ASYNCHRONOUS NEUROMUSCULAR ELECTRICAL STIMULATION

By

RYAN JAMES DOWNEY

A DISSERTATION PRESENTED TO THE GRADUATE SCHOOL
OF THE UNIVERSITY OF FLORIDA IN PARTIAL FULFILLMENT
OF THE REQUIREMENTS FOR THE DEGREE OF
DOCTOR OF PHILOSOPHY

UNIVERSITY OF FLORIDA

2015

To my parents, Michael and Denise Downey, for their invaluable support

ACKNOWLEDGMENTS

I would like to express sincere gratitude towards Dr. Warren E. Dixon. Since I first joined the lab as an undergraduate student six years ago, he has not only been my academic advisor but my mentor as well. As an academic advisor, he has provided me intellectual freedom when desired and guidance when needed. As a mentor, his constant encouragement and advice has been instrumental to my career by providing focus and direction. As I have witnessed over the years, Dr. Dixon truly cares for his students and his actions always have the best interests of their future careers in mind. He has provided me with valuable insights into an academic career, involved me in grant writing, encouraged me to mentor undergraduate and Masters students, helped me prepare application packets, involved me in IRB submissions, and even sent me abroad to collaborate with another lab. Looking toward my future career, I honestly would not be as prepared as I am today if it were not for Dr. Dixon. I would also like to extend my gratitude towards my committee members Dr. Scott Banks, Dr. Benjamin Fregly, Dr. Chris Gregory, and Dr. Bruce Wheeler for their time and the valuable recommendations they have provided. I would also like to thank my colleagues at the University of Florida Nonlinear Controls and Robotics laboratory for the countless discussions that have helped shape the ideas in this dissertation. I acknowledge that this dissertation would not have been possible without the support and encouragement provided by my family and my friends and without the financial support provided by the National Science Foundation.

TABLE OF CONTENTS

LIST OF TABLES

LIST OF FIGURES

LIST OF ABBREVIATIONS

ANOVA   Analysis of Variance

FES   Functional Electrical Stimulation

LEM   Leg Extension Machine

MVC   Maximal Voluntary Contraction

NMES   Neuromuscular Electrical Stimulation

RISE   Robust Integral of the Sign of the Error

RMS   Root-Mean-Square

SCI   Spinal Cord Injury

SEM   Standard Error of the Mean

SRT   Successful Run Time

Abstract of Dissertation Presented to the Graduate School
of the University of Florida in Partial Fulfillment of the
Requirements for the Degree of Doctor of Philosophy

ASYNCHRONOUS NEUROMUSCULAR ELECTRICAL STIMULATION

By

Ryan James Downey

May 2015

Chair: Warren E. Dixon
Major: Mechanical Engineering

Neuromuscular electrical stimulation (NMES) has been shown to impart a number of health benefits. NMES can also be used to produce functional outcomes such as grasping, walking, reaching, and cycling where it is termed functional electrical stimulation (FES). However, one limitation to NMES/FES is the rapid onset of NMES-induced fatigue. Fatigue limits the duration that NMES can be applied, and thus, the health benefits of NMES may be enhanced by reducing NMES-induced fatigue and allowing NMES to be applied for extended periods of time. Fatigue is also a limitation to FES as it limits the duration that functional tasks can be performed. Two methods to address fatigue include sequential stimulation and asynchronous stimulation. During both sequential stimulation and asynchronous stimulation, multiple stimulation channels are utilized to either segregate the desired muscle into multiple groups of motor units or to segregate multiple synergistic muscles. The stimulus is then switched between stimulation channels as time progresses, thereby reducing the average stimulation frequency of the recruited motor units.

Asynchronous stimulation has been shown to reduce NMES-induced fatigue. However, during asynchronous stimulation in man, the extent that NMES-induced fatigue can be further reduced by reducing the stimulation frequency it is not presently clear. In Chapter 2, the ability of both high- and low-frequency asynchronous stimulation to reduce NMES-induced fatigue is compared to high- and low-frequency conventional

stimulation in able-bodied and spinal cord injury populations. Both asynchronous stimulation protocols are shown to result in less fatigue than conventional stimulation. Furthermore, low-frequency asynchronous stimulation is shown to be advantageous compared to high-frequency conventional stimulation.

While asynchronous stimulation can reduce fatigue, each stimulation channel is likely to recruit a different number and/or type of motor unit for a given stimulus. Thus, asynchronous stimulation may also exhibit a force ripple (i.e., contractions that are not fully fused, thus exhibiting non-smooth force tracings). The amount of force ripple present during asynchronous stimulation in man is not presently clear, and thus, in Chapter 3, the force ripple is quantified during asynchronous and conventional single-channel transcutaneous stimulation across a range of stimulation frequencies. While high-frequency asynchronous stimulation is shown to evoke ripple similar to that of volitional contractions, low-frequency asynchronous stimulation is found to induce significant ripple.

Asynchronous stimulation and sequential stimulation have been shown to reduce NMES-induced fatigue, and thus, these methods may extend the time that functional tasks may be performed if they are combined with feedback control. However, one limitation of both methods is that switching between stimulation channels introduces discontinuities due to a differing response to stimulation by each group of recruited motor units. Therefore, there is a need to design controllers which consider the switching dynamics and muscle response to stimulation. A continuous closed-loop feedback controller is developed in Chapter 4 to yield semi-global asymptotic tracking of a desired trajectory for a person's knee-shank complex. In Chapter 5, a closed-loop feedback controller is developed through a switched systems analysis to improve upon the work in Chapter 4. The developed controller yields semi-global exponential tracking while allowing for instant switching, relaxing gain conditions, and removing an implicit assumption that there is zero activation overlap. The results in Chapters 4 and 5 indicate that

11

asynchronous stimulation can successfully extend the duration of successful tracking (compared to conventional stimulation) during feedback control, despite statistically different responses between stimulation channels. These results are therefore promising for the implementation of asynchronous stimulation for closed-loop rehabilitative procedures and in assistive devices as a method to limit NMES-induced fatigue while tracking a desired trajectory.

Chapter 6 concludes the dissertation with a discussion of the developed contributions and future efforts.

CHAPTER 1
INTRODUCTION

Neuromuscular electrical stimulation (NMES) is defined as the use of an electrical stimulus to elicit muscle contractions and is commonly used in rehabilitative settings where the goal is typically to increase muscle size, strength, and function [1–5]. NMES has been shown to impart a number of health benefits such as increased bone mineral density [6, 7], improved muscular strength [8, 9], improved motor control [10, 11], increased lean muscle mass and sensory ability [12], improved range of motion [9, 13], improved cardiovascular parameters [14, 15], and improved gait parameters [16]. However, one limitation to NMES is the rapid onset of NMES-induced fatigue compared to volitional contractions. Fatigue limits the duration that NMES can be applied. Therefore, the aforementioned health benefits of NMES may be enhanced by utilizing stimulation methods which reduce NMES-induced fatigue, thereby allowing for increased dosage of rehabilitative treatment.

NMES can also be used to produce functional outcomes such as grasping [17–19], walking [20–22], reaching [23], stair climbing [24], and cycling [25–31] where it is termed functional electrical stimulation (FES). However, NMES-induced fatigue limits the duration that functional tasks can be performed, motivating researchers to examine alternative stimulation methods that may reduce fatigue such as doublets [32–34], N-let pulse trains [35], and modulation of the stimulation parameters [36–40].

One suggested cause of NMES-induced fatigue is a reversal of the Henneman's size principle [41] whereby slow-fatiguing motor units are preferentially recruited over fast-fatiguing motor units; however, this assertion has recently been contended [42, 43]. Another suggested cause of NMES-induced fatigue is that, in contrast to physiological contractions, conventional single-channel stimulation exhibits a nonselective, spatially fixed, synchronous recruitment of motor units [42, 43]. Due to a temporal summation of the muscle twitch response, higher stimulation frequencies are required to achieve

13

a smooth force output when motor units are recruited synchronously rather than asynchronously. Higher stimulation frequencies are associated with increased rates of fatigue [44–46], and thus, when the goal is to minimize fatigue or to sustain a desired functional outcome, low stimulation frequencies should be utilized. While doublets, N-let pulse trains, and modulating the stimulation parameters have been shown to reduce fatigue, these methods do not directly address the suggested cause of fatigue in [42, 43]. Thus, researchers have developed two methods to more directly address the problem of fatigue.

The first method is sequential stimulation [47, 48] (although it has also been referred to as alternating [49] and cyclical stimulation [50]). During sequential stimulation, multiple stimulation channels are used either to segregate multiple synergistic muscles [49, 50] or to segregate the desired muscle into multiple groups of motor units [47, 48]. Pulse trains are then sequentially delivered to each stimulation channel, thereby allowing motor units to rest when the corresponding stimulation channel is not active. Lower rates of fatigue can be attributed to a reduced duty cycle (i.e., a lower average stimulation frequency) for the recruited motor units compared to conventional single-channel stimulation.

A similar and more commonly used method to reduce fatigue is asynchronous stimulation [51–53] (although it has also been referred to as rotary [54], distributed [55–57], interleaved [58–61], sequential [62], and spatially distributed sequential stimulation [63]). Similar to sequential stimulation, asynchronous stimulation utilizes multiple stimulation channels to segregate motor units or synergistic muscles. However, during asynchronous stimulation, the stimulus pulses are delivered in an interleaved fashion (i.e., switching the active stimulation channel following each individual pulse rather than after each pulse train). By interleaving the pulses, lower stimulation frequencies are achieved at each stimulation channel while retaining a high composite stimulation frequency. Similar to sequential stimulation, the ability of asynchronous stimulation to

reduce NMES-induced fatigue can be attributed to the reduced stimulation frequency of the recruited motor units compared to conventional single-channel stimulation. An illustrative comparison of sequential stimulation, asynchronous stimulation, and conventional stimulation is provided in Figure 1-1.

Both sequential stimulation and asynchronous stimulation have been shown to reduce NMES-induced fatigue [47, 49–52, 55, 56, 58–65]. Moreover, one study [50] found that a shorter on-time (i.e., the time to keep one stimulation channel activated before switching to the next channel) resulted in less fatigue, motivating the use of asynchronous stimulation over sequential stimulation. However, only a limited number of studies have examined asynchronous stimulation in human subjects [51, 52, 56, 63–65]. Furthermore, it is well known that higher stimulation frequencies increase the rate of fatigue during conventional single-channel stimulation [44–46], and thus, it is reasonable to assume that the same frequency-fatigue relationship exists with asynchronous stimulation. Two studies in cats indicate that lower stimulation frequencies may lead to reduced fatigue during asynchronous stimulation [55, 60]. However, in each of the aforementioned studies in man, one asynchronous stimulation protocol is compared to one conventional stimulation protocol. In other words, the effect of stimulation frequency on fatigue was not examined. Therefore, during asynchronous stimulation in man, the extent that NMES-induced fatigue can be further reduced by reducing the stimulation frequency it is not presently clear. Furthermore, asynchronous stimulation has been examined in able-boded individuals [52, 65], individuals post-stroke [51], and individuals with spinal cord injury (SCI) [56, 63, 64]; however, asynchronous stimulation has not been examined in both able-bodied and SCI populations simultaneously.

In Chapter 2, the ability of both high- and low-frequency asynchronous stimulation to reduce NMES-induced fatigue is compared to high- and low-frequency conventional stimulation in both able-bodied and SCI populations. Low frequency asynchronous stim-ulation is found to have significant fatigue benefits over high frequency asynchronous

15

stimulation as well as high- and low-frequency conventional stimulation, motivating its use for rehabilitation and FES.

While the results of Chapter 2 and previous research have demonstrated the effectiveness of asynchronous stimulation as a method to reduce fatigue [51, 52, 55, 56, 58–60, 62–64], each stimulation channel is likely to recruit a different number and/or type of motor unit for a given stimulus, leading to differing force responses for the same stimulus. Therefore, similar to low-frequency conventional stimulation, asynchronous stimulation may also exhibit a force ripple (i.e., contractions that are not fully fused, thus exhibiting non-smooth force tracings).

Few results have examined force ripple with asynchronous stimulation [54, 57, 58, 60]. Hughes et al. [58] studied epimysial stimulation of the plantaris longus muscle in frogs. The authors found that asynchronous stimulation with 4 channels at 15 Hz (resulting in a composite frequency equivalent to 60 Hz single-channel stimulation) produced less ripple than conventional (i.e., synchronous) single-channel stimulation at 15 Hz while producing more ripple than conventional single-channel 60 Hz stimulation. Similarly, McDonnall et al. [60] studied asynchronous intrafascicular stimulation of the sciatic nerve in cats and reported that 15 Hz stimulation with 4 channels (resulting in a composite frequency equivalent to 60 Hz single-channel stimulation) resulted in less ripple than conventional single-channel stimulation at 15 Hz. Lind and Petrofsky [54] studied asynchronous stimulation through surgically divided groups of ventral roots in cats, targeting the plantaris, medial gastrocnemius, and soleus. They showed that asynchronous stimulation of 10 Hz with 3, 5, and 10 channels (composite frequencies of 30, 50, and 100 Hz) produced smoother contractions, greater tension, and a faster rate of tension rise than conventional stimulation with a single channel at 10 Hz. Furthermore, as the number of channels was increased, thereby increasing the composite frequency, the tension increased in amplitude and became smoother. They also examined the tension developed during asynchronous stimulation with 3, 5, or 10 stimulation channels

16

at various stimulation frequencies and found that maximal tetanic tensions were always reached at a lower frequency with asynchronous stimulation than with conventional single-channel stimulation, but force ripple was not quantified. Brown et al. [57] studied asynchronous stimulation of the soleus and medial gastrocnemius in cats by activating the muscle through cut ventral roots with 6 channels of stimulation. They compared the force ripple during asynchronous stimulation at multiple stimulation frequencies where the pulses were delivered with equal time intervals or with unequal time intervals in an attempt to reduce the ripple. They found that shifting the stimulus times could reduce the ripple.

While there have been a few reports on force ripple during asynchronous stimulation in cat and frog [54, 57, 58, 60], the amount of force ripple present during asynchronous stimulation in man is not presently clear. Furthermore, in the aforementioned studies, the authors utilized epimiysial or intrafasicular stimulation or the stimulus was delivered through surgically divided ventral roots. Therefore, the amount of force ripple present during asynchronous transcutaneous stimulation (i.e., stimulation with surface electrodes, a method often used since it is noninvasive) in man is presently unknown. Furthermore, it is expected that force ripple can be decreased by utilizing higher stimulation frequencies; however, lower stimulation frequencies are preferred to reduce NMES-induced fatigue. Thus, knowledge of the interplay between stimulation frequency and force ripple may guide the choice of stimulation frequency during asynchronous FES.

In Chapter 3, the force ripple is quantified during asynchronous and conventional single-channel transcutaneous stimulation across a range of stimulation frequencies in isometric conditions. The ripple was measured during five asynchronous stimulation protocols, two conventional stimulation protocols, and three volitional contractions in twelve able-bodied individuals. Conventional 40 Hz and asynchronous 16 Hz stimulation

17

were found to induce contractions that were as smooth as volitional contractions; however, asynchronous 8, 10, and 12 Hz stimulation induced contractions with significant ripple.

During both sequential stimulation and asynchronous stimulation, multiple stimulation channels are utilized to either segregate the desired muscle into multiple groups of motor units or to segregate multiple synergistic muscles. The stimulus is then switched between stimulation channels as time progresses in an effort to avoid synchronous recruitment of motor units, thereby reducing the average stimulation frequency of the recruited motor units. Both asynchronous stimulation [51, 52, 55, 56, 58–67] and sequential stimulation [47–50] have been shown to reduce NMES-induced fatigue compared to conventional single-channel stimulation [47, 49–52, 55, 56, 58–65], and thus, these methods may extend the time that functional tasks may be performed if they are combined with feedback control. However, previous studies have primarily focused on isometric contractions with fixed stimulation parameters (i.e., open-loop stimulation) [47, 50, 55, 56, 58–65, 67]. Therefore, it is presently unclear if the fatigue benefits reported for open-loop stimulation similarly applies to feedback control of NMES in man. One study [50] found that a shorter on-time (i.e., the time to keep one stimulation channel activated before switching to the next channel) resulted in less fatigue, motivating the use of asynchronous stimulation over sequential stimulation. However, incorporating either of these stimulation strategies with a closed-loop controller is challenging due to the need to switch between different synergistic muscles (or different groups of motor units within a given muscle) while maintaining stability of the closed-loop system. Specifically, the muscle's response to a given stimulus will differ for each stimulation channel since each channel activates a different number and/or type of motor units. Thus, there is a need to design a controller that considers the switching dynamics and muscle response to stimulation. Since both stimulation methods exhibit the same closed-loop control challenges and asynchronous stimulation is more commonly used, the subsequent limb

18

model, control development, and experiment sections of the dissertation will refer only to asynchronous stimulation without loss of generality.

While constructive control developments and associated stability analyses have been previously developed for conventional single-channel stimulation [27, 30, 68–71], limited development has been provided for multi-channel asynchronous stimulation. Lau et al. [66] studied standing in cats and found that the duration of standing achieved during closed-loop control of asynchronous stimulation was longer than that for open-loop control. However, the closed-loop controller implemented was a logic-based if-then-else algorithm without modeling or stability analysis. Similarly, Frankel et al. [72] implemented an iterative learning controller for isometric force control in cats; however, no modeling or stability analysis was included. Based on the preliminary work in [73], a closed-loop tracking controller is developed for asynchronous stimulation in Chapter 4. The associated stability analysis yields semi-global asymptotic tracking despite switching between stimulation channels, parametric uncertainties in the nonlinear dynamics, and the presence of exogenous disturbances. As a result of the designed transition period, which can be made arbitrarily short by adjusting the control gains, switching is arbitrary in the sense that the switching signal is not dependent on the states and the switching can be arbitrarily fast. The developed controller is applied to both asynchronous and conventional stimulation in experiments with a modified leg extension machine to compare the ability of each stimulation method to maintain trajectory tracking. Asynchronous stimulation with the developed closed-loop controller is found to significantly prolong the functional movements of the lower limb. This result is promising for the implementation of asynchronous stimulation in closed-loop rehabilitative procedures and in assistive devices as a method to reduce fatigue while maintaining a person's ability to track a desired limb trajectory.

While the continuous control law developed in Chapter 4 achieves semi-global asymptotic tracking despite bounded time-varying disturbances, the control design

required there to be a finite window of time where the control voltage is transitioned from one channel to another. Heuristically, a transition period is expected to lead to increased muscle fatigue since each stimulation channel will be activated longer than otherwise desired. Furthermore, in practice, stimulation channels are instantly switched, motivating the design of a control law that allows for instant switching. Although the transition period in Chapter 4 can be made arbitrarily small to approximate instant switching, increased control gains are required to compensate for smaller transition periods. Furthermore, the work in Chapter 4 implicitly assumes that the motor units recruited by each stimulation channel are independent. Yet, some degree of activation overlap is expected in practice, and therefore, it is motivated to remove this assumption in the control design. In Chapter 5, a switched systems analysis is used to examine an alternative control approach which allows for instantaneous switching between stimulation channels, without additional requirements on the control gains. The work in Chapter 5 also removes the implicit assumption that there is no activation overlap. A closed-loop feedback controller is developed to yield semi-global exponential tracking where the switching is arbitrary in the sense that the switching signal can be defined a priori and is not dependent on the states. The developed controller is implemented on four individuals with asynchronous and conventional stimulation. While it is expected that each asynchronous stimulation channel would respond differently to stimulation (resulting in different recruitment curves), it has not previously been examined. There-fore, tests were also conducted to examine the differences in the responses between each asynchronous stimulation channel. Asynchronous stimulation is found to result in statistically longer durations of successful tracking for the knee-joint angle despite statis-tically different responses between the stimulation channels. The results of Chapters 4 and 5 are promising for the implementation of asynchronous stimulation for closed-loop rehabilitative treatments and for assistive devices as a method to limit NMES-induced fatigue while tracking a desired trajectory.
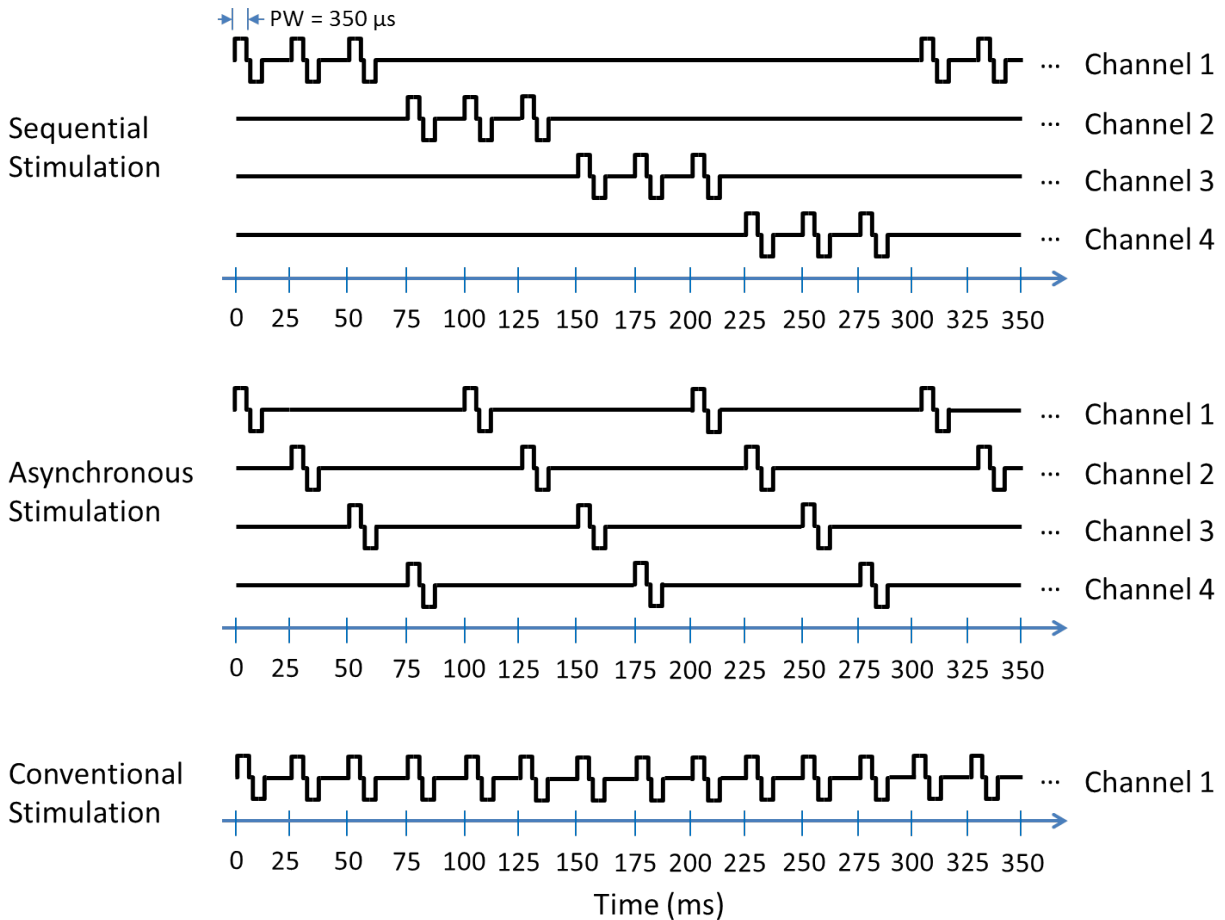
Figure 1-1. Asynchronous stimulation, sequential stimulation, and conventional stimulation diagram.

During sequential stimulation, multiple channels are utilized where high frequency pulse trains are delivered sequentially to each channel resulting in a lower average stimulation frequency per channel. In the present example, each stimulation channel receives pulses at 40 Hz; however, the average stimulation frequency is 10 Hz per channel. During asynchronous stimulation, multiple channels are utilized where high composite stimulation frequencies are achieved by interleaving the pulses. Depicted is asynchronous 10 Hz stimulation with 4 channels where each channel receives pulse trains at 10 Hz, but the composite stimulation frequency is 40 Hz. During conventional stimulation, only a single stimulation channel is utilized and higher stimulation frequencies are required to achieve a strong and smooth force output resulting in the onset of fatigue. Depicted in the present example is 40 Hz conventional stimulation. Note that the width of the pulses is not drawn to scale for illustrative purposes.

CHAPTER 2
LOW FREQUENCY ASYNCHRONOUS STIMULATION REDUCES NMES-INDUCED FATIGUE IN SCI AND ABLE-BODIED INDIVIDUALS

Multi-channel asynchronous stimulation has been previously shown to reduce NMES-induced fatigue compared to conventional single-channel stimulation. However, in previous studies in man, the effect of stimulation frequency on the NMES-induced fatigue has not been examined for asynchronous stimulation. Low stimulation frequencies are known to reduce fatigue during conventional stimulation, and thus, it is reasonable to assume that the same frequency-fatigue relationship exists with asynchronous stimulation. In this chapter, the ability of both high- and low-frequency asynchronous stimulation to reduce NMES-induced fatigue is compared to high- and low-frequency conventional stimulation in both able-bodied and spinal cord injury populations. Low frequency asynchronous stimulation is found to have significant fatigue benefits over high frequency asynchronous stimulation as well as high- and low-frequency conventional stimulation, motivating its use for rehabilitation and FES.

2.1 Methods

2.1.1 Subjects

Asynchronous and conventional stimulation were examined in both able-bodied and spinal cord injured populations to better understand the NMES-induced fatigue characteristics of the stimulation protocols. Four individuals with SCI (3 male, 1 female, aged 35 to 63) participated in the study at the Medical University of South Carolina. Prior to participation, written informed consent was obtained from all participants, as approved by the institutional review board at the Medical University of South Carolina. All participants were medically stable, but a physical therapist was present during the study to monitor vital signs as needed and to monitor for signs of autonomic dysreflexia. Demographics are listed in Table 2-1 for the four individuals with SCI. Four able-bodied individuals (3 male, 1 female, aged 20 to 27) also participated in the study at the

Table 2-1. Demographics of the SCI study group.

Subject	Age	Sex	Injury	Months Since Injury
A	55	M	C6	28.7
B	36	M	C7	65.6
C	63	F	T10	77.8
D	35	M	C4	179.3

University of Florida. Prior to participation, written informed consent was obtained from all participants, as approved by the institutional review board at the University of Florida.

2.1.2 Apparatus

All testing was performed using an apparatus that consisted of the following: 1) a current-controlled 8-channel stimulator (RehaStim, Hasomed GmbH, Germany), 2) a data acquisition device (Quanser Q8-USB), 3) a personal computer running Matlab/Simulink, and 4) a dynamometer to measure the isometric knee-joint torque. At the University of Florida, the dynamometer is a modified leg extension machine (LEM) fitted with force transducers while a Biodex System 4 Pro dynamometer was utilized at the Medical University of South Carolina and is depicted in Figure 2-1. The LEM and Biodex allow for seating adjustments to ensure that the center of rotation of the knee joint could be aligned with the center of rotation of the dynamometers. In both apparatuses, the thigh was parallel to the ground and the shank was in a gravity eliminated position. In general, the hips were flexed approximately 75 degrees, though a reclined (i.e., more extended) position was utilized for SCI individuals that did not have adequate trunk control (i.e., those with cervical level injuries) and straps were used to stabilize the torso.

2.1.3 Stimulation Protocols

Four stimulation protocols were examined: 8 Hz asynchronous stimulation (A8), 16 Hz asynchronous stimulation (A16), 32 Hz conventional stimulation (C32), and 64 Hz conventional stimulation (C64). Conventional stimulation consists of a single stimulation channel with a pair of 3" by 5" Valutrode® surface electrodes placed over the quadriceps
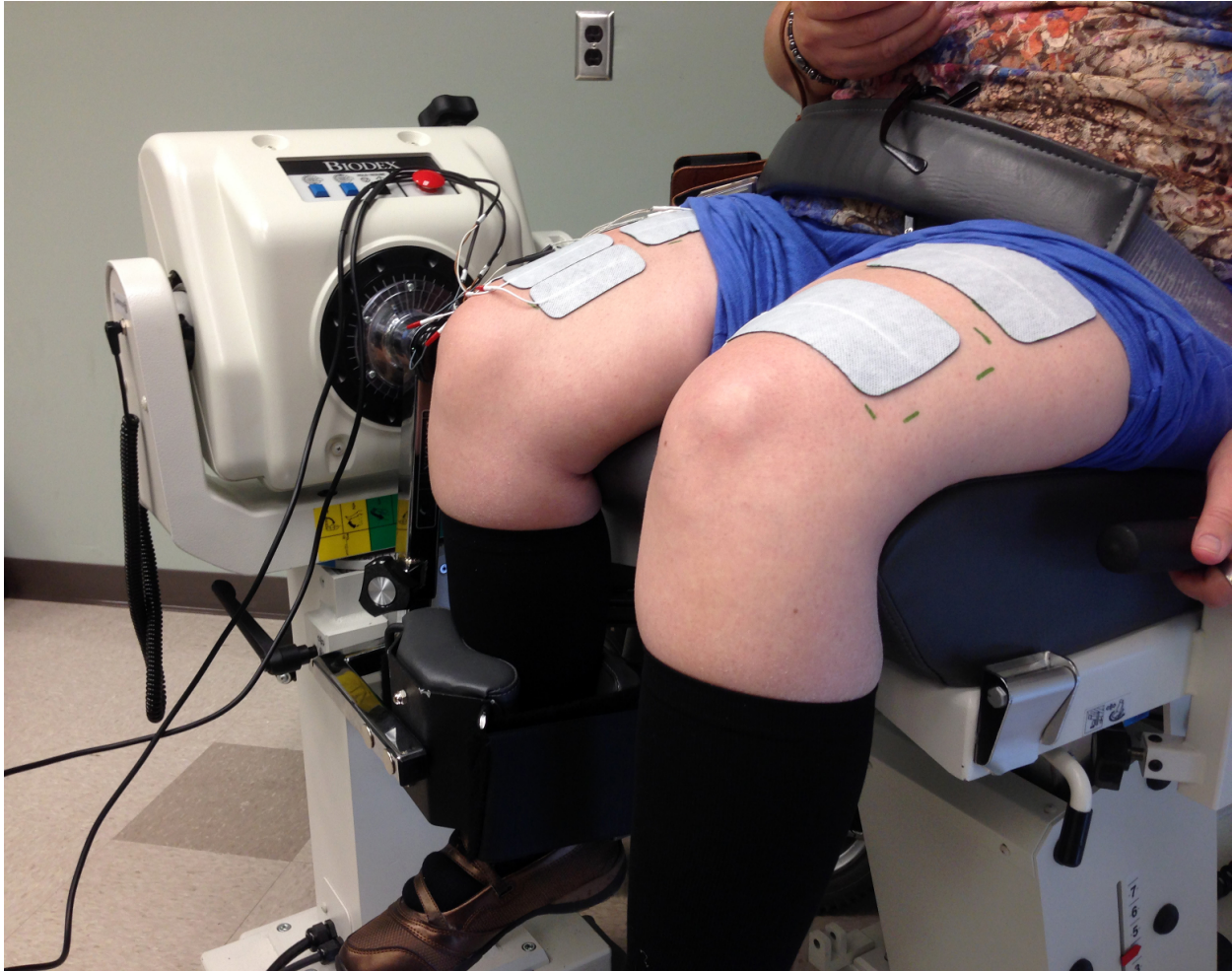
Figure 2-1. Biodex dynamometer.
Individuals with SCI were seated at the Biodex dynamometer to measure isometric knee joint torque as the muscle fatigues during four stimulation protocols. The protocol order was randomized and electrode positions were marked so that the positioning could be replicated when switching between asynchronous and conventional electrode config- urations. Pictured above is single-channel conventional stimulation on the individual's left leg and four-channel asynchronous stimulation on the individual's right leg. Seating adjustments were made to ensure that the center of rotation of the knee joint could be aligned with the center of rotation of the dynamometer. Photo courtesy of Ryan Downey.

femoris muscle group, while asynchronous stimulation consists of four channels of stimulation utilizing four electrodes placed distally (1.5" by 3.5" Valutrode®) and two electrodes placed proximally (2" by 3.5" Valutrode®).[1] For asynchronous stimulation, each channel utilized the same current amplitude, but the stimulation pulses were interleaved across the stimulation channels. In other words, asynchronous stimulation of 16 Hz with four channels results in a composite stimulation frequency of 64 Hz. The electrode configuration utilized during asynchronous stimulation is depicted in Figure 2-2, and the method of interleaving the pulses across the stimulation channels is the same as previously depicted for asynchronous stimulation in Figure 1-1.

2.1.4 Determining the Desired Initial Torque

In the subsequently described fatigue trials, the current amplitude is adjusted before the start of each fatigue trial to match the initial torque to a predetermined level. To account for variability in each individual's strength, the desired torque level was determined specifically for each leg in a pretrial (i.e., before any fatigue trials were conducted) test with conventional 64 Hz stimulation. The pretrial test also served as a warm-up session and allowed for individuals to become accustomed to the sensation of the electrical pulses. During the pretrial test, pulse trains were delivered 5 seconds at a time with 25 seconds of rest between pulse trains. The resulting torque was analyzed immediately following each contraction and the current amplitude was adjusted during the rest period preceding the following contraction. Since all four stimulation protocols were examined on the same day, it was expected that there would be some layover effect of fatigue, even with rest between fatigue trials. Therefore, the subsequently described criteria were used to determine the desired initial torque so that the layover effect of fatigue would not later preclude torque matching.

---

[1] Surface electrodes for the study were provided compliments of Axelgaard Manufacturing Co., Ltd.
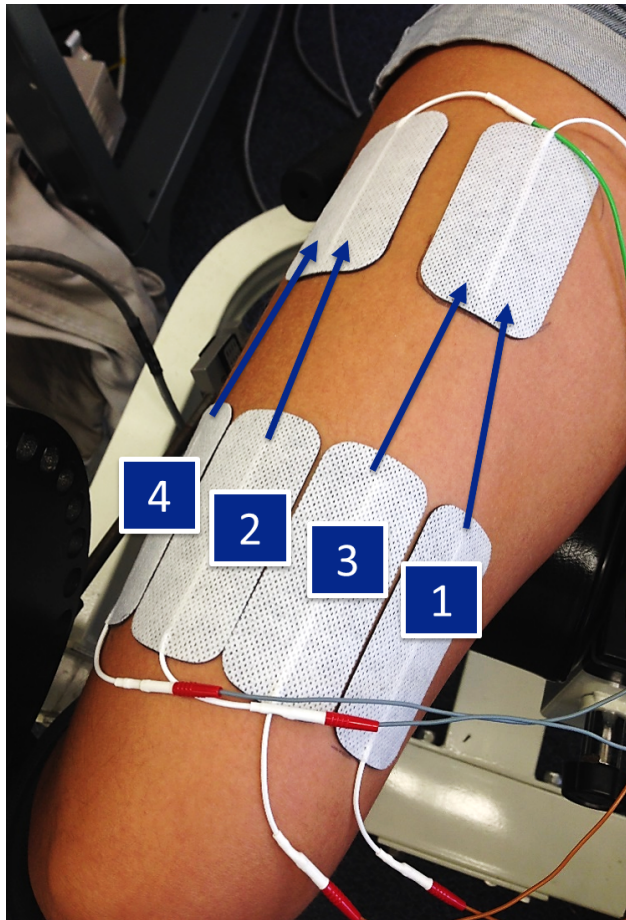
Figure 2-2. Asynchronous electrode configuration.
Electrode configuration utilized for four-channel asynchronous stimulation with two electrodes placed proximally and four electrodes placed distally. Stimulation channels 1 and 3 share the most medial and proximal electrode, while stimulation channels 2 and 4 share the most lateral and proximal electrode. Photo courtesy of Ryan Downey.

2.1.4.1 SCI

For individuals with SCI, the current amplitude was incremented between contractions until one of the following three conditions were met: 1) the isometric torque reached 20 $N \cdot m$, 2) the torque output began to plateau with increases in current amplitude, or 3) the current amplitude reached 100 mA, whichever occurred first. If the torque reached 20 $N \cdot m$ during this phase of the experiment, then the desired torque was set to 20 $N \cdot m$ for the subsequent fatigue trials. Otherwise, the desired torque was set to 75% of the maximum torque achieved during the pretrial test in an effort to account for

any layover effect of fatigue between trials. The torque reached $20 \mathrm{~N} \cdot \mathrm{m}$ for only one leg of one individual in the pretrial test. After determining the desired torque based on the aforementioned criteria, this value was used as the targeted initial torque for all subsequent fatigue trials on the same leg.

2.1.4.2 Able-bodied

For able-bodied individuals, the current amplitude was incremented between contractions until one of the following three conditions were met: 1) the isometric torque reached 10% of their maximal voluntary contraction (MVC), 2) the torque output began to plateau with increases in current amplitude, or 3) the individual experienced discomfort in response to the stimulation, whichever occurred first. If the torque reached 10% of the MVC during this phase of the experiment, then the desired torque was set to 10% of the MVC for the subsequent fatigue trials. Otherwise, the desired torque was set to 75% of the maximum torque achieved during the pretrial test in an effort to account for any layover effect of fatigue between trials. The torque reached 10% of the MVC for all able-bodied individuals in the pretrial test. After determining the desired torque based on the aforementioned criteria, this value was used as the targeted initial torque for all subsequent fatigue trials on the same leg.

2.1.5 Fatigue Trials

After the desired torque level was determined for each leg, fatigue trials were conducted for each of the four stimulation protocols. Fatigue trials consisted of 5 minutes of intermittent stimulation where pulse trains were delivered for 5 seconds and then the muscle was allowed to rest for 5 seconds. To increase subject comfort during delivery of each 5-second pulse train, the current amplitude was increased as a ramp from 0 mA to the desired current amplitude over the course of 1 second. The current amplitude then remained constant for 3 seconds before returning to 0 mA over the course of 1 second.

2.1.5.1 Precautionary measures

Since all four stimulation protocols were examined on the same day, the protocol order was randomized and participants were allowed to rest between trials. A minimum of 20 minutes of rest was given between trials although participants were allowed to rest longer if they so desired. Electrode positions were marked so that the placement could be replicated when switching between asynchronous and conventional electrode configurations.

2.1.5.2 Setting the current amplitude

Before the start of each fatigue trial, the current amplitude was adjusted in order to match the initial value of torque to the desired initial torque that was determined previously (Section 2.1.4). During this phase of the experiment, pulse trains were delivered 5 seconds at a time with 25 seconds of rest between pulse trains. The resulting torque was analyzed immediately following each contraction and the current amplitude was adjusted during the rest period preceding the following contraction. Fatigue trials were initiated immediately after determining the appropriate current amplitude.

An alternative approach to the study would have been to utilize the same current amplitude for all stimulation protocols in an effort to recruit the same number of fibers for each protocol. However, there is no guarantee that matching the current amplitude across asynchronous and conventional stimulation would recruit the same number of fibers. Given the non-selective recruitment patterns for NMES [42, 43], the relative drop in force should be consistent across stimulation intensities (i.e., current amplitudes). Therefore, similar to [60, 63–65], the current amplitude was adjusted for each stimulation protocol in order to reach a desired value of torque.

2.1.6 Data Analysis

The mean isometric torque was calculated for each contraction (30 contractions per fatigue trial). To account for intersubject variability in strength and intrasubject

variability in the initial contraction, the torque was then normalized by the mean torque of the first contraction. The four stimulation protocols were compared according to the following metrics: fatigue time, and fatigue index. Fatigue time denotes the time elapsed between the first contraction and the contraction at which the torque decreased below 80% of the initial contraction. Fatigue index is the ratio of the mean torque produced in the final three contractions to the torque produced in the first contraction. To account for intersubject variability in terms of fatigability of the muscle, fatigue times were normalized by the mean fatigue time of all stimulation protocols for each leg. The same normalization process was applied to the fatigue index. Analysis of variance (ANOVA) was performed on the normalized fatigue time and fatigue index of the group data at a significance level of $\alpha = 0.05$. Post hoc analysis (Tukey–Kramer method) was used to determine differences between individual stimulation protocols at a significance level of $\alpha = 0.05$.

2.2   Results

2.2.1   Torque Matching

Matching the initial torque to the desired level proved to be difficult in the SCI population as the torque mismatch was greater than 25% of the desired initial torque in six of the 32 fatigue trials (note there were 32 fatigue trials in the SCI population as four protocols were tested on both legs of the four individuals). In five of these six instances, the maximum possible current amplitude for the stimulator (126 mA) was reached and in the remaining instance, the torque plateaued with respect to increasing current amplitude. These results suggest that there may have been some layover effect of fatigue in the SCI population, even after 20 minutes of rest. Meanwhile, in the able-bodied population, the torque mismatch was greater than 25% of the desired initial torque in only one of the 32 fatigue trials.

2.2.2 Fatigue

2.2.2.1 SCI

Figure 2-3 shows the normalized torque for each protocol across all SCI partici-
pants as a function of the contraction number. Fatigue times are provided in Table 2-2
and the fatigue indices are provided in Table 2-3. ANOVA revealed differences in the
fatigue time of the four protocols ($F = 71.41$, $p = 3.110E - 13$) as well as the fatigue
index ($F = 22.33$, $p = 1.379E - 7$). Post hoc analysis indicated that the mean fatigue
time of A8 was significantly longer than that of A16, C32, and C64; A16 was significantly
longer than C32 and C64; and C32 was significantly longer than C64. Further, post hoc
analysis indicated that the mean fatigue index of A8 was significantly larger than C32
and C64; and A16 and C32 were significantly larger than C64. Significant differences
between the mean fatigue index of A8 and A16 could not be concluded. Significant
differences could also not be concluded between the mean fatigue index of A16 and
C32.

Table 2-2. Fatigue time (in seconds) - SCI.

Subject-Leg	A8	A16	C32	C64
A - Left	170.0	160.0	50.0	20.0
A - Right	190.0	70.0	40.0	20.0
B - Left	170.0	140.0	60.0	10.0
B - Right	130.0	60.0	40.0	10.0
C - Left	70.0	70.0	50.0	10.0
C - Right	100.0	80.0	50.0	30.0
D - Left	180.0	140.0	60.0	10.0
D - Right	110.0	80.0	60.0	20.0
Mean	**140.0**[a,b,c]	**100.0**[a,b]	**51.3**[a]	**16.3**
SD	**43.8**	**39.6**	**8.3**	**7.4**

[a] *Significantly longer fatigue time than C64*
[b] *Significantly longer fatigue time than C32*
[c] *Significantly longer fatigue time than A16*
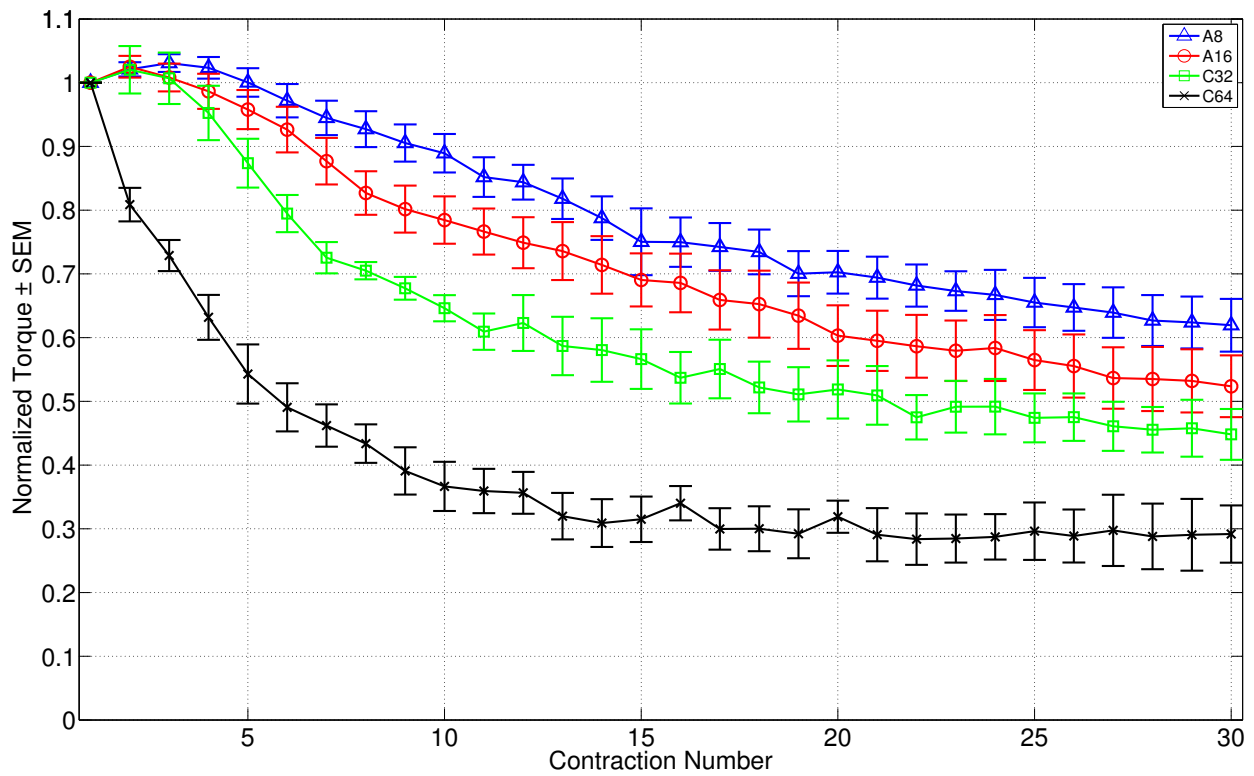
Figure 2-3. Isometric muscle fatigue in SCI individuals.
Fatigue in SCI individuals represented by the normalized torque produced $\pm$ the standard error of the mean (SEM) as a function of the contraction number.

Table 2-3. Fatigue index - SCI.

Subject-Leg	A8	A16	C32	C64
A - Left	0.689	0.617	0.566	0.238
A - Right	0.720	0.746	0.526	0.361
B - Left	0.604	0.413	0.353	0.170
B - Right	0.615	0.300	0.274	0.090
C - Left	0.384	0.444	0.354	0.157
C - Right	0.628	0.523	0.526	0.358
D - Left	0.746	0.609	0.440	0.432
D - Right	0.544	0.541	0.558	0.473
Mean	**0.616**[a,b]	**0.524**[a]	**0.450**[a]	**0.285**
SD	**0.115**	**0.139**	**0.111**	**0.140**

[a] *Significantly larger fatigue index than C64*
[b] *Significantly larger fatigue index than C32*

2.2.2.2 Able-bodied

Figure 2-4 shows the normalized torque for each protocol across all able-bodied participants as a function of the contraction number. Fatigue times are provided in Table 2-4 and the fatigue indices are provided in Table 2-5. ANOVA revealed differences in the fatigue time of the four protocols ($F = 59.61$, $p = 2.814E-12$) as well as the fatigue index ($F = 37.27$, $p = 6.527E-10$). Post hoc analysis indicated that the mean fatigue time of A8 was significantly longer than that of A16, C32, and C64; and A16 was significantly longer than C32 and C64. Statistical differences could not be concluded between C32 and C64. Further, post hoc analysis indicated that the mean fatigue index of A8 was significantly larger than A16, C32 and C64; A16 was significantly larger than C32 and C64; and C32 was significantly larger than C64.

2.3 Discussion

Previous studies have suggested that asynchronous stimulation may reduce NMES-induced fatigue compared to conventional single-channel stimulation. Popovic et al. examined isometric knee torque and found that asynchronous 16 Hz stimulation with
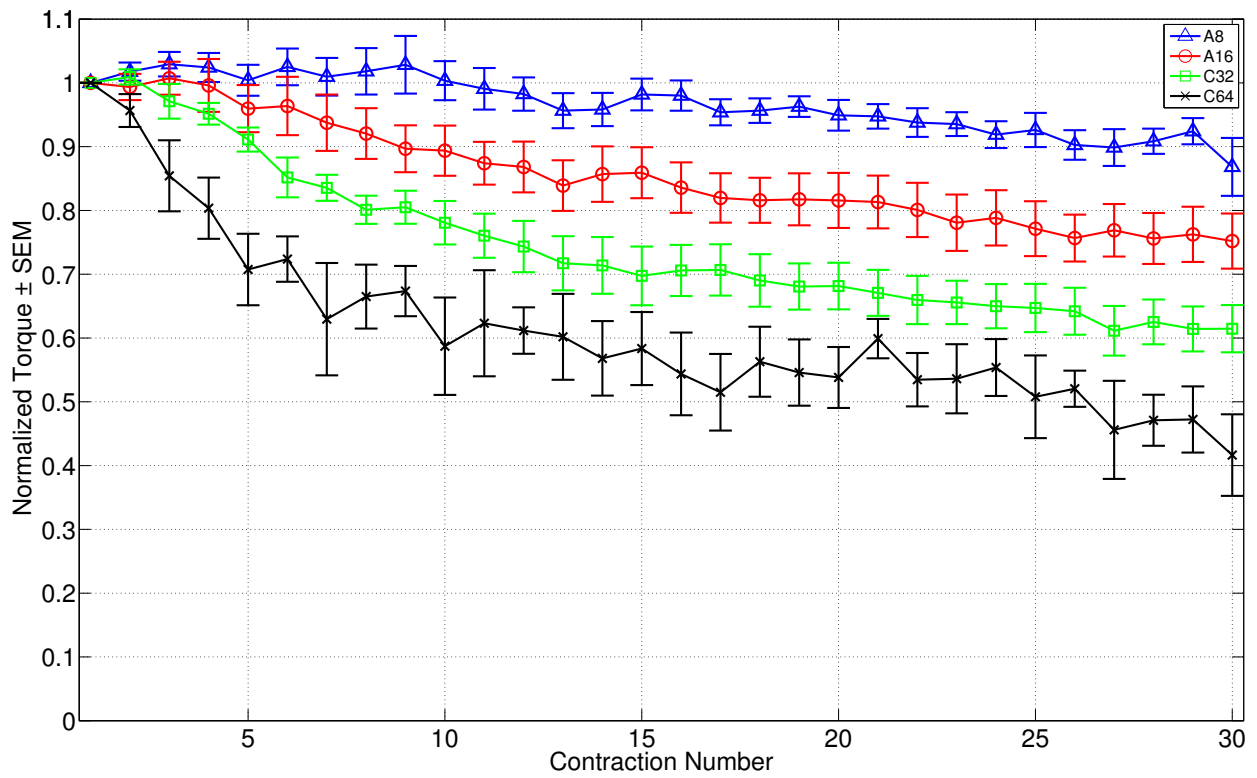
Figure 2-4. Isometric muscle fatigue in able-bodied individuals.
Fatigue in able-bodied individuals represented by the normalized torque produced $\pm$ the standard error of the mean (SEM) as a function of the contraction number.

Table 2-4. Fatigue time (in seconds) - able-bodied.

Subject-Leg	A8	A16	C32	C64
A - Left	300.0	100.0	60.0	20.0
A - Right	300.0	100.0	40.0	30.0
B - Left	260.0	80.0	50.0	40.0
B - Right	300.0	90.0	90.0	70.0
C - Left	240.0	150.0	100.0	40.0
C - Right	300.0	300.0	70.0	40.0
D - Left	300.0	120.0	60.0	30.0
D - Right	300.0	300.0	180.0	50.0
Mean	**287.5**^{a,b,c}	**155.0**^{a,b}	**81.3**	**40.0**
SD	**23.8**	**92.0**	**44.5**	**15.1**

[a] *Significantly longer fatigue time than C64*
[b] *Significantly longer fatigue time than C32*
[c] *Significantly longer fatigue time than A16*

four channels prolonged the average fatigue interval by 153% compared to conventional 40 Hz stimulation in six individuals with SCI [64]. In a follow up study to [64], Malesevic et al. found that asynchronous 16 Hz stimulation with four channels resulted in 26% longer fatigue intervals compared to conventional 30 Hz stimulation in six individuals with SCI [56]. Nguyen et al. examined isometric ankle torque and found asynchronous 10 Hz stimulation with four channels resulted in a 280% longer time to fatigue and a 234% higher fatigue index than conventional 40 Hz stimulation in one individual with SCI [63]. Downey et al. examined FES cycling and found that asynchronous 16.67 Hz stimulation with 6 channels almost doubled the fatigue time compared to conventional 30 Hz stimulation in two able-bodied individuals [52]. Maneski et al. examined grasping pressure and found that asynchronous 10 Hz stimulation with four channels more than doubled the time interval before the onset of fatigue compared to conventional 40 Hz stimulation in six individuals post-stroke [51]. Sayenko et al. concluded that asynchronous 10 Hz stimulation with four stimulation channels is more effective at reducing muscle fatigue compared to 40 Hz conventional stimulation in able-bodied

Table 2-5. Fatigue index - able-bodied.

Subject-Leg	A8	A16	C32	C64
A - Left	0.894	0.740	0.617	0.235
A - Right	0.970	0.640	0.658	0.661
B - Left	0.756	0.661	0.612	0.284
B - Right	0.962	0.721	0.681	0.510
C - Left	0.894	0.617	0.488	0.337
C - Right	0.849	0.958	0.683	0.528
D - Left	0.813	0.793	0.451	0.436
D - Right	0.977	0.898	0.736	0.605
Mean	**0.889**^{a,b,c}	**0.754**^{a,b}	**0.616**^{a}	**0.450**
SD	**0.080**	**0.123**	**0.099**	**0.154**

^{a}*Significantly larger fatigue index than C64*
^{b}*Significantly larger fatigue index than C32*
^{c}*Significantly larger fatigue index than A16*

individuals and the reason is that different sets of muscle fibers are activated alternately by the different electrodes [65].

In the SCI population of the present study, asynchronous stimulation resulted in a longer fatigue time than conventional stimulation with A16 yielding a 513% increase over C64 and A8 yielding a 173% increase over C32. In the able-bodied population, asynchronous stimulation also resulted in a longer fatigue time than conventional stimulation with A16 yielding a 287% increase over C64 and A8 yielding a 253% increase over C32. However, it should be noted that the muscle did not fatigue beyond the 80% threshold in six of the A8 trials and two of the A16 trials. Therefore, the true fatigue times are likely to be longer than the reported values of 300 seconds (i.e., the entire duration of the fatigue trials) in Table 2-4. Asynchronous stimulation also resulted in less total fatigue at the end of the trials compared to conventional stimulation. In the SCI population, A16 yielded an 84% larger fatigue index than C64 and A8 yielded a 37% larger fatigue index than C32. Similarly, in the able-bodied population, A16 yielded a 68% larger fatigue index than C64 and A8 yielded a 44% larger fatigue index than C32.

While it is well known that asynchronous stimulation reduces NMES-induced fatigue compared to conventional stimulation, lower frequency asynchronous stimulation may also be preferred over high frequency asynchronous stimulation. Wise et al. examined six-channel asynchronous stimulation in cats at both 6 Hz and 10 Hz [55]. The authors found that 6 Hz stimulation resulted in less fatigue than 10 Hz during intermittent stimulation, but it did not result in less fatigue during continuous stimulation. However, data was only collected in two cats for 10 Hz continuous stimulation and in three cats for 6 Hz continuous stimulation. Furthermore, the authors stated that the discrepancy between intermittent and continuous stimulation may be due to the fact that there was a large amount of potentiation present at the beginning of the 10 Hz continuous stimulation protocol. Although lowering the stimulation frequency did not reduce fatigue during continuous asynchronous stimulation in [55], a more recent study by McDonnall et al. also examined continuous asynchronous stimulation in cats. The authors found that four-channel asynchronous stimulation at 15 Hz resulted in a greater fatigue index (i.e., less fatigue) than two-channel asynchronous stimulation at 30 Hz [60].

In the present study, there was significant advantage to utilizing lower stimulation frequencies, even for asynchronous stimulation, as post hoc analysis determined that A8 resulted in significantly longer fatigue times than A16 (40% longer on average in the SCI population and 85% longer on average in the able-bodied population). Post hoc analysis also determined there to be a statistically significant difference in the mean fatigue indices of A8 and A16 for the able-bodied population but a statistical difference could not be concluded for the SCI population. However, the data suggests that A8 leads to less total fatigue as A8 resulted in an 18% greater fatigue index than A16 on average for both populations. While there are obvious differences between the able-bodied and SCI populations in the sense that the SCI population exhibited higher rates of fatigue (cf. Tables 2-2 and 2-4) and more total fatigue at the end of the

trials (cf. Tables 2-3 and 2-5), both populations exhibited the same general trend in the performance of the four protocols.

While the present results are promising in that the fatigue benefits of asynchronous stimulation can be extended by reducing the stimulation frequency, care should be taken when using low frequency asynchronous stimulation in certain applications because low frequency asynchronous stimulation may result in a significant force ripple [74]. Force ripple is unlikely to be a major concern if asynchronous stimulation is used for muscle strengthening, increasing bone mineral density, or other rehabilitative efforts. However, it may pose a problem to FES where feedback control may be required, although efforts have been made to develop controllers that allow for limbs to track a desired trajectory during asynchronous stimulation [73]. Furthermore, while asynchronous stimulation may reduce NMES-induced fatigue, conventional stimulation may be preferred for muscle strengthening therapy as indicated by one study [56]. However, when the goal of NMES is to increase bone mineral density [6], improve cardiovascular parameters [14, 15], or achieve other health related benefits other than muscle strengthening, asynchronous stimulation is preferred over conventional stimulation since it allows the treatment duration to be extended. Similarly, asynchronous stimulation is also preferred over conventional stimulation in FES applications where desired tasks and movements need to be accomplished for as long as possible. In conclusion, the present work demonstrated that NMES-induced fatigue is significantly reduced with asynchronous stimulation and that low frequency asynchronous stimulation significantly reduces fatigue compared to high frequency asynchronous stimulation. The results are promising both for clinical adoption of asynchronous stimulation and for its use in assistive devices.

CHAPTER 3
COMPARING THE FORCE RIPPLE DURING ASYNCHRONOUS AND CONVENTIONAL STIMULATION

Asynchronous stimulation has been shown to reduce fatigue during electrical stimulation; however, it may also exhibit a force ripple. In this chapter, ripple is quantified during asynchronous and conventional single-channel transcutaneous stimulation across a range of stimulation frequencies. The ripple was measured during five asynchronous stimulation protocols, two conventional stimulation protocols, and three volitional contractions in twelve healthy individuals. Conventional 40 Hz and asynchronous 16 Hz stimulation were found to induce contractions that were as smooth as volitional contractions. Asynchronous 8, 10, and 12 Hz stimulation induced contractions with significant ripple. Thus, while lower stimulation frequencies can reduce fatigue, they may also lead to increased ripple.

3.1 Methods

Twelve healthy individuals (age 28.5 ± 7.5 years) participated in the study. Prior to participation, written informed consent was obtained from each individual, as approved by the institutional review board at the University of Florida. Individuals were asked to sit in a modified leg extension machine (LEM). The LEM allows for seating adjustments such that the axis of rotation of the knee joint could be aligned with the axis of rotation of the LEM. The LEM was fitted with a force transducer such that the isometric knee-joint torque could be measured. Isometric torque was recorded during five asynchronous stimulation protocols with stimulation frequencies ranging from 8 to 16 Hz in 2 Hz steps as well as during two conventional (i.e., synchronous) single-channel stimulation protocols with stimulation frequencies of 20 and 40 Hz. Isometric torque was also acquired during volitional contractions to provide a reference for the smoothness of volitional contractions in healthy individuals. As stated previously, a force ripple is characterized by contractions that are not fully fused, thus exhibiting force tracings (or equivalently, torque tracings) which are not smooth. Recorded isometric torque

38
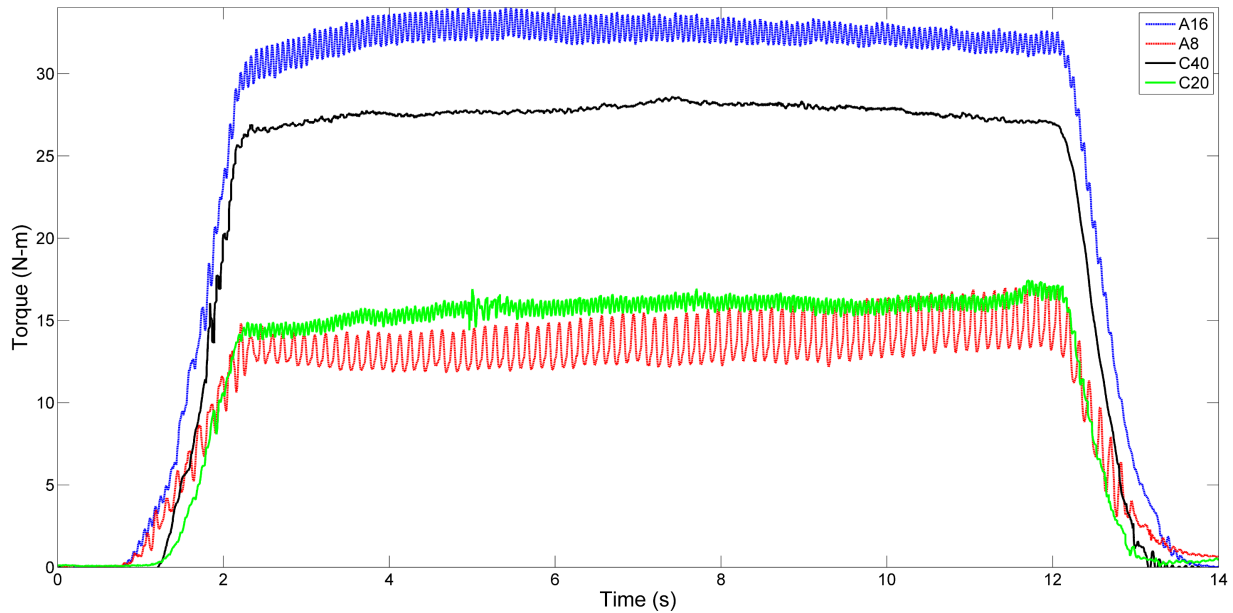
Figure 3-1. Isometric torque measurements.
Example isometric torque measurements acquired from a single individual which illustrates the presence of ripple (i.e., contractions exhibiting force tracings which are not smooth) during asynchronous stimulation. A16 and A8 refer to asynchronous multi-channel stimulation of 16 and 8 Hz, respectively. C40 and C20 refer to conventional single-channel stimulation of 40 and 20 Hz, respectively. In this example, A16, C40, C20, and A8 evoked mean torques of 32.4, 27.8, 16.1, and 14.1 N-m, respectively.

measurements from a single individual are shown in Figure 3-1 to better illustrate the difference between smooth contractions and those which exhibit a ripple. The root mean square (RMS) ripple was computed for each volitional and NMES-induced contraction, expressed as a percentage of the mean torque.

Stimulation pulses were delivered by a current-controlled 8-channel stimulator (RehaStim, Hasomed GmbH, Germany), which was controlled by a personal computer. Conventional stimulation consisted of a single stimulation channel with a pair of surface electrodes placed over the quadriceps femoris muscle, while asynchronous stimulation consisted of four channels of stimulation. For asynchronous stimulation, the stimulation pulses were interleaved across the stimulation channels. In other words, asynchronous stimulation of 10 Hz with 4 channels results in a composite stimulation frequency of 40 Hz. The electrode configuration utilized during asynchronous stimulation is depicted in

Figure 3-2, and the method of interleaving the pulses across the stimulation channels is the same as previously depicted for asynchronous stimulation in Figure 1-1.
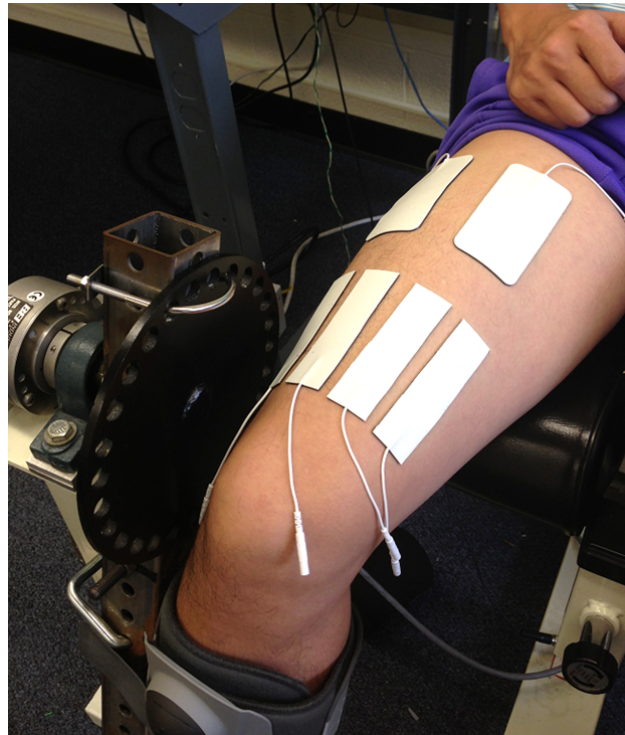
Figure 3-2. Asynchronous electrode configuration.
Electrode configuration for asynchronous stimulation with 2 electrodes placed proximally and 4 electrodes placed distally. The stimulation channels corresponding to the 2 most medial and distal electrodes share the most medial and proximal electrode, while the stimulation channels corresponding to the 2 most lateral and distal electrodes share the most lateral and proximal electrode. A force transducer was fixed to the leg extension machine to acquire the isometric torque. Photo courtesy of Ryan Downey.

At the beginning of each experiment, each individual was asked to perform a maximal voluntary contraction (MVC) while the isometric torque was recorded. The individual was then asked to perform contractions at 50% and subsequently 25% of his or her MVC. To aid the individual's ability to reach the desired torque, visual feedback of the torque was provided via a display. The individual then received asynchronous 16 Hz stimulation, while the current amplitude was slowly incremented. This served as a warm-up session while also providing a guideline to select the desired current amplitude. For each individual, the desired current amplitude was selected as either the

current amplitude which evoked a contraction of at least 20% of the MVC or the current amplitude beyond which increases in current amplitude caused discomfort, whichever occurred first. Due to subject discomfort, 20% of the MVC was not always obtained during the warm-up session with asynchronous 16 Hz stimulation. The mean current amplitude selected for each individual was 39.7 ± 10.1 mA.

The ripple present during asynchronous and conventional stimulation was then examined by delivering biphasic pulses with a pulsewidth of 350 μs and the desired current amplitude previously determined in the warm up session. While it is possible to adjust the current amplitude for each protocol in an effort to match the mean torque output, doing so may induce fatigue. Therefore, to provide a fair comparison of protocols while minimizing the effect of fatigue, the ripple was quantified as a percentage of mean torque. For subject comfort, the current amplitude was increased as a ramp from 0 mA to the desired amplitude over the course of 2 seconds. The current amplitude then remained constant for 10 seconds before decreasing back to 0 mA over the course of 2 seconds. The duration of constant stimulation was chosen as 10 seconds in an effort to reduce potential fatigue; however, the duration was sufficiently long so that the ripple could be measured. To further reduce any effect of fatigue, the order of stimulation protocols was randomized for each individual, and the individuals were allowed to rest for a minimum of 2 minutes between each trial. A simple linear regression was performed with the protocol order as the independent variable and the mean torque output as the dependent variable in an effort to examine whether or not fatigue occurred throughout the trials. Since conventional and asynchronous stimulation utilize different electrode configurations and the protocol order was randomized, the electrode positions were marked so that the positioning could be replicated when donning and doffing the electrodes.

3.2 Results

Isometric knee-joint torque was recorded during five asynchronous stimulation pro-
tocols with stimulation frequencies of 8, 10, 12, 14, and 16 Hz (subsequently described
as A8, A10, A12, A14, and A16) as well as during two conventional stimulation protocols
with stimulation frequencies of 20 and 40 Hz (subsequently described as C20 and C40).
Isometric torque was also acquired during volitional contractions at 100%, 50%, and
25% of each individual's MVC (subsequently described as V100, V50, and V25). The
RMS values of the ripple measured during volitional and NMES-induced contractions
are presented in Table 3-1 and the corresponding box plot is provided in Figure 3-3.
Higher stimulation frequencies resulted in less ripple during asynchronous stimulation
than low stimulation frequencies. The two asynchronous stimulation protocols with
the highest stimulation frequencies (A16 and A14) were found to induce contractions
with mean RMS ripple values of 1.06% and 2.68%, respectively. Meanwhile, the three
asynchronous protocols with the lowest stimulation frequencies (A12, A10, and A8) were
found to induce contractions with mean RMS ripple values of 6.77%, 6.04%, and 8.64%,
respectively.

The mean torque evoked during each stimulation protocol is presented in Table
3-2. Asynchronous stimulation was found to produce stronger contractions on average,
with mean torques of 33.9, 32.1, 27.0, 23.7, and 14.2 N-m for A16, A14, A12, A10,
and A8, respectively. Meanwhile, conventional stimulation produced generally weaker
contractions, with mean torques of 16.8 and 13.4 N-m for C40 and C20, respectively.
To examine if fatigue due to protocol order affected the data, a simple linear regression
was performed with the protocol order as the independent variable and the mean
torque output as the dependent variable. While the linear regression resulted in a linear
curve fit with a downward slope, regression analysis resulted in a P-value of 0.0596.
Thus, there is not enough evidence to conclude that there is a relationship between
the protocol order and the mean torque at a significance level of $\alpha = 0.05$. While the

Table 3-1. RMS ripple expressed as a percentage of mean torque.

	RMS Ripple (%DC)									
Subject	A16	A14	A12	A10	A8	C40	C20	V100	V50	V25
A	2.43	3.68	4.49	3.89	9.61	0.33	4.55	0.82	2.67	1.15
B	0.30	0.95	2.85	6.95	8.29	0.64	1.06	0.94	1.28	0.54
C	0.46	1.72	3.95	3.04	4.01	0.44	1.73	1.12	1.28	0.54
D	1.09	5.62	14.36	7.44	4.86	0.30	3.04	1.79	1.56	0.75
E	1.65	4.18	6.43	7.05	8.42	0.21	1.97	1.53	0.39	0.27
F	0.56	1.51	12.77	6.88	9.30	0.45	1.12	0.78	0.63	0.55
G	0.99	5.09	4.79	7.21	18.07	0.57	4.33	0.50	0.73	0.41
H	2.15	4.98	9.54	13.03	13.08	1.42	5.11	1.22	0.57	0.44
I	1.29	1.45	2.51	1.45	4.82	0.41	4.02	0.98	0.57	0.66
J	0.94	0.59	6.89	4.00	8.28	0.32	1.91	1.11	0.63	0.40
K	0.46	1.94	5.80	7.84	8.90	1.30	1.47	1.44	1.46	0.62
L	0.43	0.45	6.84	3.69	6.01	0.58	1.81	1.17	1.65	0.50
Mean	**1.06**	**2.68**	**6.77**	**6.04**	**8.64**	**0.58**	**2.68**	**1.12**	**1.12**	**0.60**
SD	**0.70**	**1.90**	**3.73**	**3.05**	**3.90**	**0.39**	**1.46**	**0.35**	**0.66**	**0.24**

A16, A14, A12, A10, and A8 refer to asynchronous 16, 14, 12, 10, and 8 Hz stimulation, respectively. C40 and C20 refer to conventional 40 and 20 Hz stimulation, respectively. V100, V50, and V25 refer to volitional contractions at 100%, 50%, and 25% of the maximal voluntary contraction, respectively.

possibility that some fatigue occurred with the order of contractions cannot be excluded, the coefficient of determination was found to be 0.0426, further indicating that the protocol order explained less than 5% of the variation in torque. The linear fit to the evoked torque as a function of the protocol order is shown in Figure 3-4.

3.3 Discussion

The results indicate that both asynchronous 16 Hz stimulation and conventional 40 Hz stimulation can induce contractions which are as ripple-free as volitional contractions in healthy individuals (Figure 3-3 and Table 3-1). However, on average, asynchronous 16 Hz stimulation induced contractions that were more than twice as strong as conventional 40 Hz stimulation, given the same current amplitude (Table 3-2). Asynchronous 16 Hz stimulation with four channels has been previously shown to induce less fatigue than conventional 40 Hz stimulation [64]. Thus, when smooth, strong, fatigue resistant
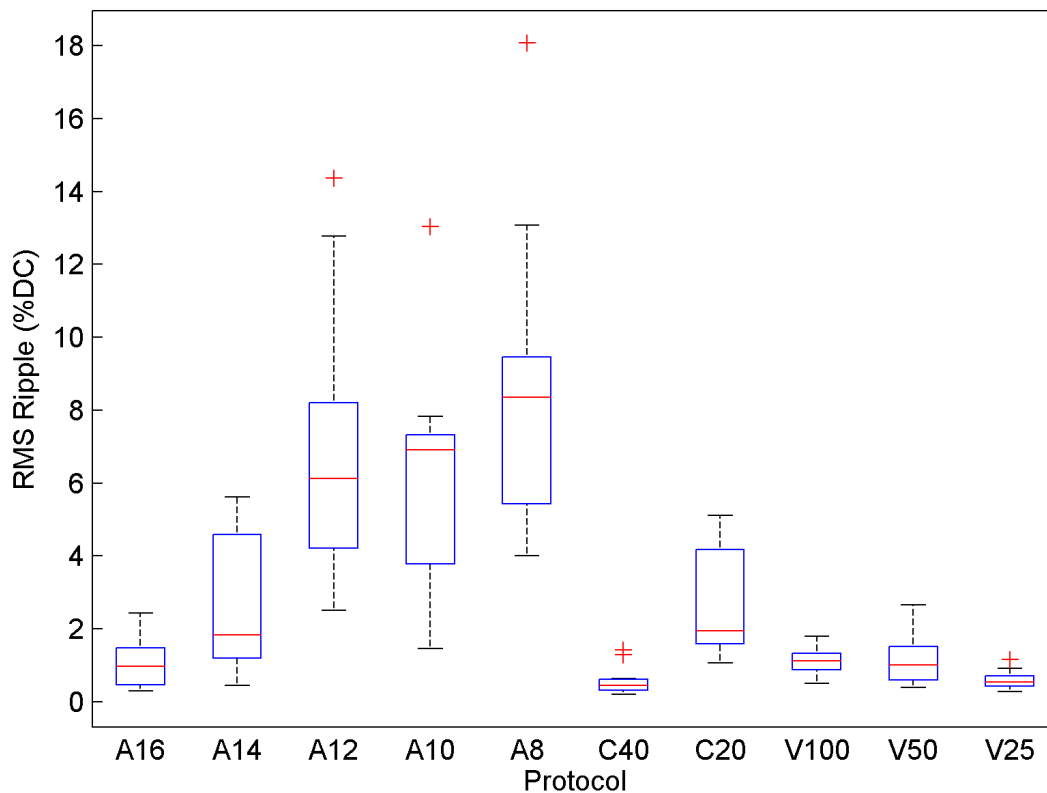
Figure 3-3. RMS ripple box plot.
Box plot of the RMS value of the ripple expressed as a percentage of the mean torque produced. The central marks in the boxes represent the median, the edges of the boxes represent the 25th and 75th percentiles, and the whiskers extend to the most extreme data points not considered to be outliers, as the outliers are plotted separately as plus signs.

contractions are desired, asynchronous 16 Hz stimulation is preferred over conventional 40 Hz stimulation.

Asynchronous 14 Hz stimulation induced contractions with similar ripple to that of conventional 20 Hz stimulation; however, neither protocol was as ripple-free as volitional contractions (see Figure 3-3 and Table 3-1). On average, asynchronous 14 Hz stimulation induced contractions that were more than twice as strong as conventional 20 Hz stimulation, given the same current amplitude (see Table 3-2). While it is expected that asynchronous 14 Hz stimulation would induce less fatigue than conventional 20

Table 3-2. Mean torque (N·m) produced by each stimulation protocol.

	Mean Evoked Torque (N-m)						
Subject	A16	A14	A12	A10	A8	C40	C20
A	24.2	23.8	21.3	20.8	10.4	22.1	15.2
B	33.2	32.6	31.9	18.1	9.9	6.3	6.1
C	19.2	21.1	16.7	17.7	13.4	18.9	19.0
D	27.8	31.4	18.4	24.5	18.9	24.7	11.7
E	32.4	31.4	27.6	23.5	14.1	27.8	16.1
F	20.2	18.3	14.7	11.3	6.5	11.3	8.4
G	28.3	17.6	18.7	10.1	7.5	7.0	4.5
H	25.8	25.1	16.3	12.3	6.9	6.6	5.7
I	38.6	39.5	35.2	37.7	16.4	19.1	22.9
J	48.6	43.7	42.4	38.0	22.5	36.2	20.6
K	48.6	36.6	34.5	26.7	22.6	4.9	17.4
L	60.5	63.8	46.0	43.3	21.8	16.5	12.8
Mean	**33.9**	**32.1**	**27.0**	**23.7**	**14.2**	**16.8**	**13.4**
SD	**12.8**	**13.0**	**10.8**	**11.0**	**6.1**	**9.9**	**6.2**

A16, A14, A12, A10, and A8 refer to asynchronous 16, 14, 12, 10, and 8 Hz stimulation, respectively. C40 and C20 refer to conventional 40 and 20 Hz stimulation, respectively.

Hz stimulation, previous studies have not compared the NMES-induced fatigue of the 2 protocols. Thus, it is not presently clear if asynchronous 14 Hz stimulation provides a significant fatigue benefit over conventional 20 Hz stimulation, in addition to producing stronger contractions.

Asynchronous 10 Hz stimulation was found to induce 40% stronger contractions than conventional 40 Hz stimulation on average, given the same current amplitude (see Table 3-2). This result is in agreement with previous findings, where asynchronous 10 Hz stimulation required 20% less current to reach the same desired torque [63]. Asynchronous 10 Hz stimulation has been shown previously to induce less fatigue than conventional 40 Hz stimulation [51, 63], and thus, asynchronous 10 Hz stimulation would be the preferred FES protocol if it exhibited similar ripple to conventional 40 Hz stimulation. In theory, asynchronous 10 Hz stimulation with four channels is capable of eliciting contractions which are as smooth as conventional 40 Hz stimulation; however, the results indicate that asynchronous 10 Hz stimulation may exhibit significantly more
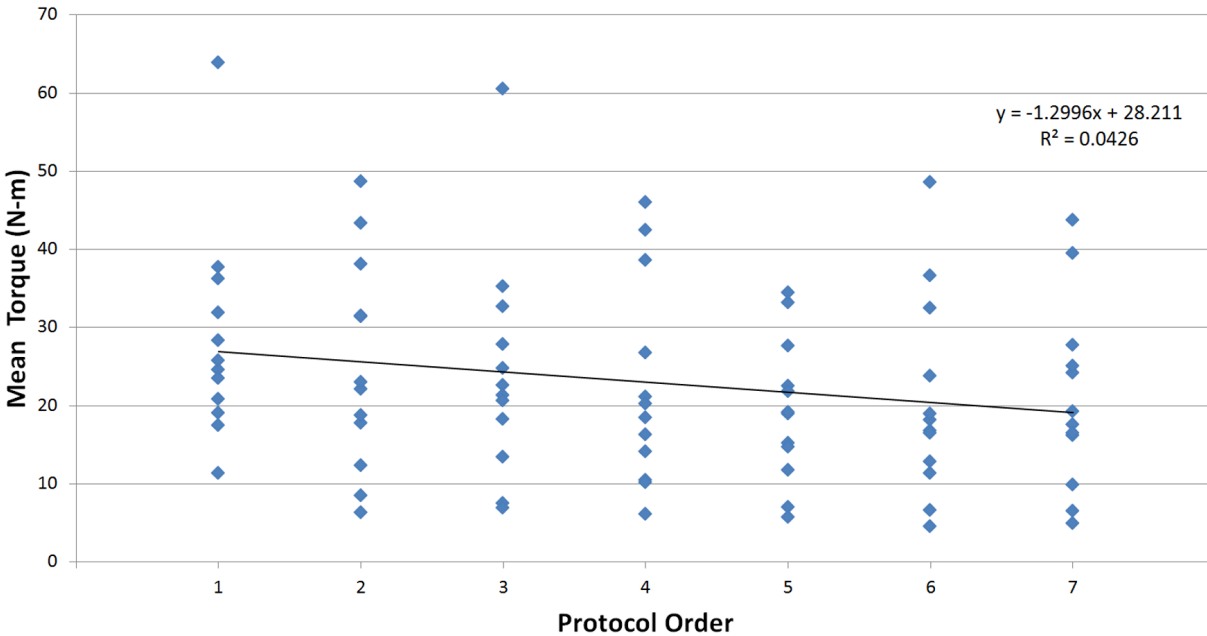
Figure 3-4. Torque versus protocol order scatter plot.
Scatter plot of the mean torque produced as a function of the protocol order with the corresponding linear fit. While the linear regression resulted in a linear curve fit with a downward slope, regression analysis resulted in a P-value of 0.0596. Thus, there is not enough evidence to conclude that there is a relationship between the protocol order and the mean torque at a significance level of $\alpha = 0.05$. Further, the coefficient of determination was found to be 0.0426, indicating that the protocol order explained less than 5% of the variation in torque.

ripple than conventional 40 Hz stimulation (Figure 3-3 and Table 3-1). Further, the three asynchronous stimulation protocols with the lowest stimulation frequencies (8, 10, and 12 Hz) were found to produce significant ripple compared to volitional contractions (Figure 3-3 and Table 3-1). While these three protocols are expected to reduce NMES-induced fatigue, the results suggest that 8, 10, and 12 Hz asynchronous stimulation with 4 channels may not be suitable for FES applications that require contractions which are as smooth as volitional contractions in healthy individuals.

It should be noted that different electrode configurations (i.e., electrode size, shape, placement, and the number of stimulation channels) could alter the amount of ripple during asynchronous stimulation. However, the electrode configuration of this study was selected in an effort to prevent activation overlap which could otherwise limit the

46

effectiveness of asynchronous stimulation as a method to reduce fatigue. Low stim-
ulation frequencies have been shown to reduce fatigue, but this study indicates that
low frequency asynchronous stimulation can lead to increased ripple. Thus, future re-
search should investigate methods to reduce ripple so that low frequency asynchronous
stimulation may produce strong, smooth, and fatigue-resistant contractions.

The extent that force ripple impacts FES control and the smoothness of FES-
induced movement remains an unanswered question. The force ripple was investigated
during volitional contractions of healthy individuals under the assumption that stimulation
protocols resulting in a similar amount of force ripple are sufficient to produce move-
ments similar to that of healthy individuals. However, since the relationship between
isometric force ripple and the smoothness of FES-induced movement is not presently
known, future studies should investigate this relationship as a means to determine
the lowest suitable stimulation frequency to elicit movements similar to that of healthy
individuals. Future efforts should also examine the relationship between stimulation
frequency and NMES-induced fatigue during asynchronous stimulation. Low stimulation
frequencies have been shown to reduce NMES-induced fatigue; however, there may be
a lower bound on the stimulation frequency beyond which there is no discernible change
in NMES-induced fatigue. Thus, the choice of an optimal asynchronous stimulation
frequency that elicits fatigue-resistant movements similar to the volitional movements of
healthy individuals is a topic of interest for future studies on NMES-induced fatigue and
the effect of force ripple on the FES-induced movement.

CHAPTER 4
RISE-BASED TRACKING CONTROL OF A HUMAN LIMB DURING ASYNCHRONOUS NEUROMUSCULAR ELECTRICAL STIMULATION

Both asynchronous stimulation and sequential stimulation can reduce NMES-induced fatigue; however, one limitation of to these methods is that switching between stimulation channels introduces discontinuities due to a differing response to stimulation by each group of recruited motor units. Thus, there is a need to design a controller which considers the switching dynamics and muscle response to stimulation during both asynchronous and sequential stimulation. A continuous closed-loop feedback controller is developed in this chapter to yield semi-global asymptotic tracking of a desired trajectory for a person's knee-shank complex during either asynchronous or sequential stimulation. The result is promising for the implementation of asynchronous and sequential stimulation for closed-loop rehabilitative treatments and in assistive devices as methods to reduce fatigue while tracking a desired trajectory.

4.1 Limb Model

The knee-joint dynamics are modeled as in [68] as

$$M_I + M_e + M_g + M_v + \tau_d = \tau, \tag{4–1}$$

where $M_I : \mathbb{R} \to \mathbb{R}$ denotes the inertial effects of the shank-foot complex about the knee-joint; $M_e : \mathbb{R} \to \mathbb{R}$ denotes the elastic effects due to joint stiffness; $M_g : \mathbb{R} \to \mathbb{R}$ denotes the gravitational effects on the limb; $M_v : \mathbb{R} \to \mathbb{R}$ denotes the viscous effects due to damping in the musculotendon complex; $\tau_d \in \mathbb{R}$ denotes an unknown time-varying disturbance that is assumed to be sufficiently smooth in the sense that $\tau_d, \dot{\tau}_d, \ddot{\tau}_d \in \mathcal{L}_\infty$; and $\tau \in \mathbb{R}$ denotes the torque produced at the knee-joint due to stimulation. The inertial and gravitational effects in (4–1) are modeled as

$$M_I \triangleq J\ddot{q}, \quad M_g \triangleq mgl \sin(q), \tag{4–2}$$

where J, m, g, $l \in \mathbb{R}$ are positive, unknown constants, and q, $\dot{q}$, $\ddot{q} \in \mathbb{R}$ denote the angular position (depicted in Figure 4-1), velocity, and acceleration of the shank about the knee-joint, respectively. The terms J, m, and l denote the unknown inertia of the combined shank and foot, the unknown combined mass of the shank and foot, and the unknown distance between the knee-joint and the lumped center of mass of the shank and foot, respectively, while g denotes the gravitational acceleration constant. The elastic and viscous effects are modeled as in [68] as

$$M_e \triangleq k_{e1}(\exp(-k_{e2}q))(q - k_{e3}), \tag{4--3}$$

where k_{e1}, k_{e2}, $k_{e3} \in \mathbb{R}$ are unknown constants and

$$M_v \triangleq -B_1 \tanh(-B_2\dot{q}) + B_3\dot{q}, \tag{4--4}$$

where B_1, B_2, $B_3 \in \mathbb{R}$ are unknown, positive constants.

Asynchronous stimulation involves switching between $N \in \mathbb{N}$ stimulation channels. Since each channel activates different sets of motor units, the corresponding dynamics are different depending on which stimulation channel is active. Let $\mathbb{S} \subset \mathbb{N}$ be the finite index set for all stimulation channels, defined as

$$\mathbb{S} \triangleq \{1, 2, 3, \cdots, N\}.$$

Then, the torque produced by stimulation of the ith subsystem is related to the musculo-tendon force as

$$\tau_i \triangleq \varsigma_i F_{T,i}, \ i \in \mathbb{S}, \tag{4--5}$$

where $\varsigma_i \in \mathbb{R}$ denotes an unknown, positive moment arm that changes with extension and flexion of the leg. The musculotendon force $F_{T,i} \in \mathbb{R}$ is defined as

$$F_{T,i} \triangleq F_i \cos(a_i), \ i \in \mathbb{S}, \tag{4--6}$$
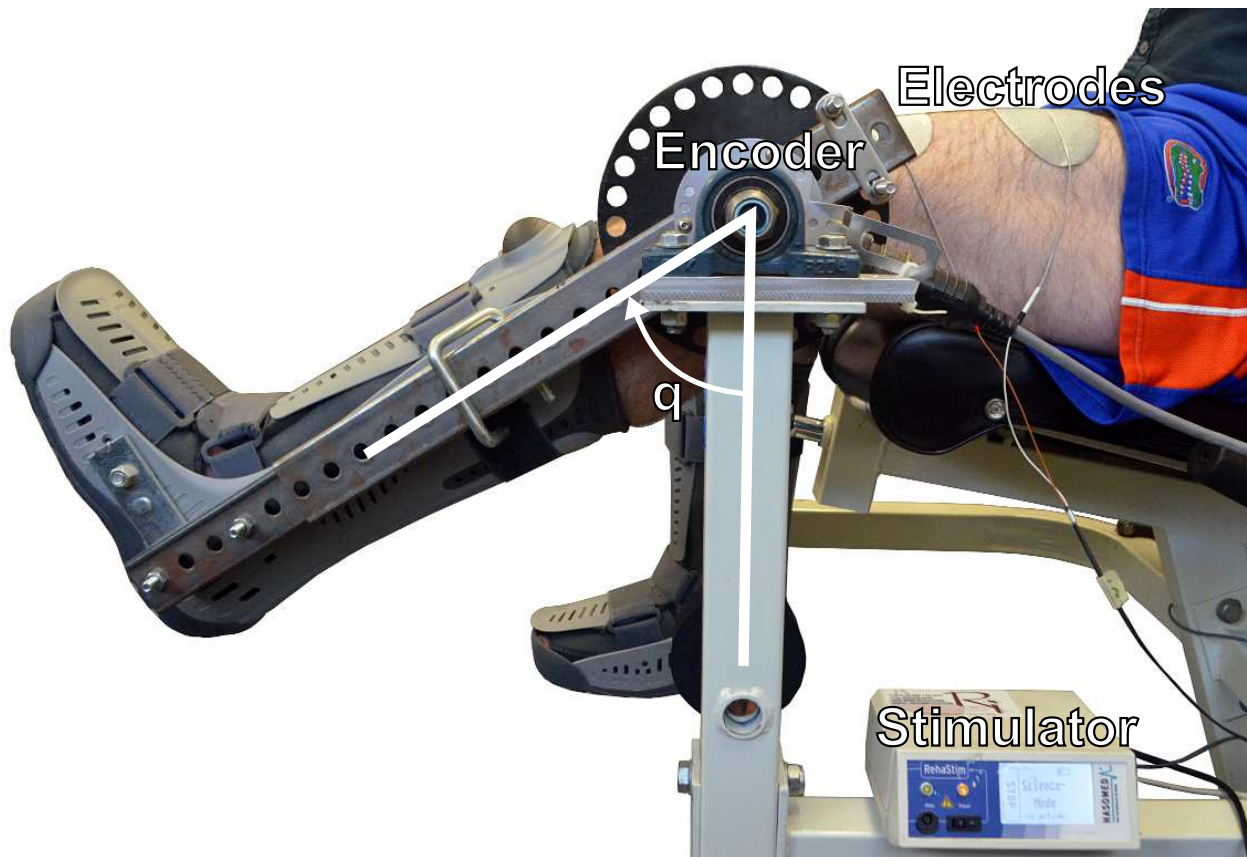
Figure 4-1. Modified leg extension machine for feedback control.
A modified leg extension machine was fitted with optical encoders to measure the knee joint angle q and provide feedback to the developed control algorithm running on a personal computer. Participants were seated at the leg extension machine with the thighs parallel to the ground and hips flexed approximately 75 degrees. The desired stimulation parameters were sent in real time from a personal computer to the stimulator via USB. Photo courtesy of Ryan Downey.

where $a_i \in \mathbb{R}$ denotes the pennation angle between the tendon and the muscle, which changes with extension and flexion of the leg, and $F_i \in \mathbb{R}$ denotes the force produced by the recruited motor units in the ith subsystem. The relationship between muscle force and applied voltage is defined as

$$F_i \triangleq \varphi_i \eta_i V_i, \; i \in \mathbb{S}, \tag{4–7}$$

where $V_i \in \mathbb{R}$ represents the voltage applied to the ith subsystem by electrical stimulation; $\eta_i \in \mathbb{R}$ is an unknown function of q and $\dot{q}$ (i.e., η_i represents unknown muscle force-length and force-velocity relationships); and $\varphi_i \in \mathbb{R}$ is an unknown time-varying function that represents fatigue.

Typically, during asynchronous stimulation, only one channel is activated at a given time. However, if only one stimulation channel is activated at a given time, immediately switching the applied voltage from one subsystem to another subsystem would introduce discontinuities in the torque produced at the knee. Therefore, switching in the subsequent development is designed to include an arbitrarily short period of time during which both subsystems are simultaneously activated (each receiving a percentage of the input voltage). During the transition period, the voltage input transitions from being applied solely to the original subsystem to being applied to the new subsystem designated by the switching signal. Without loss of generality, the knee-joint dynamics during stimulation of up to two subsystems at a time can be modeled as

$$M_I + M_e + M_g + M_v + \tau_d = \tau_i + \tau_j, \tag{4–8}$$

where $\tau_i, \tau_j \in \mathbb{R}$ denote the torque produced by stimulation of the ith and j^{th} subsystems, respectively, for $i, j \in \mathbb{S}, \; i \neq j$. The inertial, gravitational, elastic, and viscous components are common to all subsystems since all subsystems act on the same knee joint, and the unknown, bounded disturbance torque can also be modeled as being common to all subsystems.

Remark 4.1. Equation ([4–8](#)) implicitly assumes that there is no activation overlap between any of the stimulation channels (i.e., a specific muscle fiber generates tension in response to only one channel), although there is likely to be some overlap. Activation overlap would cause some motor units to be activated more frequently than desired, leading to increased muscle fatigue. Therefore, overlap should be avoided in practice since the motivation for asynchronous stimulation is to reduce fatigue. However, activation overlap would not have a negative effect from a control perspective. For example, 100% activation overlap for all of the channels would imply that there is effectively only one stimulation channel, and thus, the tracking control problem would simplify to single-channel conventional stimulation.

4.2 Control Development

The control objective is to enable the knee joint to track a specified desired angular trajectory. To quantify this objective, the position tracking error is defined as

$$e_1 \triangleq q_d - q, \tag{4–9}$$

where $q_d \in \mathbb{R}$ denotes the desired angular trajectory for the knee joint, designed such that $q_d, q_d^k \in \mathcal{L}_\infty$, where q_d^k denotes the kth derivative of q_d for $k = 1, 2, 3, 4$. To facilitate the subsequent development, auxiliary tracking errors $e_2, r \in \mathbb{R}$ are defined as

$$e_2 \triangleq \dot{e}_1 + \alpha_1 e_1, \tag{4–10}$$

$$r \triangleq \dot{e}_2 + \alpha_2 e_2, \tag{4–11}$$

where $\alpha_1, \alpha_2 \in \mathbb{R}$ are selectable positive constants. The filtered tracking error r facilitates the stability analysis but is not used in the control development due to the dependence on the angular acceleration about the knee, which is assumed to be unmeasurable.

After multiplying (4–11) by J, and utilizing (4–2) and (4–8)-(4–10), the open-loop dynamics during stimulation of up to two subsystems can be written as

$$Jr = W - \tau_i - \tau_j + \tau_d, \ i, j \in \mathbb{S}, \ i \neq j, \tag{4–12}$$

where $W \in \mathbb{R}$ denotes an auxiliary term defined as

$$W \triangleq J(\ddot{q}_d + \alpha_1 \dot{e}_1 + \alpha_2 e_2) + M_e + M_g + M_v.$$

After utilizing (4–5)-(4–7), the open-loop dynamics in (4–12) can be expressed as

$$Jr = W - V_i \Omega_i - V_j \Omega_j + \tau_d, \ i, j \in \mathbb{S}, \ i \neq j, \tag{4–13}$$

where $V_i \in \mathbb{R}$ denotes the voltage applied by the ith stimulation channel, and $\Omega_i \in \mathbb{R}$ denotes an unknown positive auxiliary function of the leg angle and velocity that varies with time and relates the voltage applied by the ith channel to the torque produced by the activated motor neurons, defined based on [68] as

$$\Omega_i \triangleq \varsigma_i \varphi_i \eta_i \cos(a_i), \ i \in \mathbb{S}. \tag{4–14}$$

Assumption 4.1. The moment arm ς_i is assumed to be a non-zero, positive, and bounded function [75] where the first two partial derivatives of ς_i with respect to q exist and are bounded for a bounded argument. Likewise, the function η_i is assumed to be a non-zero, positive, and bounded function [76] provided the muscle is not fully stretched or contracting concentrically at its maximum shortening velocity [77], where the first two partial derivatives of η_i with respect to q and $\dot{q}$ exist and are bounded for a bounded argument. The unknown fatigue function φ_i is assumed to be a non-zero, positive, and bounded function of time with bounded first and second time derivatives. Thus, from (4–14), the first two partial derivatives of Ω_i with respect to q and $\dot{q}$ are assumed to exist and be bounded for a bounded argument; the first two partial derivatives of Ω_i with respect to time (via the time derivatives of φ_i) are assumed to exist and be

bounded; and Ω_i is assumed to be a non-zero, positive, and bounded function such that $\Omega_i > \varepsilon > 0, \ \forall i \in \mathbb{S}$, where $\varepsilon \in \mathbb{R}$ is a known positive constant.

Let $\sigma : [0, \infty) \to \mathbb{S}$ denote a piecewise constant signal that selects a stimulation channel from $\mathbb{S}$ to be activated at time $t \in [0, \infty)$. The instants when the value of σ changes are called the switching times, t_k. Immediately following each switching time, there is a transition period $\triangle t$ during which the input voltage is transitioned from one channel to another.

Property 1. The designed switching signal σ has a finite number of discontinuities on any bounded time interval. Any two consecutive switching times, t_k and t_{k+1} satisfy $t_k + \Delta t < t_{k+1} \ \forall k \in \mathbb{N} \cup \{0\}$, and the switching signal σ remains constant for $t \in [t_k, \ t_{k+1})$.

Let $V \in \mathbb{R}$ denote the voltage input to the system such that $V \triangleq V_i + V_j$, where

$$V_i \triangleq \chi V, \quad V_j \triangleq (1 - \chi) V, \tag{4–15}$$

where $\chi \in \mathbb{R}$ is an auxiliary signal designed such that $0 \leq \chi \leq 1$ so that the transition period from one stimulation channel to another is continuous. Figure 4-2 illustrates a particular choice of χ that facilitates the transition between channels based on the switching signal σ, where χ is selected as

$$\chi \triangleq \begin{cases} 1 & t \in [t_0, t_1) \\[2mm] \frac{1 + \cos(\omega(t - t_k))}{2} & t \in \bigcup_{k \in \mathbb{N}_{\text{odd}}} [t_k, t_k + \Delta t) \\[2mm] 0 & t \in \bigcup_{k \in \mathbb{N}_{\text{odd}}} [t_k + \Delta t, t_{k+1}) \\[2mm] \frac{1 - \cos(\omega(t - t_k))}{2} & t \in \bigcup_{k \in \mathbb{N}_{\text{even}}} [t_k, t_k + \Delta t) \\[2mm] 1 & t \in \bigcup_{k \in \mathbb{N}_{\text{even}}} [t_k + \Delta t, t_{k+1}) \end{cases} \tag{4–16}$$

where $\mathbb{N}_{\text{even}}$ and $\mathbb{N}_{\text{odd}}$ are used to denote the even and odd natural numbers, respectively. Based on the design in (4–16), χ and its first time derivative are bounded and
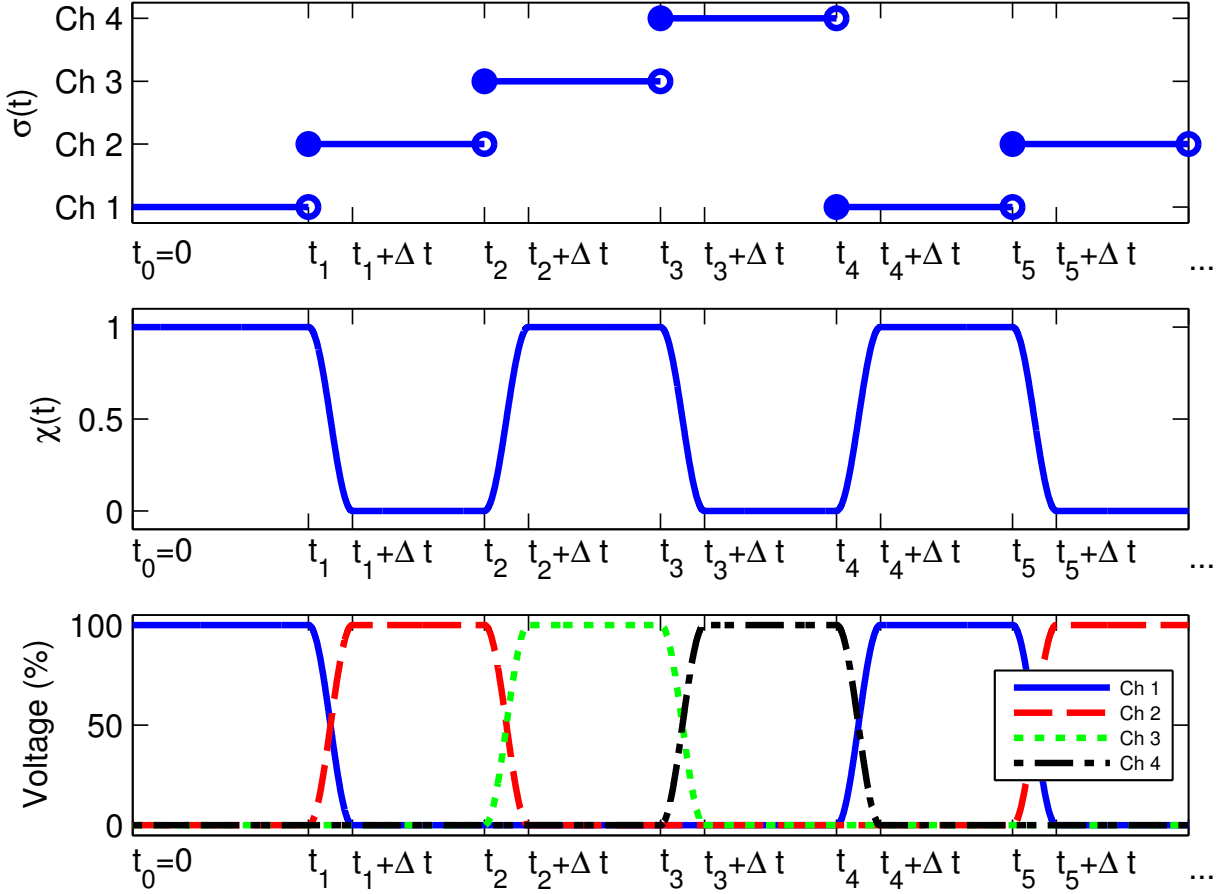
Figure 4-2. Example switching signal.
Depicted is an example piecewise constant switching signal σ that selects a desired stimulation channel to be active. Combining the switching signal with the corresponding signal χ results in a smooth transition of the control voltage between stimulation channels as seen in the bottommost subplot.

continuous, and the second time derivative of χ is bounded. The transition period in (4–16) is defined as $\Delta t \triangleq \frac{\pi}{\omega}$ and can be made arbitrarily short through the choice of ω.

After substituting (4–15) into (4–13), the open-loop error dynamics can be expressed as

$$Jr = W - \bar{\Omega}V + \tau_d, \tag{4–17}$$

where

$$\bar{\Omega} \triangleq \chi\Omega_i + (1 - \chi)\Omega_j, \; i, j \in \mathbb{S}, \; i \neq j. \tag{4–18}$$

From (4–16), (4–18), and Assumption 4.1, $\bar{\Omega}$ is non-zero, positive, and bounded; the first two partial derivatives of $\bar{\Omega}$ with respect to q and $\dot{q}$ are bounded for a bounded argument; and the first two partial derivatives of $\bar{\Omega}$ with respect to time (via the time derivatives of φ_i and χ) are bounded. Furthermore, $\bar{\Omega} > \varepsilon > 0$, and thus, $\bar{\Omega}$ is invertible.

After multiplying (4–17) by $\bar{\Omega}^{-1}$, the open-loop error dynamics can be expressed as

$$J_\Omega r = W_\Omega - V + \tau_{d\Omega}, \tag{4–19}$$

where

$$J_\Omega \triangleq \bar{\Omega}^{-1} J, \ W_\Omega \triangleq \bar{\Omega}^{-1} W, \ \tau_{d\Omega} \triangleq \bar{\Omega}^{-1} \tau_d.$$

To facilitate the subsequent stability analysis, the time derivative of (4–19) is expressed as

$$J_\Omega \dot{r} = -\frac{1}{2} \dot{J}_\Omega r + \tilde{N} + N_d - e_2 - \dot{V}, \tag{4–20}$$

where $\tilde{N}, N_d \in \mathbb{R}$ denote the following auxiliary[1] terms

$$\tilde{N} \triangleq N - N_d,$$

$$N \triangleq \dot{W}_\Omega + e_2 - \frac{1}{2} \dot{J}_\Omega r + \dot{\tau}_{d\Omega},$$

$$N_d \triangleq \frac{1}{\bar{\Omega}_d} N_{d1} - \frac{\dot{\bar{\Omega}}_d}{\left(\bar{\Omega}_d\right)^2} N_{d2},$$

$$N_{d1} \triangleq J \dddot{q}_d + \dot{M}_e(q_d) + \dot{M}_g(q_d) + \dot{M}_v(\dot{q}_d) + \dot{\tau}_d,$$

$$N_{d2} \triangleq J \ddot{q}_d + M_e(q_d) + M_g(q_d) + M_v(\dot{q}_d) + \tau_d.$$

$$\bar{\Omega}_d \triangleq \bar{\Omega}(q_d, \dot{q}_d, t)$$

---

[1] The terms $\tilde{N}$ and N_d are not available for use in the controller and are introduced only to facilitate the stability analysis. These terms are not used in the controller because they depend on the dynamics that contain parametric uncertainty (e.g., J, m, l, B_1, k_{e1}, η, τ_d, and $\dot{\tau}_d$ are uncertain). Moreover, $\tilde{N}$ contains r, which depends on angular acceleration measurements. Motivation to exclude r from the controller is that acceleration measurements contain high frequency measurement/numerical artifacts that can inject high frequency content in the controller.

Motivation for expressing the open-loop error system as in (4–20) is to separate the model into groups that are bounded by state-dependent bounds or by constants. Specifically, by applying the Mean Value Theorem [78, Lemma 5], $\tilde{N}$ can be upper-bounded by state-dependent terms as

$$\left| \tilde{N} \right| \leq \rho(\|z\|) \, \|z\| , \tag{4–21}$$

where $\|\cdot\|$ denotes the standard 2-norm, $z \in \mathbb{R}^3$ is defined as

$$z \triangleq [e_1, \ e_2, \ r]^T , \tag{4–22}$$

and $\rho : \mathbb{R} \to \mathbb{R}$ is a positive, strictly increasing function. The definition of the desired trajectory can be used to prove the upper bounds for N_d as

$$|N_d| \leq \zeta_{N_d}, \quad \left| \dot{N}_d \right| \leq \zeta_{\dot{N}_d}, \tag{4–23}$$

where ζ_{N_d}, $\zeta_{\dot{N}_d} \in \mathbb{R}$ are known, positive constants.

Remark 4.2. The bounds on N_d and $\dot{N}_d$ depend on the signal χ since $\dot{\chi}$ and $\ddot{\chi}$ appear through $\dot{\Omega}$ and $\ddot{\Omega}$. A sufficient condition for stability of the closed-loop error system will later be shown to depend on the bounds of N_d and $\dot{N}_d$. Therefore, a sufficient condition for stability of the closed-loop error system depends on the transition period Δt. However, the transition period can be made arbitrarily small by selecting control gains based on the desired length of the transition period.

Based on the open-loop error system in (4–20) and the subsequent stability analysis, a RISE-based (Robust Integral of the Sign of the Error) controller [79] is designed as

$$V \triangleq (k_s + 1) \, (e_2 - e_2(0)) + \nu, \tag{4–24}$$

where ν is the generalized Filippov solution to

$$\dot{\nu} = (k_s + 1)\alpha_2 e_2 + \beta \, \mathrm{sgn}(e_2), \ \nu(0) = \nu_0, \tag{4–25}$$

where k_s, $\beta \in \mathbb{R}$ are positive, selectable control gains, ν_0 is a user-defined initial voltage, and $\mathrm{sgn}(\cdot)$ denotes the signum function.

Remark 4.3. In the subsequent experiments, the pulsewidth will be adjusted according to the control law in (4–24) and (4–25) rather than the voltage. During NMES, there are three stimulation parameters that affect the resulting torque: pulse amplitude (voltage amplitude or equivalently current amplitude), pulsewidth, and pulse frequency. Typically two of these three parameters are fixed while the final parameter is varied to evoke the desired muscle response. The uncertain model in (4–19) relating the stimulus input V to the evoked torque is equivalent regardless of which parameter is varied. Therefore, the stimulus input was referred to as a voltage in the control development and modeling sections to be consistent with the RISE-based controller that was developed for conventional stimulation in [68]. Meanwhile, the pulsewidth was varied during experiments in the present work since the utilized stimulator has a greater resolution on pulsewidth (20-500 μs in steps of 1 μs) than current amplitude (0 to 126 mA in steps of 2 mA).

After substituting (4–24) into (4–20) and using the definition of r in (4–11), the closed-loop dynamics can be written as

$$J_\Omega \dot{r} = -\frac{1}{2}\dot{J}_\Omega r + \tilde{N} + N_d - e_2$$
$$- (k_s + 1)r - \beta\,\mathrm{sgn}(e_2). \tag{4–26}$$

The closed-loop system in (4–26) yields semi-global asymptotic tracking of a desired knee-joint trajectory as described in Theorem 4.1 and its associated stability proof in Section 4.3.

4.3 Stability Analysis

Theorem 4.1. *The controller designed in (4–24) yields semi-global asymptotic tracking in the sense that*

$$|e_1| \to 0 \quad as \, t \to \infty$$

under any switching signal satisfying Property 1, provided that the control gain k_s, introduced in (4–24) and (4–25), is selected sufficiently large according to the initial conditions, and the control gains α_1, α_2, and β introduced in (4–10), (4–11), and (4–25) are selected according to the following sufficient conditions:

$$\alpha_1 > \frac{1}{2}, \quad \alpha_2 > 1, \tag{4–27}$$

$$\beta > \left(\zeta_{N_d} + \frac{1}{\alpha_2} \zeta_{\dot{N}_d} \right), \tag{4–28}$$

where ζ_{N_d}, and $\zeta_{\dot{N}_d}$ were introduced in (4–23).

Proof. Let $y \in D \subset \mathbb{R}^{3+1}$, defined as

$$y \triangleq \left[z^T, \, \sqrt{P} \right]^T, \tag{4–29}$$

where z was defined in (4–22) and $P \in \mathbb{R}$ is the Filippov solution to

$$\dot{P} = -r \left[N_d - \beta \operatorname{sgn}(e_2) \right], \tag{4–30}$$

$$P(e_2(0), \, 0) = -e_2(0) N_d(0) + |e_2(0)| \, \beta.$$

Provided the gain condition for β in (4–28) is satisfied, P is guaranteed to satisfy $P \geq 0$ [79, Lemma 1].

Let $V_L : \, D \to \mathbb{R}$ be a continuously differentiable function, defined as

$$V_L \triangleq e_1^2 + \frac{1}{2} e_2^2 + \frac{1}{2} J_\Omega r^2 + P, \tag{4–31}$$

which satisfies the following inequalities:

$$U_1 \leq V_L \leq U_2, \tag{4–32}$$

where U_1, $U_2 \in \mathbb{R}$ are continuous, positive definite functions defined as $U_1 \triangleq \lambda_1 \|y\|^2$, $U_2 \triangleq \lambda_2 \|y\|^2$, where y was defined in (4–29) and λ_1, $\lambda_2 \in \mathbb{R}$ are positive constants.

The time derivative of (4–31) exists almost everywhere (a.e.)[2] , i.e., for almost all $t \in [0, \infty)$, and $\dot{V}_L \stackrel{a.e.}{\in} \dot{\tilde{V}}_L$ where

$$\dot{\tilde{V}}_L \triangleq \bigcap_{\xi \in \partial V_L} \xi^T K \left[\dot{e}_1, \ \dot{e}_2, \ \dot{r}, \ \frac{1}{2} P^{-\frac{1}{2}} \dot{P}, \ 1 \right]^T, \tag{4–33}$$

where $K[\cdot]$ is defined in [80], and ∂V_L is the generalized gradient of V_L. Since V_L is continuously differentiable with respect to y, (4–33) can be rewritten as

$$\dot{\tilde{V}}_L \subset \nabla V_L^T K \left[\dot{e}_1, \ \dot{e}_2, \ \dot{r}, \ \frac{1}{2} P^{-\frac{1}{2}} \dot{P}, \ 1 \right]^T, \tag{4–34}$$

where

$$\nabla V_L \triangleq \left[2e_1, \ e_2, \ rJ_\Omega, \ 2P^{\frac{1}{2}}, \ \frac{1}{2} \dot{J}_\Omega r^2 \right]^T.$$

Substituting (4–9)-(4–11) and (4–26) into (4–34) yields

$$\begin{aligned}
\dot{\tilde{V}}_L \subset {} & 2e_1(e_2 - \alpha_1 e_1) + e_2(r - \alpha_2 e_2) + \frac{1}{2} r \dot{J}_\Omega r \\
& + r \left(-\frac{1}{2} \dot{J}_\Omega r + N_d - e_2 \right) + K \left[\dot{P} \right] \\
& + r \left(\tilde{N} - (k_s + 1)r - \beta K \left[\mathrm{sgn} \right] (e_2) \right),
\end{aligned} \tag{4–35}$$

where $K\left[\mathrm{sgn}\right](e_2) = 1$ if $e_2 > 0$, $[-1, \ 1]$ if $e_2 = 0$, and -1 if $e_2 < 0$. After substituting $\dot{P}$ from (4–30) and canceling common terms, (4–35) can be rewritten and upper-bounded

---

[2] The time derivative of the Lyapunov function has a discontinuous right-hand side (due to $\dot{V}$ and $\dot{P}$), causing the time derivative of the Lyapunov function to exist almost everywhere and motivating the nonsmooth analysis.

as

$$\dot{V}_L \overset{a.e.}{\leq} -2\alpha_1 e_1^2 - \alpha_2 e_2^2 + 2\,|e_1|\,|e_2|$$
$$+ r\tilde{N} - (k_s + 1)r^2, \tag{4–36}$$

where the set in (4–35) reduces to the scalar inequality in (4–36) since the right hand side is continuous almost everywhere, i.e., the right hand side is continuous except for the Lebesgue negligible set of times when

$$r\beta K\,[\mathrm{sgn}]\,(e_2) - r\beta K\,[\mathrm{sgn}]\,(e_2) \neq \{0\}.$$

After utilizing Young's Inequality and (4–21), the inequality in (4–36) can be further upper-bounded as

$$\dot{V}_L \overset{a.e.}{\leq} -(2\alpha_1 - 1)e_1^2 - (\alpha_2 - 1)e_2^2$$
$$- (k_s + 1)r^2 + \rho(\|z\|)\,\|z\|\,|r|. \tag{4–37}$$

After completing the square, (4–37) can be expressed as

$$\dot{V}_L \overset{a.e.}{\leq} -\left(\lambda - \frac{\rho^2(\|z\|)}{4k_s}\right)\|z\|^2$$
$$\overset{a.e.}{\leq} -U_3 \triangleq -c\,\|z\|^2,\ \forall y \in D, \tag{4–38}$$

where $\lambda \triangleq \min\{2\alpha_1 - 1,\ \alpha_2 - 1,\ 1\}$, $c \in \mathbb{R}$ is a positive constant, and D is defined as

$$D \triangleq \left\{y \in \mathbb{R}^{3+1} \mid \rho(\|y\|) < \sqrt{4\lambda k_s}\right\},$$

where ρ was introduced in (4–21). From the inequalities in (4–32) and (4–38), $V_L \in \mathcal{L}_\infty$, and hence, $e_1,\ e_2,\ r \in \mathcal{L}_\infty$. The remaining signals in the closed-loop dynamics can be proven to be bounded. Let $D_z \subset D$ be defined as

$$D_z \triangleq \left\{y \in D \mid \rho\left(\sqrt{\frac{\lambda_2}{\lambda_1}}\,\|y\|\right) < \sqrt{4\lambda k_s}\right\}. \tag{4–39}$$

From (4–38), [81, Corollary 1] can be invoked to show that $c \|z\|^2 \rightarrow 0$ as $t \rightarrow \infty, \ \forall y(0) \in D_z$. Based on the definition of z, $e_1 \rightarrow 0$ as $t \rightarrow \infty, \ \forall y(0) \in D_z$. Note that the region of attraction in (4–39) can be expanded arbitrarily by increasing k_s. Provided that the gain conditions in (4–27) and (4–28) are satisfied, the result of the stability analysis is independent of the designed switching signals σ satisfying Property 1, so that the asymptotic tracking result is satisfied where the only restriction on the switching signal is that there be an arbitrarily short transition period during which two stimulation channels are simultaneously activated. $\quad\square$

4.4 Experiments

Asynchronous and conventional stimulation were examined during dynamic contractions to better understand the NMES-induced fatigue characteristics of the stimulation protocols. For both asynchronous and conventional stimulation, the control algorithm in (4–24) and (4–25) was used to vary the pulsewidth in real time while the current amplitude and stimulation frequency remained constant.

4.4.1 Subjects

Four able-bodied individuals (male, aged 20 to 27) participated in the study. Prior to participation, written informed consent was obtained from all participants, as approved by the institutional review board at the University of Florida.

4.4.2 Apparatus

All testing was performed using an apparatus that consisted of the following:

1. A current-controlled 8-channel stimulator (RehaStim, Hasomed GmbH, operating in ScienceMode)

2. A data acquisition device (Quanser Q8-USB)

3. A personal computer running Matlab/Simulink

4. A leg extension machine (shown previously in Figure 4-1) that was modified to include sensors as well as boots to securely fasten the shank and foot

5. Optical encoders to measure the leg angle (BEI Technologies)

6. Surface electrodes (Axelgaard Manufacturing Co.)[3]

4.4.3 Stimulation Protocols

Two stimulation protocols were examined: 16 Hz asynchronous stimulation (A16) with four channels and 64 Hz conventional stimulation (C64) with a single channel. These two protocols were selected because A16 has a composite stimulation frequency equivalent to C64. Conventional stimulation consisted of a single stimulation channel with a pair of 3" by 5" Valutrode® surface electrodes placed distally and proximally over the quadriceps femoris muscle group, while asynchronous stimulation consisted of four channels of stimulation utilizing four electrodes placed distally (1.5" by 3.5" Valutrode®) and two electrodes placed proximally (2" by 3.5" Valutrode®). For asynchronous stimulation, the electrical pulses were interleaved across the stimulation channels. In other words, asynchronous stimulation of 16 Hz with four channels resulted in a composite stimulation frequency of 64 Hz. The electrode configurations utilized for conventional and asynchronous stimulation are depicted in Figure 4-3, and the method of interleaving the pulses across the stimulation channels was as previously depicted for asynchronous stimulation in Figure 1-1.

4.4.4 Precautions

To prevent any layover effect of fatigue, each leg received only one stimulation protocol per day. On the first day of experiments, the two stimulation protocols (A16 and C64) were randomly divided between the individual's left and right legs. While a minimum of 24 hours of rest was required before the individual completed the remaining protocol for each leg, additional rest was allowed if the individual reported symptoms of muscle fatigue.

---

[3] Surface electrodes for the study were provided compliments of Axelgaard Manufacturing Co., Ltd.
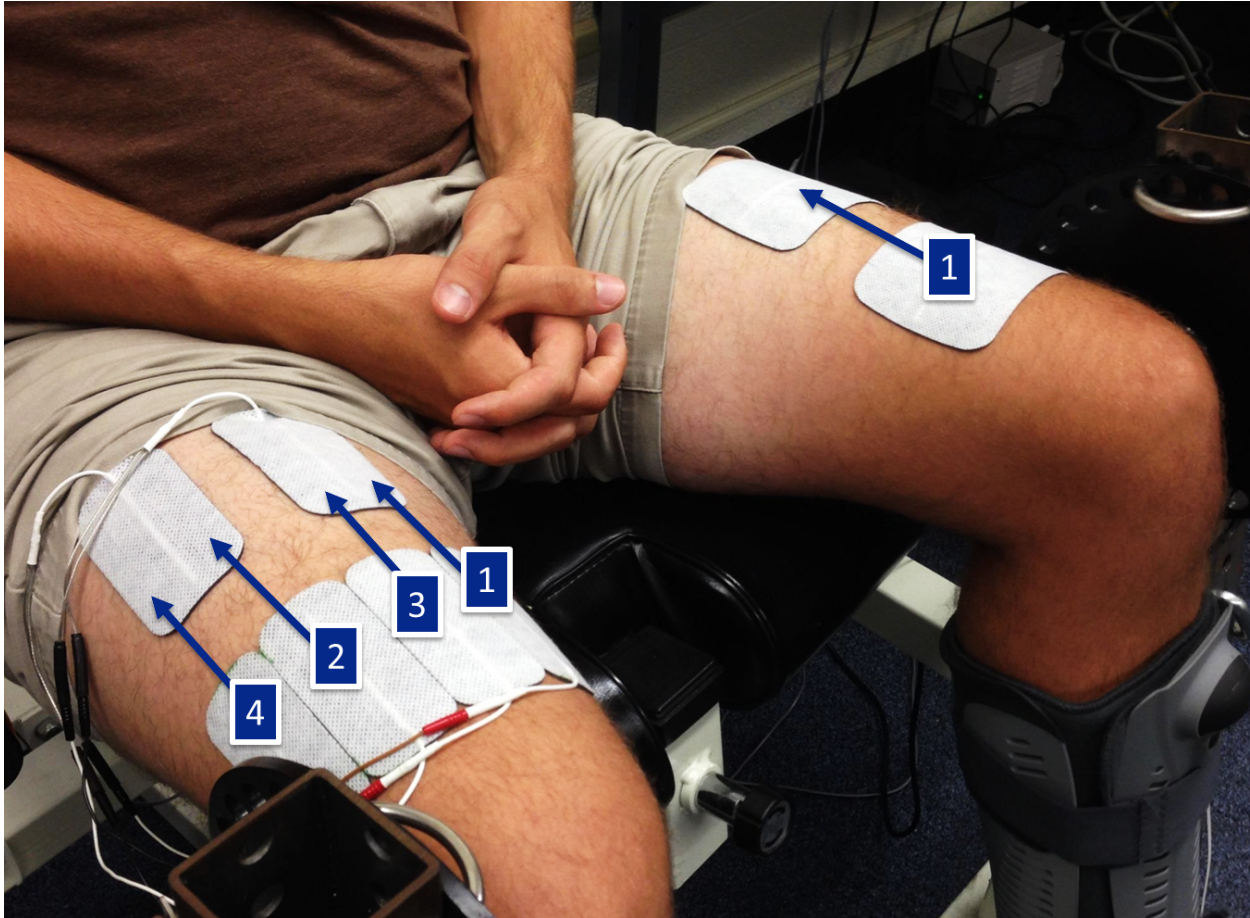
Figure 4-3. Asynchronous and conventional electrode configurations.
Electrode configurations utilized for conventional and asynchronous stimulation. Pictured above is single-channel conventional stimulation on the individual's left leg and four-channel asynchronous stimulation on the individual's right leg. Conventional stimulation consists of one stimulation channel with one electrode placed proximally and one electrode placed distally. Asynchronous stimulation consists of four stimulation channels with two electrodes placed proximally and four electrodes placed distally. Stimulation channels 1 and 3 share the most medial and proximal electrode, while stimulation channels 2 and 4 share the most lateral and proximal electrode. Photo courtesy of Ryan Downey.

4.4.5 Pretrial Tests

The control gains[4] were adjusted in pretrial tests to achieve trajectory tracking where the desired angular trajectory[5] of the knee joint was selected as a sinusoid ranging from 5 to 50 degrees with a period of 2 seconds. The root mean square (RMS) position tracking error was calculated in real time with a moving window of 2 seconds to assist the gain tuning process. After determining appropriate control gains in the pretrial tests, fatigue trials were subsequently conducted on the same day. Since there is a finite pulsewidth resolution for the stimulator (steps of 1 μs), the current amplitude must be selected small enough so that there is a sufficient range of pulsewidth values corresponding to the desired range of motion. However, the current amplitude must also be selected large enough so that the pulsewidth does not saturate. Furthermore, the muscle response to stimulation varies from person to person and asynchronous stimulation has been commonly reported to require less current amplitude to reach the same value of torque as conventional stimulation [63, 64, 74]. Therefore, the current amplitude was selected for each leg/protocol during the pretrial tests so that the resulting pulsewidth (calculated by the control algorithm) had sufficient range to elicit controlled limb movement without saturating.

4.4.6 Fatigue Trials

Fatigue trials were conducted where the pulsewidth was adjusted according to the developed feedback control algorithm in (4–24) and (4–25) to compare each stimulation protocol in terms of its ability to maintain trajectory tracking. The baseline RMS tracking

---

[4] To ensure a fair comparison, efforts were made to utilize the same control gains for asynchronous and conventional stimulation. While this is not always possible due to general variability in the muscle response to stimulation, the control gains (other than the general scaling factor k_s) were the same for both asynchronous and conventional stimulation in 5 out of the 8 legs tested.

[5] The desired trajectory was based on the comfortable range of motion.

error was calculated when the tracking error had reached steady state.[6] The successful run time (SRT) of each fatigue trial was then calculated as the elapsed time from the onset of steady state tracking to the time that the RMS tracking error increased by 3 degrees above the baseline measurement.

4.4.7 Statistical Analysis

The difference between the SRTs for asynchronous and conventional stimulation was calculated (i.e., paired data). A sign test was performed at a significance level of $\alpha = 0.05$ to test for statistically significant differences between the two protocols. Similarly, a sign test was used to test for statistically significant differences between the baseline RMS errors. In addition to the sign test, a 95% confidence interval was constructed for the median difference between the SRTs of asynchronous and conventional stimulation to better quantify the relative performance of the two protocols.

4.5 Results

The SRTs for each fatigue trial are listed in Table 4-1, and the corresponding baseline RMS errors are listed in Table 4-2. Asynchronous stimulation yielded a significantly longer SRT than conventional stimulation (p-value = 0.0078). Meanwhile, the baseline RMS errors were not significantly different (p-value = 0.7266). The 95% confidence interval for the median difference between the SRTs of asynchronous and conventional stimulation was found to be (30.8, 67.3) seconds. The mean current amplitude was 65 and 85 mA for the asynchronous and conventional stimulation fatigue trials, respectively. Example fatigue trials comparing asynchronous and conventional stimulation are shown in Figure 4-4.

---

[6] The onset of steady state tracking is defined as the point at which the RMS error begins to flatten (no longer decreasing from the large initial error). Steady state tracking occurred approximately 10 seconds after starting the trial, on average.

Table 4-1. Successful run time (in seconds).

Subject-Leg	C64	A16	Difference
A - Left	53.4	85.1	31.7
A - Right	37.3	76.3	38.9
B - Left	26.2	45.4	19.2
B - Right	21.3	64.7	43.3
C - Left	27.1	93.6	66.4
C - Right	20.9	66.6	45.7
D - Left	33.7	94.8	61.1
D - Right	34.0	113.4	79.4
25th Percentile	**22.6**	**65.1**	**33.5**
Median	**30.4**	**80.7**	**44.5***
75th Percentile	**36.5**	**94.5**	**65.1**

$*$ *SRT of asynchronous stimulation is significantly longer than that of conventional stimulation*

For the left leg of Subject B, the electrodes for both asynchronous and conventional stimulation were moved farther towards the medial side of the leg. The electrode positions were different in this particular instance because the muscle consistently exhibited an "all-or-nothing" response to stimulation whenever an electrode was placed superficial to the vastus lateralis. The necessary shifting of electrodes for the left leg of Subject B may explain why this trial exhibited the shortest SRT of all asynchronous stimulation trials (Table 4-1) since crowding the electrodes to the medial side may have caused overlap in the muscle activation. In other words, some muscle fibers may have been activated by more than one electrode in this particular trial thereby reducing the fatigue benefits of asynchronous stimulation.

4.6   Discussion

Asynchronous stimulation has been previously shown to have significant advantages over conventional stimulation [51, 52, 55, 56, 58–67] in terms of reduced fatigue. However, studies comparing asynchronous to conventional stimulation have primarily
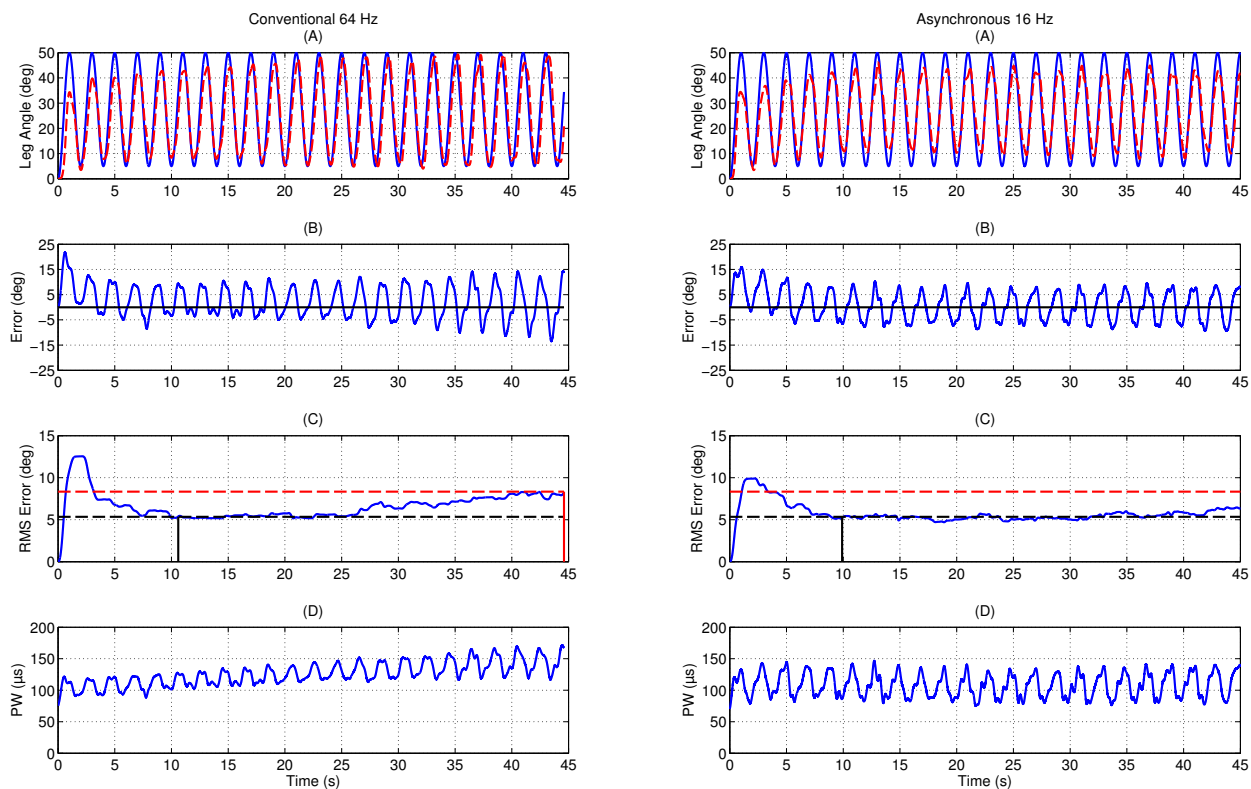
Figure 4-4. Example tracking performance for RISE control.
Example tracking performance for conventional stimulation (left column) and asynchronous stimulation (right column) taken from the right leg of Subject D. Plot A depicts the desired (solid line) and actual (dashed line) leg angle. Plot B depicts the position tracking error. Plot C depicts the RMS tracking error calculated over a moving 2 second window. The dashed lines in Plot C indicate the baseline error and the threshold that determines when to terminate stimulation (3 degrees of RMS error above the baseline measurement). Vertical solid lines correspond to the time that steady state tracking began and the time that the RMS error increased by 3 degrees. Note that the end time is not shown for asynchronous stimulation so that the two protocols can be visually compared over the same time scale. Plot D depicts the pulsewidth (i.e., the control input) that was calculated according to the developed control algorithm and delivered to the quadriceps femoris muscle group.

Table 4-2. Baseline RMS error (degrees).

Subject-Leg	C64	A16	Difference
A - Left	5.16	5.03	-0.13
A - Right	4.88	4.69	-0.19
B - Left	5.64	4.52	-1.12
B - Right	4.37	5.19	0.82
C - Left	4.78	4.71	-0.07
C - Right	5.69	5.91	0.22
D - Left	4.82	4.88	0.07
D - Right	5.34	5.34	-0.00
25th Percentile	**4.79**	**4.69**	**-0.18**
Median	**5.02**	**4.96**	**-0.04**
75th Percentile	**5.57**	**5.30**	**0.18**

focused on isometric contractions with fixed stimulation parameters [55, 56, 58–65, 67], due to the fact that it is easier to control for variation in the data. Sequential stimulation has also been shown to be advantageous over conventional stimulation as a method to reduce fatigue in isometric contractions [47, 50]. However, one study [50] found that a shorter on-time (i.e. the time to keep one stimulation channel activated before switching to the next channel) resulted in less fatigue, motivating the use of asynchronous stimulation over sequential stimulation. Furthermore, depending on the application, sequential stimulation may not be viable. For example, due to the segregation of motor units and the fact that sequential stimulation switches between stimulation channels less frequently, the torque required to accomplish a task may be greater than the torque that a single stimulation channel can maintain. Meanwhile, for asynchronous stimulation, even if one stimulation channel elicits a particularly weak response, the more frequent switching provides an averaging effect such that a larger torque can be maintained. In the present study, the developed control method is theoretically applicable to both sequential stimulation and asynchronous stimulation. However, in preliminary tests,

asynchronous stimulation was reported to be more comfortable than sequential stimulation. Therefore, the experimental work of the present study focused on asynchronous stimulation.

While experiments reported in literature have primarily been conducted with isometric contractions, a few studies have examined contractions yielding limb motion. Asynchronous stimulation [52] and sequential stimulation [49] were shown to reduce fatigue during FES cycling. Asynchronous stimulation has also been shown to be beneficial for isotonic gripping [51]. However, in the three aforementioned studies, the stimulus was delivered in an open-loop manner. Normann et al. used asynchronous stimulation to reduce fatigue during standing in cats [82]. While stimulation was also delivered in an open-loop manner, the authors stated that feedback information would be required if the method were to be used for a clinical neuroprosthesis. Similarly, Lau et al. studied standing in cats with both asynchronous and conventional stimulation [66]. As expected, the authors found that asynchronous resulted in less fatigue than conventional stimulation. Furthermore, the authors also compared open-loop and closed-loop control and found that the duration of standing achieved during closed-loop control was longer than that for open-loop control. However, the closed-loop controller implemented was a logic-based if-then-else algorithm. More recently, Frankel et al. implemented an iterative learning controller for isometric force control in cats; however, no modeling or stability analysis was included and the results were not compared with conventional stimulation [72].

In the current result, a controller that enables limb trajectory tracking was designed based on a constructive stability analysis (Section 4.3) that included the nonlinear, uncertain muscle/limb dynamics, and the controller performance was experimentally demonstrated in both legs of four able-bodied individuals. The experiments indicate that asynchronous stimulation can successfully extend the duration of successful limb

70

tracking compared to conventional stimulation in man. This result is promising for various rehabilitative treatments since a longer SRT means a larger dose of rehabilitative stimulation can be delivered before the onset of fatigue. The result is also promising for the development of neuroprostheses that may require the use of feedback control since asynchronous stimulation could slow the rate of fatigue, and thereby extend the duration that a neuroprosthesis enables functional movements or activities of daily living. Although experiments were conducted only in able-bodied individuals in the present study, asynchronous stimulation has been previously shown to slow the rate of fatigue (without feedback control) in individuals post-stroke [51] and in individuals with spinal cord injury [56, 63, 64, 67]. Therefore, it is expected that feedback control with asynchronous stimulation would result in longer durations of successful limb tracking than conventional stimulation in patient populations, similar to the able-bodied population of the present study. Nonetheless, experimental validation is still required to know the extent that the SRT can be prolonged during feedback control for individuals with spinal cord injury and other neurological disorders. Furthermore, experimental validation is still required to investigate the clinical significance of longer SRTs (and thus larger rehabilitative doses) in a patient population.

While the present results are promising, additional opportunities exist for closed-loop asynchronous stimulation. For example, since the muscle response to stimulation is different for each stimulation channel, it may be beneficial to develop a controller where the control gains can be selected independently for each channel. Independent gains may be particularly important if multiple heads of a large muscle are stimulated since different heads could have different recruitment and fatigue properties. Additionally, low-frequency asynchronous stimulation can lead to force ripple [74]. While the 16 Hz asynchronous stimulation protocol utilized in the present study resulted in smooth traces (Figure 5-2) and has been previously shown to induce equivalent ripple to volitional contractions [74], future efforts could focus on reducing force ripple for

low-frequency asynchronous stimulation either through independent gains or adaptive control laws. Adaptive controllers may also prove to be beneficial for asynchronous stimulation since they typically require less control effort and result in better tracking performance than robust controllers in practice. Future efforts could also focus on developing and/or implementing asynchronous stimulation with closed-loop control for other activities such as standing or cycling.

4.7   Concluding Remarks

A novel feedback controller is developed to yield trajectory tracking for a human limb during asynchronous or sequential neuromuscular electrical stimulation. The developed controller overcomes a potential drawback of asynchronous stimulation whereby switching between stimulation channels may introduce discontinuities. The controller yields semi-global asymptotic tracking where the only restriction on the switching signal is that there is an arbitrarily short transition period during which two subsystems are simultaneously activated. The sole purpose of this switching period is to ensure that the muscle response to stimulation remains continuous when switching between subsystems so that the switching signal is not required to be state dependent. Since the switching signal is not state dependent and the transition period can be made arbitrarily short, the proposed controller is suitable for both methods of asynchronous stimulation where the switching signal is either fast (i.e., interleaved pulses) or slow (i.e., sequential pulse trains). However, it should be noted that the control gains β and α_2 should be selected sufficiently large according to the duration of the desired transition period.

72

CHAPTER 5
SWITCHED TRACKING CONTROL OF A HUMAN LIMB DURING ASYNCHRONOUS NEUROMUSCULAR ELECTRICAL STIMULATION

In the previous chapter, a continuous RISE-based control law was developed which achieves semi-global asymptotic tracking despite bounded time-varying disturbances [73]. However, the control design required there to be a finite window of time where the control voltage is transitioned from one channel to another. Heuristically, a transition period is expected to lead to increased muscle fatigue since each stimulation channel will be activated longer than otherwise desired. Furthermore, in practice, stimulation channels are instantly switched, motivating the design of a control law that allows for instant switching. Although the transition period in Chapter 4 can be made arbitrarily small to approximate instant switching, increased control gains are required to compensate for smaller transition periods. Furthermore, the work in Chapter 4 implicitly assumes that the motor units recruited by each stimulation channel are independent. Yet, some degree of activation overlap is expected in practice, and therefore, it is motivated to remove this assumption in the control design. In the present chapter, a switched systems analysis is used to examine an alternative control approach to the sequential stimulation and asynchronous stimulation problem which allows for instantaneous switching between stimulation channels without additional requirements on the control gains. The contribution of this chapter is the development of a closed-loop tracking controller and the associated stability analysis that yields semi-global exponential tracking despite instantaneous switching between stimulation channels. An additional contribution is that the work is the first to show that response between stimulation channels is significantly different. Yet, tracking was still achieved and asynchronous stimulation yielded longer durations of successful tracking that conventional stimulation.

5.1   Limb Model

The knee-joint dynamics are modeled as previously in (4–1)-(4–4). During asynchronous stimulation, there are $N \in \mathbb{N}$ stimulation channels in the system. Since each

stimulation channel is expected to activate differing sets of motor units, the resulting dynamics depend on the active stimulation channel. Let $\mathbb{S} \subset \mathbb{N}$ be the finite index set for all involved subsystems (i.e., the stimulation channels) defined as $\mathbb{S} = \{1, 2, 3, \cdots, N\}$. To facilitate the subsequent analysis a positive auxiliary term $\Omega_i \in \mathbb{R}$ is defined as in (4–14). The torque produced by stimulation of the ith subsystem is then related to the voltage applied to the ith subsystem as

$$\tau_i = \Omega_i V_i, \ i \in \mathbb{S}. \tag{5–1}$$

Assumption 5.1. The moment arm ς_i is assumed to be a continuous, non-zero, positive, bounded function [75]. The function η_i is assumed to be a continuous, non-zero, positive, and bounded function [76]. Thus from (4–14), Ω_i is assumed to be a continuous, non-zero, positive, and bounded function such that $\Omega_i > \underline{\Omega} > 0, \ \forall i \in \mathbb{S}$ where $\underline{\Omega} \in \mathbb{R}$ is a known positive constant.

During asynchronous stimulation, the active stimulation channel is switched according to a predefined sequence (selected by the user) where only one channel is activated at a given time. To describe this phenomenon, let $\sigma : [t_0, \infty) \to \mathbb{S}$ denote a piecewise constant signal which selects a subsystem from $\mathbb{S}$ to be activated at time t, where $t_0 \in \mathbb{R}$ is the initial time. The voltage delivered to each subsystem, V_i, is then described in terms of the switching signal as

$$V_i(t) = \begin{cases} \nu_i(t) & \sigma(t) = i, \ i \in \mathbb{S} \\ 0 & \text{otherwise} \end{cases}, \tag{5–2}$$

where $\nu_i \in \mathbb{R}$ denotes the subsequently designed control voltage for the ith subsystem.

Property 2. The designed switching signal σ has a finite number of switching instances on any bounded time interval and the switching signal σ remains constant for $t \in [t_k, t_{k+1}), \ k \in \mathbb{N}$, where t_k denotes the instances of time when the active stimulation channel is switched.

After utilizing (5–1) and (5–2), the knee-joint dynamics in (4–1) can be expressed as

$$M_I + M_e + M_g + M_v + \tau_d = \Omega_{\sigma(t)}\nu_{\sigma(t)}, \tag{5–3}$$

where the inertial, gravitational, elastic, and viscous components are common to all subsystems since all subsystems act on the same knee-joint. In (5–3), while each of the terms vary with time in general, the time dependence of $\Omega_{\sigma(t)}$ is explicitly written to highlight that the control effectiveness instantly switches its value due to the switching signal σ, which characterizes the switching nature of asynchronous stimulation.

5.2 Control Development

The goal is to develop a controller that enables the knee-joint to track a desired angular trajectory. To facilitate the subsequent development, let $e_0 \in \mathbb{R}$ be defined as

$$e_0 \triangleq \int_{t_0}^{t} \left(q_d(s) - q(s) \right) ds, \tag{5–4}$$

where $q_d \in \mathbb{R}$ is a desired angular trajectory for the knee-joint, which is designed such that $q_d, \dot{q}_d, \ddot{q}_d \in \mathcal{L}_\infty$. To facilitate the subsequent development, the auxiliary tracking errors $e_1, e_2 \in \mathbb{R}$ are defined as

$$e_1 \triangleq \dot{e}_0 + \alpha_0 e_0, \tag{5–5}$$

$$e_2 \triangleq \dot{e}_1 + \alpha_1 e_1, \tag{5–6}$$

where $\alpha_0, \alpha_1 \in \mathbb{R}$ denote selectable positive constants.

Remark 5.1. Part of the motivation for designing e_1 and e_2 as in (5–5) and (5–6) is to include an integrator in the subsequently developed controller. It will later be shown that $|e_0|, |e_1| \to 0$, which implies $|q_d - q| \to 0$, thereby achieving the control objective.

After multiplying the time derivative of (5–6) by J, and utilizing (4–2), (5–3), (5–4), and (5–5), the open-loop dynamics during asynchronous stimulation can be expressed

as

$$J\dot{e}_2 = W + \tau_d - \Omega_{\sigma(t)}\nu_{\sigma(t)}, \tag{5–7}$$

where J is the same inertia for each subsystem since each subsystem acts on the same knee-shank complex, and $W \in \mathbb{R}$ denotes an auxiliary term defined as

$$W \triangleq J\left(\ddot{q}_d + \alpha_0\left(\dot{q}_d - \dot{q}\right) + \alpha_1\dot{e}_1\right) + M_e + M_g + M_v.$$

To facilitate the subsequent stability analysis, (5–7) is expressed as

$$J\dot{e}_2 = \tilde{W} + W_d - e_1 + \tau_d - \Omega_{\sigma(t)}\nu_{\sigma(t)}, \tag{5–8}$$

where $\tilde{W}, W_d \in \mathbb{R}$ denote the auxiliary terms

$$\tilde{W} \triangleq W - W_d + e_1,$$

$$W_d \triangleq J\ddot{q}_d + M_e(q_d) + M_g(q_d) + M_v(\dot{q}_d).$$

The motivation for expressing the open-loop error system as in (5–8) is to separate the model into groups that are bounded by states or by constants. Specifically, by applying the Mean Value Theorem [78, Lemma 5], $\tilde{W}$ can be upper bounded by state-dependent terms as

$$\left|\tilde{W}\right| \le \rho(\|z\|)\|z\|, \tag{5–9}$$

where $\|\cdot\|$ denotes the standard 2-norm, $z \in \mathbb{R}^3$ is defined as

$$z \triangleq [e_0,\ e_1,\ e_2]^T, \tag{5–10}$$

and $\rho : \mathbb{R} \to \mathbb{R}$ is a positive, radially unbounded, nondecreasing function. Based on the assumption that the desired angular trajectory of the knee-joint is bounded, an upper bound for W_d can be developed as

$$|W_d| \le \overline{W}_d, \tag{5–11}$$

where $\overline{W}_d \in \mathbb{R}$ is a known positive constant.

Based on the open-loop error system in (5–8) and the subsequent stability analysis, a sliding-mode-based controller is designed as

$$\nu_i \triangleq (k_{1,i} + k_{2,i})e_2 + k_{3,i}\,\mathrm{sgn}(e_2), \ i \in \mathbb{S}, \tag{5–12}$$

where $k_{1,i}$, $k_{2,i}$, $k_{3,i} \in \mathbb{R}$ are positive, constant control gains, and $\mathrm{sgn}(\cdot)$ denotes the signum function. To facilitate the subsequent analysis, let the minimum control gains for all stimulation channels be defined as

$$k_{1,\mathrm{min}} \triangleq \min_{i \in \mathbb{S}} \{k_{1,i}\}, \tag{5–13}$$

$$k_{2,\mathrm{min}} \triangleq \min_{i \in \mathbb{S}} \{k_{2,i}\}, \tag{5–14}$$

$$k_{3,\mathrm{min}} \triangleq \min_{i \in \mathbb{S}} \{k_{3,i}\}. \tag{5–15}$$

After substituting (5–12) into (5–8), the closed-loop dynamics can be written as

$$J\dot{e}_2 = \tilde{W} + W_d - e_1 + \tau_d - \Omega_{\sigma(t)}(k_{1,\sigma(t)} + k_{2,\sigma(t)})e_2$$
$$- \Omega_{\sigma(t)}k_{3,\sigma(t)}\,\mathrm{sgn}(e_2).$$

As described in Section 5.3, Theorem 5.1 and its associated stability proof establish that the switching asynchronous controller in (5–2) and (5–12) yields exponential tracking of a desired knee-joint trajectory.

5.3 Stability Analysis

Let $\mathcal{D}$ be the interior of the set $\{\xi \in \mathbb{R}^3 \mid \rho(\|\xi\|) < \sqrt{4\lambda k_{2,\mathrm{min}}\underline{\Omega}}\}$ where

$$\lambda \triangleq \min\left\{\left(\alpha_0 - \frac{1}{2}\right), \left(\alpha_1 - \frac{1}{2}\right), k_{1,\mathrm{min}}\underline{\Omega}\right\}, \tag{5–16}$$

and $\underline{\Omega}$ was defined in Assumption 5.1. Let $V_L : \mathcal{D} \to \mathbb{R}$ be a common Lyapunov function candidate, defined as

$$V_L \triangleq \frac{1}{2}e_0^2 + \frac{1}{2}e_1^2 + \frac{1}{2}Je_2^2, \tag{5–17}$$

which satisfies the following inequalities:

$$\lambda_1 \|z\|^2 \leq V_L \leq \lambda_2 \|z\|^2, \tag{5–18}$$

where $\lambda_1 \triangleq \min\left\{\frac{1}{2}, \frac{1}{2}J\right\}$, $\lambda_2 \triangleq \max\left\{\frac{1}{2}, \frac{1}{2}J\right\}$, and z was defined in (5–10). Let the region of attraction $\mathcal{D}_z \subset \mathcal{D}$ be the interior of $\left\{\xi \in \mathcal{D} \mid \rho\left(\sqrt{\frac{\lambda_2}{\lambda_1}} \|\xi\|\right) < \sqrt{4\lambda k_{2,\min}\underline{\Omega}}\right\}$.

Theorem 5.1. *The controller designed in (5–2) and (5–12) yields semi-global exponential tracking in the sense that*

$$|q_d(t) - q(t)| \leq (1 + \alpha_0)\sqrt{\frac{\lambda_2}{\lambda_1}} \|z(t_0)\| e^{-\frac{c}{2\lambda_2}(t-t_0)}, \tag{5–19}$$

where t_0 is the initial time, and $c \in \mathbb{R}$ is some positive constant, provided that the control gain $k_{2,\min}$ is selected sufficiently large so that the initial condition $z(t_0) \in \mathcal{D}_z$; $\alpha_0, \alpha_1 > \frac{1}{2}$; and the control gain $k_{3,\min}$ is selected according to the following sufficient condition:

$$k_{3,\min} > \underline{\Omega}^{-1}\left(\overline{W}_d + \overline{\tau}_d\right), \tag{5–20}$$

where $\overline{W}_d$ was introduced in (5–11), and $\overline{\tau}_d$ is a known bound on the disturbance torque.

Proof. The time derivative of (5–17) exists almost everywhere (a.e.) i.e., for almost all $t \in [t_0, \infty)$, and $\dot{V}_L \overset{a.e.}{\in} \dot{\tilde{V}}_L$ where

$$\dot{\tilde{V}}_L \triangleq \underset{\xi \in \partial V_L}{\cap} \xi^T K\left[\dot{e}_0, \ \dot{e}_1, \ \dot{e}_2, \ 1\right]^T, \tag{5–21}$$

where ∂V_L is the generalized gradient of V_L, and $K[\cdot]$ is defined as in [80]. Since V_L is continuously differentiable with respect to its arguments, (5–21) can be rewritten as

$$\dot{\tilde{V}}_L \subset \nabla V_L^T K\left[\dot{e}_0, \ \dot{e}_1, \ \dot{e}_2, \ 1\right]^T, \tag{5–22}$$

where $\nabla V_L \triangleq \left[e_0, \ e_1, \ e_2 J, \ \frac{1}{2}\dot{J}e_2^2\right]^T$. Using $K[\cdot]$ from [80], the fact that $\dot{J} = 0$, and substituting (5–5), (5–6), and (5–8) into (5–22) yields

$$\dot{\tilde{V}}_L \subset e_0(e_1 - \alpha_0 e_0) + e_1(e_2 - \alpha_1 e_1)$$

78

$$+ e_2(\tilde{W} + W_d - e_1 + \tau_d - K\left[\Omega_{\sigma(t)}\nu_{\sigma(t)}\right]).$$

First $\dot{V}_L$ is examined during the non-switching instants to prove that V_L is a common Lyapunov function. Assuming the arbitrary subsystem $p \in \mathbb{S}$ is active at time t,

$$
\begin{aligned}
\dot{V}_L \subset\, & e_0(e_1 - \alpha_0 e_0) + e_1(e_2 - \alpha_1 e_1) \\
& + e_2(\tilde{W} + W_d - e_1 + \tau_d - \Omega_p K\left[\nu_p\right]),\ p \in \mathbb{S},
\end{aligned}
\tag{5--23}
$$

where Ω_p is continuous by Assumption 5.1 and thus $K\left[\Omega_p\nu_p\right] = \Omega_p K\left[\nu_p\right]$ during the non-switching instants for arbitrary $p \in \mathbb{S}$. By canceling common terms and substituting (5–12), (5–23) can be rewritten as

$$
\begin{aligned}
\dot{V}_L =\, & -\alpha_0 e_0^2 - \alpha_1 e_1^2 + e_0 e_1 + e_2(\tilde{W} + W_d + \tau_d) \\
& - \Omega_p(k_{1,p} + k_{2,p})e_2^2 - \Omega_p k_{3,p}\left|e_2\right|,\ p \in \mathbb{S},
\end{aligned}
\tag{5--24}
$$

where the set in (5–23) reduces to the singleton in (5–24) since $e_2 K\left[\mathrm{sgn}\right](e_2) = \left|e_2\right|$. After using Young's inequality, (5–11), and the definition of the bounded disturbance, the expression in (5–24) can then be upper bounded as

$$
\begin{aligned}
\dot{V}_L \overset{a.e.}{\le}\, & -\left(\alpha_0 - \frac{1}{2}\right)e_0^2 - \left(\alpha_1 - \frac{1}{2}\right)e_1^2 - k_{1,p}\Omega_p e_2^2 \\
& - \left(k_{3,p}\Omega_p - \overline{W}_d - \overline{\tau}_d\right)\left|e_2\right| - k_{2,p}\Omega_p e_2{}^2 + e_2\tilde{W}.
\end{aligned}
\tag{5--25}
$$

After utilizing (5–9), (5–20), (5–13)-(5–15), and the fact that $\Omega_p > \underline{\Omega} > 0,\ \forall p \in \mathbb{S}$ from Assumption 5.1, the inequality in (5–25) can be further upper bounded as

$$
\begin{aligned}
\dot{V}_L \overset{a.e.}{\le}\, & -\left(\alpha_0 - \frac{1}{2}\right)e_0^2 - \left(\alpha_1 - \frac{1}{2}\right)e_1^2 - k_{1,\min}\underline{\Omega} e_2^2 \\
& - k_{2,\min}\underline{\Omega} e_2^2 + \rho(\|z\|)\|z\|\left|e_2\right|.
\end{aligned}
\tag{5--26}
$$

After completing the square, (5–26) can be expressed as

$$\dot{V}_L \overset{a.e.}{\le} -\left(\lambda - \frac{\rho^2(\|z\|)}{4k_{2,\min}\underline{\Omega}}\right)\|z\|^2,$$

$$\overset{a.e.}{\leq} -c\left\|z\right\|^2, \ \forall z \in \mathcal{D},$$

$$\overset{a.e.}{\leq} -\frac{c}{\lambda_2}V_L, \ \forall z \in \mathcal{D}, \tag{5–27}$$

where c is a positive constant, ρ was introduced in (5–9), λ_2 was introduced in (5–18), and λ was introduced in (5–16). From the inequality in (5–27), it can be concluded that V_L is in fact a common Lyapunov function since its time derivative has a common negative definite upper bound for each subsystem. From (5–27), [81, Corollary 1] can be invoked to show that $z \in D, \ \forall t \geq t_0, \ \forall z\left(t_0\right) \in D_z$, and hence, $e_0, \ e_1, \ e_2, \ V_L \in \mathcal{L}_\infty, \ \forall z(t_0) \in \mathcal{D}_z$. From (5–12) and the fact that $e_2 \in \mathcal{L}_\infty$, the control input for each channel $\nu_i \in \mathcal{L}_\infty$.

From the inequality in (5–27) and the fact that $z \in D, \ \forall t \geq t_0, \ \forall z\left(t_0\right) \in D_z$,

$$V_L(t) \leq V_L(t_0)e^{-\frac{c}{\lambda_2}(t-t_0)}, \ \forall\, z(t_0) \in \mathcal{D}_z.$$

From (5–18),

$$\begin{aligned}
\|z(t)\| &\leq \sqrt{\frac{1}{\lambda_1}V_L(t)} \\
&\leq \sqrt{\frac{1}{\lambda_1}V_L(t_0)e^{-\frac{c}{\lambda_2}(t-t_0)}}, \ \forall\, z(t_0) \in \mathcal{D}_z, \\
&\leq \sqrt{\frac{\lambda_2}{\lambda_1}\left\|z(t_0)\right\|^2 e^{-\frac{c}{\lambda_2}(t-t_0)}}, \ \forall\, z(t_0) \in \mathcal{D}_z, \\
&\leq \sqrt{\frac{\lambda_2}{\lambda_1}}\left\|z(t_0)\right\| e^{-\frac{c}{2\lambda_2}(t-t_0)}, \ \forall\, z(t_0) \in \mathcal{D}_z.
\end{aligned}$$

From the definitions of e_1 and z in (5–5) and (5–10), $|q_d - q| \leq |e_1| + \alpha_0 |e_0| \leq (1 + \alpha_0)\|z\|$, and thus, semi-global exponential tracking of the knee-joint trajectory is achieved in the sense of (5–19). The region of attraction, $\mathcal{D}_z$, can be expanded arbitrarily by increasing $k_{2,\min}$. Furthermore, the result of stability analysis is independent of the designed switching signal σ. In other words, the switching signal can be arbitrarily designed a priori by the user without needing to adhere to dwell time requirements. Limb tracking

is therefore achieved for asynchronous stimulation despite instant switching between stimulation channels. □

5.4 Experiments

Asynchronous and conventional stimulation were tested during isometric contractions to examine the muscle response to stimulation. Experiments were also conducted with dynamic contractions to test the developed controller and to better understand the NMES-induced fatigue characteristics of asynchronous and conventional stimulation during feedback control. For dynamic contractions, the developed control algorithm was used to vary the pulsewidth in real time while the current amplitude and stimulation frequency remained constant.

5.4.1 Subjects

Four able-bodied individuals (male, aged 20 to 27) participated in the study. Prior to participation, written informed consent was obtained from all participants, as approved by the institutional review board at the University of Florida.

5.4.2 Apparatus

All testing was performed using an apparatus that consisted of the following:

1. A current-controlled 8-channel stimulator (RehaStim, Hasomed GmbH, operating in ScienceMode)

2. A data acquisition device (Quanser Q8-USB)

3. A personal computer running Matlab/Simulink

4. A leg extension machine (shown previously in Figure 4-1) that was modified to include sensors as well as boots to securely fasten the shank and foot

5. Optical encoders to measure the leg angle (BEI Technologies)

6. Force Transducers to measure knee-joint torque (Transducer Techniques)

7. Surface electrodes (Axelgaard Manufacturing Co., Ltd.)[1]

5.4.3 Stimulation Protocols

Two stimulation protocols were examined: 16 Hz asynchronous stimulation (A16) with four channels and 64 Hz conventional stimulation (C64) with a single channel. These two protocols were selected because A16 has a composite stimulation frequency equivalent to C64. Conventional stimulation consisted of a single stimulation channel with a pair of 3" by 5" Valutrode® surface electrodes placed distally and proximally over the quadriceps femoris muscle group, while asynchronous stimulation consisted of four channels of stimulation utilizing four electrodes placed distally (1.5" by 3.5" Valutrode®) and two electrodes placed proximally (2" by 3.5" Valutrode®). The electrode configurations utilized for conventional and asynchronous stimulation are the same as previously depicted in Figure 4-3.

5.4.4 Precautions

The order of the two stimulation protocols (A16 and C64) were randomized for each leg. To prevent any layover effect of fatigue, each leg received only one stimulation protocol per day. A minimum of 48 hours of rest was required before the individual completed the remaining stimulation protocol for each leg.

5.4.5 Measuring the Control Effectiveness

Due to the spatial distribution of the electrodes, it is expected that the muscle response to stimulation will be different for each channel when utilizing asynchronous stimulation. To examine the extent of the differences, recruitment curves (i.e., the relationship between pulsewidth and the evoked torque) were constructed for each channel. To construct the recruitment curves, pulses were delivered at 64 Hz with a constant current amplitude of 70 mA and a pulsewidth that increased as a ramp

---

[1] Surface electrodes for the study were provided compliments of Axelgaard Manufacturing Co., Ltd.

(increasing in steps of 1 µs until the torque reached 25 N·m or the participant reported mild discomfort). The control effectiveness for each channel was then calculated as the linear slope of the recruitment curve. The control effectiveness was also calculated for conventional stimulation as a point of reference.

5.4.6 Fatigue Trials

After measuring the control effectiveness under isometric conditions, fatigue trials were conducted to compare each stimulation protocol in terms of its ability to maintain limb trajectory tracking. The desired angular trajectory[2] of the knee-joint was selected as a sinusoid ranging from 5 to 50 degrees with a period of 2 seconds. The current amplitude and stimulation frequency remained constant while the pulsewidth was adjusted according to the developed feedback control algorithm in (5–12) and the stimulation channels were switched according to (5–2). Since there is a finite pulsewidth resolution for the stimulator (steps of 1 µs), the current amplitude must be selected small enough so that there is a sufficient range of pulsewidth values corresponding to the desired range of motion. However, the current amplitude must also be selected large enough so that the pulsewidth does not saturate. Based on preliminary experiments, the current amplitude was fixed to 70 mA. However, in the specific case of conventional stimulation with Subject B, the current amplitude was increased to 90 mA since the muscle exhibited a weaker response to stimulation. This is unsurprising since conventional stimulation has been reported to require a larger current amplitude to reach the same value of torque as asynchronous stimulation [63, 64, 74].

Control gains were adjusted in pretrial tests to achieve trajectory tracking. The root mean square (RMS) position tracking error was calculated in real time with a moving window of 2 seconds to assist the gain tuning process (targeting 5 degrees of RMS error). The baseline RMS tracking error was calculated when the tracking error had

---

[2] The desired trajectory was based on the comfortable range of motion.

reached steady state.[3] The successful run time (SRT) of each fatigue trial was then calculated as the elapsed time from the onset of steady state tracking to the time that the RMS tracking error increased to 3 degrees above the baseline measurement.

5.4.7 Statistical Analysis

A Wilcoxon Signed Rank Test was performed at a significance level of $\alpha = 0.05$ to test for statistically significant differences between asynchronous and conventional stimulation in terms of SRT and the baseline RMS tracking error. A Friedman test was performed at a significance level of $\alpha = 0.05$ to test for statistically significant differences between the the four asynchronous stimulation channels in terms of the control effectiveness.

5.5 Results

Table 5-1 lists the control effectiveness for single-channel conventional stimulation as well as the control effectiveness for each channel of asynchronous stimulation. A Friedman test on the response of the four asynchronous stimulation channels indicated that there was statistically significant difference between the channels (p-value = 0.002). Figure 5-1 depicts the measured recruitment curves for the left leg of Subject C, highlighting each channel's differing response to electrical stimulation. The SRTs for each fatigue trial are listed in Table 5-2, and the corresponding baseline RMS errors are listed in Table 5-3. Asynchronous stimulation yielded a significantly longer SRT than conventional stimulation (p-value = 0.014). Meanwhile, the baseline RMS errors were not significantly different (p-value = 1.000). Example fatigue trials comparing asynchronous and conventional stimulation are shown in Figure 5-2. A detailed view

---

[3] The onset of steady state tracking is defined as the point at which the RMS error begins to flatten (no longer decreasing from the large initial error). Steady state tracking occurred approximately 10 seconds after starting the trial, on average.

highlighting the switched control input for each stimulation channel is provided in Figure 5-3.

Table 5-1. Control effectiveness (N·m·µs^{-1}).

Subject-Leg	Conv	Async			
	Ch 1	Ch 1	Ch 2	Ch 3	Ch 4
A - Left	0.483	0.743	0.566	0.403	0.289
A - Right	0.404	0.404	0.217	0.333	0.258
B - Left	0.112	0.214	0.070	0.135	0.267
B - Right	0.146	0.193	0.044	0.144	0.089
C - Left	0.396	0.367	0.115	0.318	0.322
C - Right	0.203	0.374	0.197	0.286	0.349
D - Left	0.256	0.779	0.182	0.351	0.208
D - Right	0.219	0.337	0.138	0.121	0.271
25th Percentile	**0.160**	**0.245**	**0.081**	**0.137**	**0.220**
Median	**0.237**	**0.372**	**0.160**	**0.300**	**0.269**
75th Percentile	**0.402**	**0.658**	**0.212**	**0.347**	**0.294**

5.6 Discussion

Asynchronous stimulation is a promising stimulation method that has been previously shown to reduce fatigue during isometric contractions with fixed stimulation parameters [55, 56, 58–65, 67]. Asynchronous stimulation may also reduce fatigue during isotonic gripping [51] and FES cycling [52]. The desire to use asynchronous stimulation for rehabilitative procedures or neuroprostheses, coupled with the challenges of switching between sets of motor units, motivates the developed control design. A challenge to designing an asynchronous stimulation controller is that, due to the spatial distribution of the electrodes, each channel is likely to recruit a different number or type of motor units for the same stimulation parameters. From a control perspective, this problem is represented by a switching control effectiveness ($\Omega_{\sigma(t)}$ in (5–3)). While previous studies have not directly measured the control effectiveness for each channel, there is some previous evidence to suggest that each channel's response to stimulation

Table 5-2. Successful run time (in seconds).

Subject-Leg	C64	A16	Difference
A - Left	24.5	44.3	19.7
A - Right	28.5	58.0	29.5
B - Left	25.9	56.8	30.9
B - Right	29.7	68.4	38.7
C - Left	36.7	59.6	23.0
C - Right	48.9	80.1	31.2
D - Left	27.3	234.8	207.5
D - Right	20.7	95.3	74.5
25th Percentile	**24.9**	**57.1**	**24.6**
Median	**27.9**	**64.0**	**31.0***
75th Percentile	**34.9**	**91.5**	**65.6**

$*$ *SRT of asynchronous stimulation is statistically longer than that of conventional stimulation*

Table 5-3. Baseline RMS error (degrees).

| Subject-Leg	C64	A16	Difference
A - Left	5.46	5.50	0.04
A - Right	5.29	5.32	0.02
B - Left	5.05	5.18	0.13
B - Right	5.02	5.23	0.21
C - Left	4.90	4.72	-0.18
C - Right	5.03	4.63	-0.40
D - Left	5.05	5.38	0.33
D - Right	5.36	5.10	-0.26
25th Percentile	**5.02**	**4.81**	**-0.24**
Median	**5.05**	**5.20**	**0.03**
75th Percentile	**5.34**	**5.37**	**0.19**
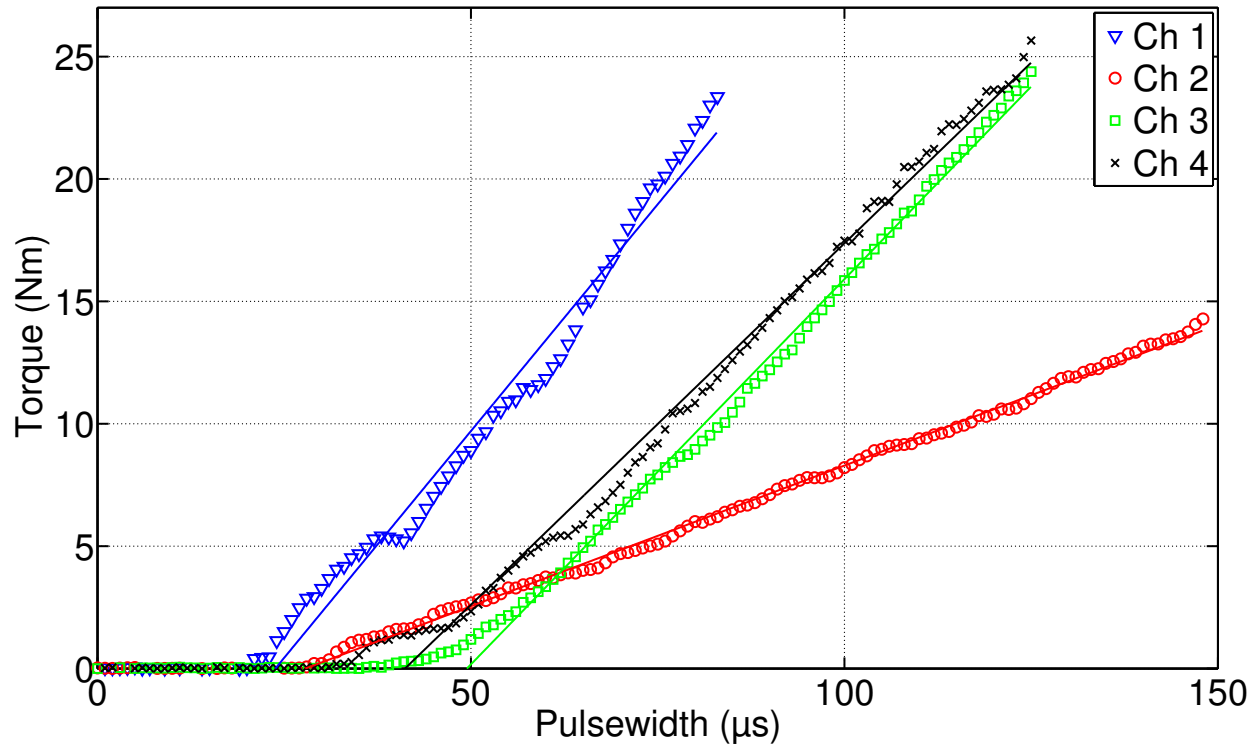
Figure 5-1. Differing control effectiveness for asynchronous stimulation. Recruitment curves corresponding to the four individual channels of asynchronous stimulation on the left leg of Subject C. Solid lines indicate the linear fit which illustrates the differences in the control effectiveness for each channel (i.e., Ω in (5–1)).

can differ since asynchronous stimulation has been shown to result in force ripple (i.e., unfused tetanus) [58, 74]. In the present study, the control effectiveness was measured for each channel during isometric contractions. The results indicate that there is in fact a significant difference, corroborating the switched model in (5–3). It should be noted that the control effectiveness for each channel is time-varying in general (e.g., due to fatigue and the muscle force-length relationship), and therefore, the control effectiveness for each channel may become more similar or dissimilar as the leg moves and the muscle fatigues during feedback control. Nevertheless, the present results highlight that the control effectiveness values should not be assumed to be equal when developing control algorithms for asynchronous stimulation.
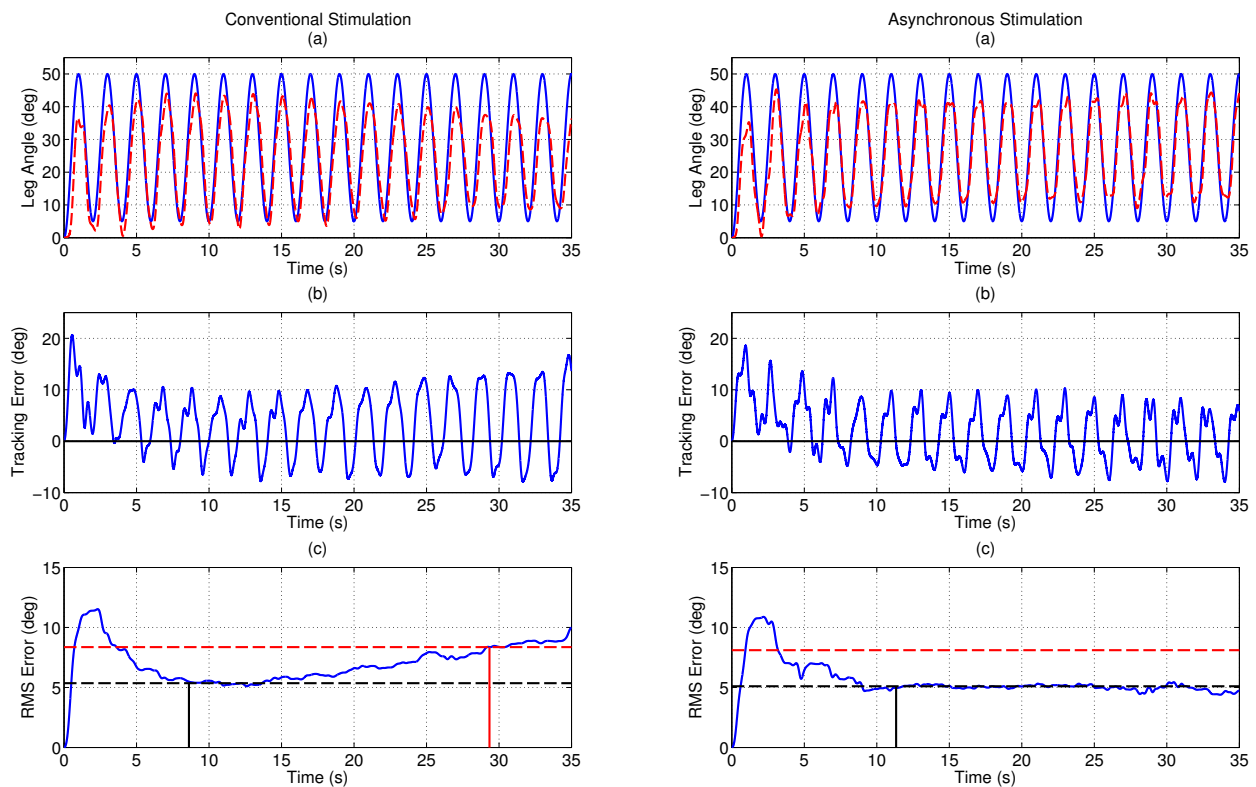
Figure 5-2. Example tracking performance for switched tracking control.
Example tracking performance taken from the right leg of Subject D comparing conventional stimulation (left column) and asynchronous stimulation (right column). Plot (a) depicts the desired (solid line) and actual (dashed line) knee-joint angle. Plot (b) depicts the angular position tracking error. Plot (c) depicts the RMS tracking error calculated over a moving 2 second window (corresponding to the period of the desired trajectory). The horizontal dashed lines in Plot (c) indicate the baseline error and the threshold that determines the end of successful tracking (set to 3 degrees of RMS error above the baseline measurement). Vertical solid lines correspond to the time that steady state tracking began and the time that the RMS error increased by 3 degrees. The end time is not shown for asynchronous stimulation so that the two protocols can be visually compared over the same time scale.
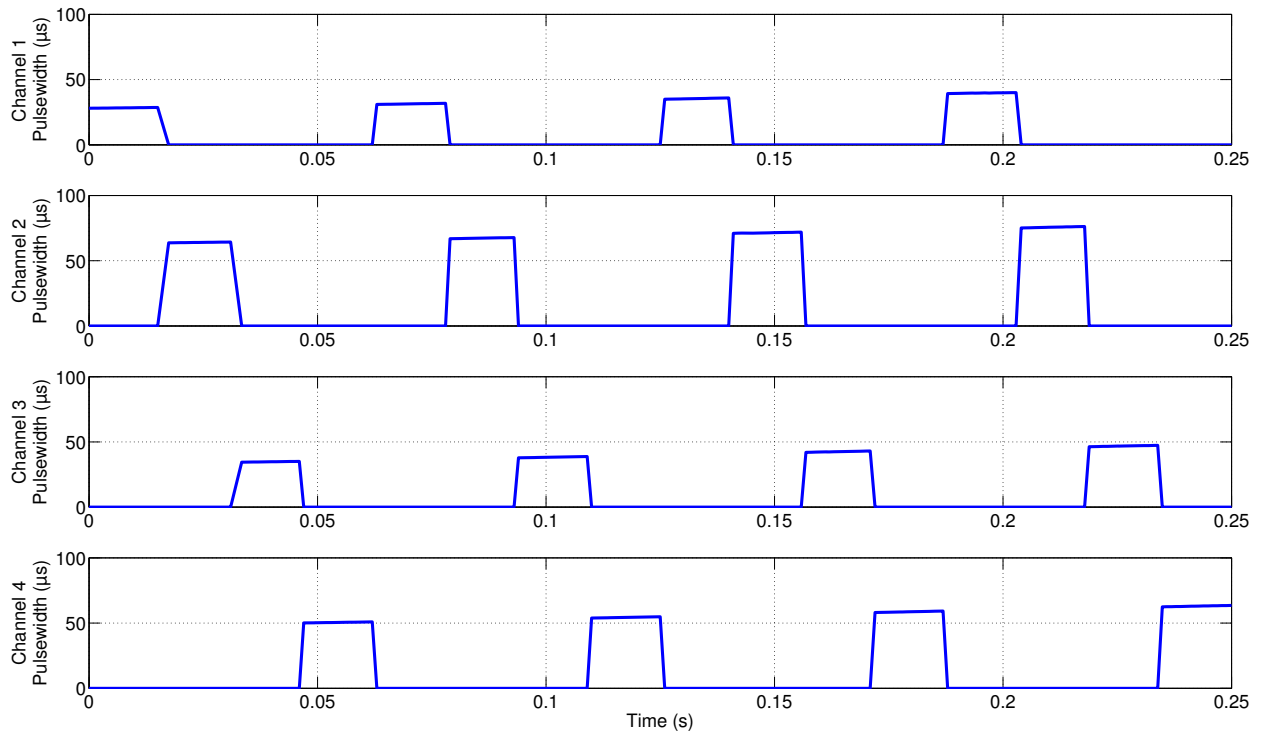
Figure 5-3. Switched pulsewidth input.

For asynchronous stimulation, the control inputs for each channel were calculated according to (5–12) and the stimulation channels were switched according to (5–2). Depicted are the control inputs for the asynchronous stimulation fatigue trial of the right leg of Subject D. For illustrative purposes, the control inputs are depicted over a period of 0.25 seconds.

Limited control development has been provided for multi-channel asynchronous stimulation. Lau et al. [66] implemented a closed-loop, logic-based, if-then-else algorithm for standing in cats. Frankel et al. [72] implemented an iterative learning controller for isometric force control in cats. However, no modeling or stability analysis were included in the aforementioned studies. In [73], a RISE-based control law was developed for knee-joint tracking with asynchronous stimulation. While the work considered that each stimulation channel could have a different control effectiveness, the control design did not allow for instantaneous switching and made an implicit assumption that there is no activation overlap between the stimulation channels. Therefore, in the present work, a switched systems analysis was used to examine and develop an alternative control approach that allows for instantaneous switching between stimulation channels and removes the assumption that there is no activation overlap. The developed controller was implemented on four individuals with asynchronous and conventional stimulation. Asynchronous stimulation was found to result in statistically longer durations of successful tracking for the knee-joint angle despite statistically different responses between the stimulation channels.

While the present results are promising, additional opportunities exist for asynchronous stimulation. An adaptive control design may prove to be beneficial for asynchronous stimulation since adaptive controllers typically require less control effort and result in better tracking performance than robust controllers in practice. Future efforts could also focus on extending the current result to other functional activities. For example, asynchronous stimulation has shown the potential to be effective for open-loop FES cycling with constant stimulation parameters [52], but combining feedback control of FES cycling [29] with asynchronous stimulation may further improve rehabilitative treatments. Along these lines, opportunities exist whereby asynchronous stimulation could be implemented along with an exoskeleton (e.g., [83, 84]) or robotic orthosis (e.g., [85]) to create a stimulation-assisted exoskeleton/orthosis that exploits the fatigue-resistant

characteristics of asynchronous stimulation. In conclusion, feedback control of asynchronous stimulation should also be examined in a patient population as the duration of successful tracking may differ from that of the able-bodied population in the present study.

5.7   Concluding Remarks

A novel feedback controller is developed to yield semi-global exponential trajectory tracking for a human limb during either sequential or asynchronous neuromuscular electrical stimulation despite instantaneous switching between stimulation channels. Since the switching signal is not state dependent and can be specified by the user a priori, the proposed controller is suitable for both methods of stimulation where the switching signal is either fast (i.e., asynchronous stimulation with interleaved pulses) or slow (i.e., sequential stimulation with sequential pulse trains). The controller is promising for the implementation of sequential and asynchronous stimulation for closed-loop rehabilitative procedures and in assistive devices as a method to reduce fatigue while tracking a desired trajectory.

CHAPTER 6
CONCLUSIONS AND FUTURE WORK

6.1 Conclusions

A promising new method of stimulation, asynchronous stimulation, was examined in the present work. Asynchronous stimulation had previously been shown to reduce NMES-induced fatigue in open-loop experiments with fixed stimulation parameters. However, there is still much to be learned about asynchronous stimulation, and therefore, the focus of the present work was further the development of the promising method. For example, while it is well known that asynchronous stimulation reduces NMES-induced fatigue compared to conventional stimulation, it was previously unclear if lower frequency asynchronous stimulation may also be preferred over high frequency asynchronous stimulation. In Chapter 2, it was determined that there is in fact a significant advantage to utilizing lower stimulation frequencies, even for asynchronous stimulation, as post hoc analysis determined that 8 Hz asynchronous stimulation resulted in significantly longer fatigue times than 16 Hz asynchronous (40% longer on average in the SCI population and 85% longer on average in the able-bodied population). Post hoc analysis also determined there to be a statistically significant difference in the mean fatigue indices of 8 Hz asynchronous and 16 Hz asynchronous for the able-bodied population but a statistical difference could not be concluded for the SCI population. However, the data suggests that 8 Hz asynchronous leads to less total fatigue as it resulted in an 18% greater fatigue index than 16 Hz asynchronous stimulation on average for both populations. While there are obvious differences between the able-bodied and SCI populations in the sense that the SCI population exhibited higher rates of fatigue (cf. Tables 2-2 and 2-4) and more total fatigue at the end of the trials (cf. Tables 2-3 and 2-5), both populations exhibited the same general trends.

While asynchronous stimulation can reduce fatigue, each stimulation channel is likely to recruit a different number and/or type of motor unit for a given stimulus. Thus,

asynchronous stimulation may also exhibit a force ripple (i.e., contractions that are not fully fused, thus exhibiting non-smooth force tracings). The amount of force ripple present during asynchronous stimulation in man was not previously clear, and therefore, in Chapter 3, the force ripple was quantified during asynchronous and conventional single-channel transcutaneous stimulation across a range of stimulation frequencies. It was found that force ripple was significant at lower frequencies but not high stimulation frequencies.

Since asynchronous stimulation has shown promise in open-loop experiments, it was previously expected to extend the time that functional tasks may be performed if they are combined with feedback control. However, closed-loop experiments had not previously been conducted in man to compare asynchronous and conventional stimulation. Furthermore, one limitation to asynchronous is that switching between stimulation channels introduces discontinuities due to a differing response to stimulation by each group of recruited motor units. However, previous literature on asynchronous stimulation neither developed nor tested feedback control of asynchronous stimulation in man. Thus, there was a need to design controllers which consider the switching dynamics and muscle response to stimulation. A continuous closed-loop feedback controller was developed in Chapter 4 to yield semi-global asymptotic tracking of a desired trajectory for a person's knee-shank complex during either asynchronous or sequential stimulation. The experiments indicated that asynchronous stimulation can successfully extend the duration of successful limb tracking compared to conventional stimulation in man. This result is promising for various rehabilitative treatments and for the development of neuroprostheses that may require the use of feedback control, since asynchronous stimulation could slow the rate of fatigue. Although experiments were conducted only in able-bodied individuals, asynchronous stimulation has been previously shown to slow the rate of fatigue (without feedback control) in individuals post-stroke [51] and in individuals with spinal cord injury [56, 63, 64, 67]. Furthermore, the results in Chapter 2

93

highlighted that the general trend in the performance of multiple stimulation protocols is the same in able-bodied SCI individuals. Therefore, it is expected that feedback control with asynchronous stimulation would result in longer durations of successful limb tracking than conventional stimulation in patient populations, similar to the able-bodied population of the present work. Nonetheless, experimental validation is still required to know the extent of the fatigue benefits during feedback control for individuals with spinal cord injury and other neurological disorders.

While the work in Chapter 4 was promising in the sense that it was the first to develop, analyze, and test and feedback controller for asynchronous stimulation (and subsequently highlight fatigue benefits of the method), there were some mathematical limitations to the control development. Specifically, the work in Chapter 4 implicitly assumed that there was zero activation overlap between stimulation channel. While zero activation overlap is desired to reduce fatigue, it can not necessarily be guaranteed, especially during transcutaneous electrical stimulation. Furthermore, the analysis dictated the introduction of a smoothing signal and a transition period, and therefore, instant switching between stimulation channels could not be obtained. While the transition could be made arbitrarily small to approximate instant switching, decreases in the transition period implied that the control gains would need to be increased (based on a sufficient condition from stability analysis). Therefore, in Chapter 5, a closed-loop feedback controller is developed through a switched systems analysis to improve upon the result in Chapter 4. The controller yields semi-global exponential tracking despite instantaneous switching between stimulation channels and removes the implicit assumption of zero activation overlap. Experimental results illustrate the performance of the newly developed controller. Additional experiments are the first to show that the recruitment curves are in fact different for each stimulation channel, confirming the modeling of the discontinuous control effectiveness for which the controller was developed. The results are promising for the implementation of asynchronous stimulation in assistive devices and closed-loop

rehabilitative procedures as methods to limit NMES-induced fatigue while tracking a desired trajectory, thereby extending treatment duration and the duration that functional tasks can be performed.

In conclusion, the work herein highlights a promising new stimulation method that can advance the field of neuromuscular electrical stimulation, its shortcomings, and methods to overcome those shortcomings. However, there is still much to learn about asynchronous stimulation and there are many opportunities to improve the method. Section 6.2 details potential topics for future work.

6.2   Future Work

While the results in the present dissertation are promising, additional opportunities exist to develop controllers for asynchronous stimulation. Specifically, the work in Chapters 4 and 5 utilize robust controllers due to the unknown time-varying nature of muscle stimulation. However, adaptive controllers may be beneficial since they typically require less control input and yield better tracking that robust controllers in practice. Along these lines, since the recruitment curves are different for each stimulation channel, methods that estimate or learn these relationships could result in better tracking since the desired torque could be directly specified (within some level of accuracy) in the controller. One possible method to learn this relationship is to utilize dynamic torque sensors so that the otherwise unknown stimulus-to-torque relationship can be measured in real time.

The optimal electrode configuration for asynchronous stimulation is presently unclear. Currently, most researchers utilize four smaller electrodes placed either distally/proximally and a larger, common electrode for all channels placed proxi-mally/distally. Since biphasic pulses are typically delivered and the ratio of larger to smaller electrodes is not significant enough to be monopolar, the motor neurons recruited by the larger electrode would still be recruited at a rate equivalent to conventional stimulation. While this configuration has been shown to induce less fatigue than

conventional stimulation, fatigue could potentially be reduced even further by utilizing unique pairs of electrodes for each channel rather than having an electrode that is common to multiple stimulation channels. In the present work, the utilized electrode configuration limited the sharing of electrodes compared to previous work (two electrodes were common to two channels each rather than one electrode common to four channels). While the decision to utilize this configuration is well motivated, no attempt was made to compare the differences in fatigue across multiple electrode configurations. Therefore, future work could examine the optimal number, size, shape, and placement of electrodes for asynchronous stimulation.

While not often discussed, one limitation to asynchronous stimulation is that the sensation of the stimulus can be more unpleasant than that during conventional stimulation. This is likely due to the fact that asynchronous stimulation utilizes smaller electrodes, thereby leading to an increased current density over a smaller surface of the skin. Along the lines of the previous point, it may be possible to reduce the sensation of skin pain through the design of an optimal electrode configuration. Additionally, rather than having only one stimulation channel active at a given time, it may be of interest to deliver a small stimulation intensity (below the threshold for muscle activation but above the threshold for sensation) to the "inactive" stimulation channels. By always delivering a low intensity stimulus, pain could be reduced via inhibitory connections between receptors. For example, it is well-known in physiology that the ability to distinguish between sharp and dull points on an object stems from the fact that a dull object causes a greater number of receptors to be activated (since it covers a wider area), and each receptor has an inhibitory effect on its neighbors.

While limb tracking was able to be achieved in the present work, opportunities exist to extend the present work to other functional movements. For example, FES cycling has been shown to be an effective rehabilitation treatment, and therefore, it is expected that prolonging the treatment duration via asynchronous stimulation could lead to

improved or quicker rehabilitative outcomes. However, this has not yet been examined. Therefore, future work could develop asynchronous stimulation controllers for functional tasks such as stepping or cycling and subsequently examine the acute and long term effects of extended closed-loop treatments in a patient population in terms of stamina, strength, neuroplasticity, etc.

The two primary goals of NMES/FES are to rehabilitate and to enable activities of daily living. While the development of feedback controllers can yield coordinated limb movement, there may be instances where the additional assistance of an exoskelton is required. For example, hip flexors are difficult to target via transcutaneous electrical stimulation, and therefore motors attached to the individual's hip could overcome this limitation. Additionally, depending on the individual, even the muscles that can be easily targeted (e.g., quadriceps femoris) might have limited force output due to atrophy. In this situation, even if feedback control via FES can theoretically lead to limb tracking, muscle weakness could necessitate the additional assistance of an exoskeleton. However, exoskeletons are not without their own limitations. Specifically, exoskeltons can be heavy due to the weight of the actuators and the power source. One advantage of muscle stimulation is that the true power source is contained within the human body and the electrical sitmuli only act a trigger to the muscle contraction. Therefore, the addition of muscle stimulation to a traditional exoskelton reduces the need for larger motors and power sources. Meanwhile, the presence of electric motors could guarantee the safety of the device and reduce the work load of the individual's muscles, as needed. Furthermore, by incorporating muscle stimulation (rather than electric motors alone), the individual will effectively receive a rehabilitative treatment, thereby regaining strength, improving cardiovascular health, etc. As muscle strength is regained, the electric motor assistance could slowly be removed. Therefore, muscle stimulation could lead to the individual becoming less dependent on assistance by the electric motor. In turn, the individual could transition to exoskeletons with smaller motors, reduced weight, and

increasingly compact form factors. Ultimately, the combination of muscle stimulation and traditional motor control in a hybrid exoskelton could result in an improved device that is less cumbersome and functions as an everyday rehabilitation treatment. By utilizing asynchronous stimulation to slow the onset of fatigue, the implementation of such a device becomes more feasible.

REFERENCES

[1] S. K. Sabut, C. Sikdar, R. Mondal, R. Kumar, and M. Mahadevappa, "Restoration of gait and motor recovery by functional electrical stimulation therapy in persons with stroke," *Disabil. Rehabil.*, vol. 32, no. 19, pp. 1594–1603, 2010.

[2] T. Yan, C. W. Y. Hui-Chan, and L. S. W. Li, "Functional electrical stimulation improves motor recovery of the lower extremity and walking ability of subjects with first acute stroke: A randomized placebo-controlled trial," *Stroke*, vol. 36, no. 1, pp. 80–85, 2005.

[3] S. K. Stackhouse, S. A. Binder-Macleod, C. A. Stackhouse, J. J. McCarthy, L. A. Prosser, and S. C. K. Lee, "Neuromuscular electrical stimulation versus volitional isometric strength training in children with spastic diplegic cerebral palsy: A preliminary study," *Neurorehabil. Neural Repair*, vol. 21, no. 6, pp. 475–485, 2007.

[4] L. Snyder-Mackler, A. Delitto, S. W. Stralka, and S. L. Bailey, "Use of electrical stimulation to enhance recovery of quadriceps femoris muscle force production in patients following anterior cruciate ligament reconstruction," *Phys. Ther.*, vol. 74, no. 10, pp. 901–907, 1994.

[5] E. Scremin, L. Kurta, A. Gentili, B. Wiseman, K. Perell, C. Kunkel, and O. U. Scremin, "Increasing muscle mass in spinal cord injured persons with a functional electrical stimulation exercise program," *Arch. Phys. Med. Rehabil.*, vol. 80, no. 12, pp. 1531–1536, 1999.

[6] T. Mohr, J. Pødenphant, F. Biering-Sørensen, H. Galbo, G. Thamsborg, and M. Kjær, "Increased bone mineral density after prolonged electrically induced cycle training of paralyzed limbs in spinal cord injured man," *Calcif. Tissue Int.*, vol. 61, no. 1, pp. 22–25, 1997.

[7] S.-C. Chen, C.-H. Lai, W. P. Chan, M.-H. Huang, H.-W. Tsai, and J.-J. J. Chen, "Iincrease in bone mineral density after functional electrical stimulatin cycling exercises in spinal cord injured patients," *Disabil. Rehabil.*, vol. 27, no. 22, pp. 1337–1341, 2005.

[8] M. Bélanger, R. B. Stein, G. D. Wheeler, T. Gordon, and B. Leduc, "Electrical stimulation: can it increase muscle strength and reverse osteopenia in spinal cord injured individuals?" *Arch. Phys. Med. Rehabil.*, vol. 81, no. 8, pp. 1090–1098, 2000.

[9] M. M. Rodgers, R. M. Glaser, S. F. Figoni, S. P. Hooker, B. N. Ezenwa, S. R. Collins, T. Mathews, A. G. Suryaprasad, and S. C. Gupta, "Musculoskeletal responses of spinal cord injured individuals to functional neuromuscular stimulation-induced knee extension exercise training," *J. Rehabil. Res. Dev.*, vol. 28, no. 4, pp. 19–26, 1991.

[10] S. Ferrante, A. Pedrocchi, G. Ferrigno, and F. Molteni, "Cycling induced by functional electrical stimulation improves the muscular strength and the motor control of

individuals with post-acute stroke," *Eur. J. Phys. Rehabil. Med.*, vol. 44, no. 2, pp. 159–167, 2008.

[11] T. J. Kimberley, S. M. Lewis, E. J. Auerbach, L. L. Dorsey, J. M. Lojovich, and J. R. Carey, "Electrical stimulation driving functional improvements and cortical changes in subjects with stroke," *Exp. Brain Res.*, vol. 154, no. 4, pp. 450–460, February 2004.

[12] L. Griffin, M. Decker, J. Hwang, B. Wang, K. Kitchen, Z. Ding, and J. Ivy, "Functional electrical stimulation cycling improves body composition, metabolic and neural factors in persons with spinal cord injury," *J. Electromyogr. Kinesiol.*, vol. 19, no. 4, pp. 614–622, 2009.

[13] P. D. Faghri, M. M. Rodgers, R. M. Glaser, J. G. Bors, C. Ho, and P. Akuthota, "The effects of functional electrical stimulation on shoulder subluxation, arm function recovery, and shoulder pain in hemiplegic stroke patients," *Arch. Phys. Med. Rehabil.*, vol. 75, pp. 73–79, 1994.

[14] S. P. Hooker, S. F. Figoni, M. M. Rodgers, R. M. Glaser, T. Mathews, A. G. Suryaprasad, and S. C. Gupta, "Physiologic effects of electrical stimulation leg cycle exercise training in spinal cord injured persons," *Arch. Phys. Med. Rehabil.*, vol. 73, no. 5, pp. 470–476, 1992.

[15] S. F. Figoni, M. M. Rodgers, R. M. Glaser, S. P. Hooker, P. D. Feghri, B. N. Ezenwa, T. Mathews, A. G. Suryaprasad, and S. C. Gupta, "Physiologic responses of paraplegics and quadriplegics to passive and active leg cycle ergometry," *J. Am. Paraplegia Soc.*, vol. 13, no. 3, pp. 33–39, 1990.

[16] R. B. Stein, "Functional electrical stimulation after spinal cord injury," *J. Neurotrauma*, vol. 16, no. 8, pp. 713–717, 1999.

[17] K. L. Kilgore, H. A. Hoyen, A. M. Bryden, R. L. Hart, M. W. Keith, and P. H. Peckham, "An implanted upper-extremity neuroprosthesis using myoelectric control," *J. Hand Surg.*, vol. 33, no. 4, pp. 539–550, 2008.

[18] R. Cornwall and M. R. Hausman, "Implanted neuroprostheses for restoration of hand function in tetraplegic patients," *J. Am. Acad. Orthop. Surg.*, vol. 12, no. 2, pp. 72–79, 2004.

[19] A. Prochazka, M. Gauthier, M. Wieler, and Z. Kenwell, "The bionic glove: An electrical stimulator garment that provides controlled grasp and hand opening in quadriplegia," *Arch. Phys. Med. Rehabil.*, vol. 78, no. 6, pp. 608 – 614, 1997.

[20] R. B. Stein, D. G. Everaert, A. K. Thompson, S. L. Chong, M. Whittaker, J. Robertson, and G. Kuether, "Long-term therapeutic and orthotic effects of a foot drop stimulator on walking performance in progressive and nonprogressive neurological disorders," *Neurorehabil. Neural Repair*, vol. 24, no. 2, pp. 152–167, 2010.

[21] T. M. Kesar, R. Perumal, D. S. Reisman, A. Jancosko, K. S. Rudolph, J. S. Higginson, and S. A. Binder-Macleod, "Functional electrical stimulation of ankle plantarflexor and dorsiflexor muscles: effects on poststroke gait." *Stroke*, vol. 40, no. 12, pp. 3821–3827, Dec 2009.

[22] S. K. Sabut, P. K. Lenka, R. Kumar, and M. Mahadevappa, "Effect of functional electrical stimulation on the effort and walking speed, surface electromyography activity, and metabolic responses in stroke subjects," *J. Electromyogr. Kinesiol.*, vol. 20, no. 6, pp. 1170–1177, 2010.

[23] S. Ferrante, E. Ambrosini, G. Ferrigno, and A. Pedrocchi, "Biomimetic NMES controller for arm movements supported by a passive exoskeleton," in *Eng. Med. Biol. Soc. (EMBC), 2012 Annu. Int. Conf. IEEE*, Sept. 2012, pp. 1888–1891.

[24] R. Kobetic, C. S. To, J. R. Schnellenberger, M. L. Audu, T. C. Bulea, R. Gaudio, G. Pinault, S. Tashman, and R. J. Triolo, "Development of hybrid orthosis for standing, walking, and stair climbing after spinal cord injury." *J. Rehabil. Res. Dev.*, vol. 46, no. 3, pp. 447–462, 2009.

[25] K. J. Hunt, D. Hosmann, M. Grob, and J. Saengsuwan, "Metabolic efficiency of volitional and electrically stimulated cycling in able-bodied subjects," *Med. Eng. Phys.*, vol. 35, no. 7, pp. 919–925, July 2013.

[26] E. Ambrosini, S. Ferrante, T. Schauer, G. Ferrigno, F. Molteni, and A. Pedrocchi, "Design of a symmetry controller for cycling induced by electrical stimulation: preliminary results on post-acute stroke patients," *Artif. Organs*, vol. 34, no. 8, pp. 663–667, August 2010.

[27] M. J. Bellman, T.-H. Cheng, R. J. Downey, and W. E. Dixon, "Stationary cycling induced by switched functional electrical stimulation control," in *Proc. Am. Control Conf.*, 2014, pp. 4802–4809.

[28] L. D. Duffell, N. d. N. Donaldson, and D. J. Newham, "Power output during functional electrically stimulated cycling in trained spinal cord injured people," *Neuromodulation: Technology at the Neural Interface*, vol. 13, no. 1, pp. 50–57, 2010.

[29] M. J. Bellman, T.-H. Cheng, R. Downey, and W. E. Dixon, "Cadence control of stationary cycling induced by switched functional electrical stimulation control," in *Proc. IEEE Conf. Decis. Control*, 2014.

[30] H. Kawai, M. J. Bellman, R. J. Downey, and W. E. Dixon, "Tracking control for FES-cycling based on force direction efficiency with antagonistic bi-articular muscles," in *Proc. Am. Control Conf.*, 2014, pp. 5484–5489.

[31] K. J. Hunt, J. Fang, J. Saengsuwan, M. Grob, and M. Laubacher, "On the efficiency of FES cycling: A framework and systematic review," *Technol. Health Care*, vol. 20, no. 5, pp. 395–422, 2012.

[32] B. M. Doucet and L. Griffin, "Maximal versus submaximal intensity stimulation with variable patterns," *Muscle Nerve*, vol. 37, no. 6, pp. 770–777, 2008.

[33] M. B. Kebaetse and S. A. Binder-Macleod, "Strategies that improve human skeletal muscle performance during repetitive, non-isometric contractions." *Pflügers Arch.*, vol. 448, no. 5, pp. 525–532, Aug 2004.

[34] B. Bigland-Ritchie, I. Zijdewind, and C. K. Thomas, "Muscle fatigue induced by stimulation with and without doublets." *Muscle Nerve*, vol. 23, no. 9, pp. 1348–1355, Sep 2000.

[35] Z. Z. Karu, W. K. Durfee, and A. M. Barzilai, "Reducing muscle fatigue in FES applications by stimulating with N-let pulse trains," *IEEE Trans. Biomed. Eng.*, vol. 42, no. 8, pp. 809–817, Aug 1995.

[36] D. Graupe, P. Suliga, C. Prudian, and K. H. Kohn, "Stochastically-modulated stimulation to slow down muscle fatigue at stimulated sites in paraplegics using functional electrical stimulation for leg extension." *Neurol. Res.*, vol. 22, no. 7, pp. 703–704, Oct 2000.

[37] A. Thrasher, G. M. Graham, and M. R. Popovic, "Reducing muscle fatigue due to functional electrical stimulation using random modulation of stimulation parameters," *Artif. Organs*, vol. 29, no. 6, pp. 453–458, Jun 2005.

[38] R. J. Downey, M. Bellman, N. Sharma, Q. Wang, C. M. Gregory, and W. E. Dixon, "A novel modulation strategy to increase stimulation duration in neuromuscular electrical stimulation," *Muscle Nerve*, vol. 44, no. 3, pp. 382–387, September 2011.

[39] S. Binder-Macleod and T. Guerin, "Preservation of force output through progressive reduction of stimulation frequency in human quadriceps femoris muscle," *Phys. Ther.*, vol. 70, no. 10, pp. 619–625, 1990.

[40] S. A. Binder-Macleod, S. Lee, and S. Baadte, "Reduction of the fatigue induced force decline in human skeletal muscle by optimized stimulation trains," *Arch. Phys. Med. Rehabil.*, vol. 78, pp. 1129–1137, 1997.

[41] E. Henneman, G. Somjen, and D. O. Carpenter, "Functional significance of cell size in spinal motoneurons," *J. Neurophysiol.*, vol. 28, pp. 560–580, 1965.

[42] C. S. Bickel, C. M. Gregory, and J. C. Dean, "Motor unit recruitment during neuromuscular electrical stimulation: a critical appraisal," *Eur. J. Appl. Physiol.*, vol. 111, no. 10, pp. 2399–2407, 2011.

[43] C. M. Gregory and C. S. Bickel, "Recruitment patterns in human skeletal muscle during electrical stimulation," *Phys. Ther.*, vol. 85, no. 4, pp. 358–364, 2005.

[44] C. M. Gregory, W. E. Dixon, and C. S. Bickel, "Impact of varying pulse frequency and duration on muscle torque production and fatigue," *Muscle Nerve*, vol. 35, no. 4, pp. 504–509, April 2007.

[45] S. A. Binder-Macleod, E. E. Halden, and K. A. Jungles, "Effects of stimulation intensity on the physiological responses of human motor units," *Med. Sci. Sports. Exerc.*, vol. 27, no. 4, pp. 556–565, Apr 1995.

[46] D. A. Jones, B. Bigland-Ritchie, and R. H. T. Edwards, "Excitation frequency and muscle fatigue: Mechanical responses during voluntary and stimulated contractions," *Exp. Neurol.*, vol. 64, no. 2, pp. 401–413, May 1979.

[47] E. D. Zonnevijlle, N. N. Somia, R. W. Stremel, C. J. Maldonado, P. M. Werker, M. Kon, and J. H. Barker, "Sequential segmental neuromuscular stimulation: an effective approach to enhance fatigue resistance." *Plast. Reconstr. Surg.*, vol. 105, no. 2, pp. 667–673, 2000.

[48] R. W. Stremel and E. D. Zonnevijlle, "Re-animation of muscle flaps for improved function in dynamic myoplasty," *Microsurgery*, vol. 21, no. 6, pp. 281–286, 2001.

[49] M. J. Decker, L. Griffin, L. D. Abraham, and L. Brandt, "Alternating stimulation of synergistic muscles during functional electrical stimulation cycling improves endurance in persons with spinal cord injury," *J. Electromyogr. Kinesiol.*, vol. 20, no. 6, pp. 1163–1169, 2010.

[50] M. Pournezam, B. J. Andrews, R. H. Baxendale, G. F. Phillips, and J. P. Paul, "Reduction of muscle fatigue in man by cyclical stimulation," *J. Biomed. Eng.*, vol. 10, no. 2, pp. 196–200, 1988.

[51] L. Z. P. Maneski, N. M. Malešević, A. M. Savić, T. Keller, and D. B. Popović, "Surface-distributed low-frequency asynchronous stimulation delays fatigue of stimulated muscles," *Muscle Nerve*, vol. 48, no. 6, pp. 930–937, 2013.

[52] R. J. Downey, E. Ambrosini, S. Ferrante, A. Pedrocchi, W. E. Dixon, and G. Ferrigno, "Asynchronous stimulation with an electrode array reduces muscle fatigue during FES cycling," in *Proc. Int. Func. Elect. Stimul. Soc.*, Banff, Canada, September 2012, pp. 154–157.

[53] S. A. Binder-Macleod and W. A. McLaughlin, "Effects of asynchronous stimulation on the human quadriceps femoris muscle," *Arch. Phys. Med. Rehabil.*, vol. 78, no. 3, pp. 294 – 297, 1997.

[54] A. R. Lind and J. Scott Petrofsky, "Isometric tension from rotary stimulation of fast and slow cat muscles," *Muscle Nerve*, vol. 1, no. 3, pp. 213–218, 1978.

[55] A. K. Wise, D. L. Morgan, J. E. Gregory, and U. Proske, "Fatigue in mammalian skeletal muscle stimulated under computer control," *J. Appl. Physiol.*, vol. 90, no. 1, pp. 189–197, 2001.

[56] N. M. Malešević, L. Z. Popović, L. Schwirtlich, and D. B. Popović, "Distributed low-frequency functional electrical stimulation delays muscle fatigue compared to conventional stimulation," *Muscle Nerve*, vol. 42, no. 4, pp. 556–562, 2010.

[57] T. Brown, Y. Huang, D. Morgan, U. Proske, and A. Wise, "A new strategy for controlling the level of activation in artificially stimulated muscle," *IEEE Trans. Rehabil. Eng.*, vol. 7, no. 2, pp. 167–173, 1999.

[58] A. C. Hughes, L. Guo, and S. P. DeWeerth, "Interleaved multichannel epimysial stimulation for eliciting smooth contraction of muscle with reduced fatigue," in *Eng. Med. Biol. Soc. (EMBC), 2010. Annu. Int. Conf. IEEE*, Sept. 2010, pp. 6226–6229.

[59] K. Yoshida and K. Horch, "Reduced fatigue in electrically stimulated muscle using dual channel intrafascicular electrodes with interleaved stimulation," *Ann. Biomed. Eng.*, vol. 21, no. 6, pp. 709–714, 1993.

[60] D. McDonnall, G. A. Clark, and R. A. Normann, "Interleaved, multisite electrical stimulation of cat sciatic nerve produces fatigue-resistant, ripple-free motor responses," *IEEE Trans. Neural Syst. Rehabil. Eng.*, vol. 12, no. 2, pp. 208–215, June 2004.

[61] V. K. Mushahwar and K. W. Horch, "Proposed specifications for a lumbar spinal cord electrode array for control of lower extremities in paraplegia," *IEEE Trans. Rehabil. Eng.*, vol. 5, no. 3, pp. 237–243, September 1997.

[62] M. Thomsen and P. H. Veltink, "Influence of synchronous and sequential stimulation on muscle fatigue," *Med. Biol. Eng. Comput.*, vol. 35, no. 3, pp. 186–192, 1997.

[63] R. Nguyen, K. Masani, S. Micera, M. Morari, and M. R. Popovic, "Spatially distributed sequential stimulation reduces fatigue in paralyzed triceps surae muscles: A case study," *Artif. Organs*, vol. 35, no. 12, pp. 1174–1180, 2011.

[64] L. Z. Popović and N. M. Malešević, "Muscle fatigue of quadriceps in paraplegics: Comparison between single vs. multi-pad electrode surface stimulation," in *Eng. Med. Biol. Soc. (EMBC), 2009. Annu. Int. Conf. IEEE*, Sept. 2009, pp. 6785–6788.

[65] D. G. Sayenko, R. Nguyen, M. R. Popovic, and K. Masani, "Reducing muscle fatigue during transcutaneous neuromuscular electrical stimulation by spatially and sequentially distributing electrical stimulation sources," *Eur. J. Appl. Physiol.*, vol. 114, no. 4, pp. 793–804, 2014.

[66] B. Lau, L. Guevremont, and V. K. Mushahwar, "Strategies for generating prolonged functional standing using intramuscular stimulation or intraspinal microstimulation," *IEEE Trans. Neural Syst. Rehabil. Eng.*, vol. 15, no. 2, pp. 273–285, 2007.

[67] R. J. Downey, M. J. Bellman, H. Kawai, C. M. Gregory, and W. E. Dixon, "Comparing the induced muscle fatigue between asynchronous and synchronous electrical stimulation in able-bodied and spinal cord injured populations," *IEEE Trans. Neural Syst. Rehabil. Eng.*, to appear.

[68] N. Sharma, K. Stegath, C. M. Gregory, and W. E. Dixon, "Nonlinear neuromuscular electrical stimulation tracking control of a human limb," *IEEE Trans. Neural Syst. Rehabil. Eng.*, vol. 17, no. 6, pp. 576–584, June 2009.

[69] N. Sharma, C. Gregory, M. Johnson, and W. E. Dixon, "Closed-loop neural network-based NMES control for human limb tracking," *IEEE Trans. Control Syst. Technol.*, vol. 20, no. 3, pp. 712–725, 2012.

[70] C. Freeman, D. Tong, K. Meadmore, A. Hughes, E. Rogers, and J. Burridge, "FES based rehabilitation of the upper limb using input/output linearization and ILC," in *Proc. Am. Control Conf.*, Montreal, June 2012, pp. 4825–4830.

[71] Q. Wang, N. Sharma, M. Johnson, C. M. Gregory, and W. E. Dixon, "Adaptive inverse optimal neuromuscular electrical stimulation," *IEEE Trans. Cybern.*, vol. 43, pp. 1710–1718, 2013.

[72] M. A. Frankel, B. R. Dowden, V. J. Mathews, R. A. Normann, G. A. Clark, and S. G. Meek, "Multiple-input single-output closed-loop isometric force control using asynchronous intrafascicular multi-electrode stimulation," *IEEE Trans. Neural Syst. Rehabil. Eng.*, vol. 19, no. 3, pp. 325–332, 2011.

[73] R. J. Downey, T.-H. Cheng, and W. E. Dixon, "Tracking control of a human limb during asynchronous neuromuscular electrical stimulation," in *Proc. IEEE Conf. Decis. Control*, Florence, IT, Dec. 2013, pp. 139–144.

[74] R. J. Downey, M. Tate, H. Kawai, and W. E. Dixon, "Comparing the force ripple during asynchronous and conventional stimulation," *Muscle Nerve*, vol. 50, no. 4, pp. 549–555, October 2014.

[75] J. L. Krevolin, M. G. Pandy, and J. C. Pearce, "Moment arm of the patellar tendon in the human knee," *J. Biomech.*, vol. 37, no. 5, pp. 785–788, 2004.

[76] T. Watanabe, R. Futami, N. Hoshimiya, and Y. Handa, "An approach to a muscle model with a stimulus frequency-force relationship for FES applications," *IEEE Trans. Rehabil. Eng.*, vol. 7, no. 1, pp. 12–18, March 1999.

[77] E. P. Widmaier, H. Raff, and K. T. Strang, *A.J. Vander, J.H. Sherman, and D.S. Luciano's Human Physiology: The Mechanisms of Body Function*, 9th ed. McGraw-Hill, New York, 2004.

[78] R. Kamalapurkar, J. A. Rosenfeld, J. Klotz, R. J. Downey, and W. E. Dixon. (2014) Supporting lemmas for RISE-based control methods. arXiv:1306.3432v3.

[79] B. Xian, D. M. Dawson, M. S. de Queiroz, and J. Chen, "A continuous asymptotic tracking control strategy for uncertain nonlinear systems," *IEEE Trans. Autom. Control*, vol. 49, no. 7, pp. 1206–1211, 2004.

[80] B. E. Paden and S. S. Sastry, "A calculus for computing Filippov's differential inclusion with application to the variable structure control of robot manipulators," *IEEE Trans. Circuits Syst.*, vol. 34, no. 1, pp. 73–82, January 1987.

[81] N. Fischer, R. Kamalapurkar, and W. E. Dixon, "LaSalle-Yoshizawa corollaries for nonsmooth systems," *IEEE Trans. Autom. Control*, vol. 58, no. 9, pp. 2333–2338, 2013.

[82] R. A. Normann, B. R. Dowden, M. A. Frankel, A. M. Wilder, S. D. Hiatt, N. M. Ledbetter, D. A. Warren, and G. A. Clark, "Coordinated, multi-joint, fatigue-resistant feline stance produced with intrafascicular hind limb nerve stimulation," *J. Neural Eng.*, vol. 9, no. 2, pp. 1–13, 2012.

[83] K. Kiguchi and Y. Hayashi, "An EMG-based control for an upper-limb power-assist exoskeleton robot," *IEEE Trans. Syst. Man Cybern. Part B Cybern.*, vol. 42, no. 4, pp. 1064–1071, August 2012.

[84] W. Yu and J. Rosen, "Neural PID control of robot manipulators with application to an upper limb exoskeleton," *IEEE Trans. Cybern.*, vol. 43, no. 2, pp. 673–684, April 2013.

[85] S. Hussain, S. Q. Xie, and P. K. Jamwal, "Adaptive impedance control of a robotic orthosis for gait rehabilitation," *IEEE Trans. Cybern.*, vol. 43, no. 3, pp. 1025–1034, June 2013.

BIOGRAPHICAL SKETCH

Ryan Downey was born in April 1987 in Boynton Beach, Florida. He received his B.S. in mechanical engineering at the University of Florida in 2010 where he completed his honor's thesis under the advisement of Dr. Warren E. Dixon. Ryan subsequently joined the Nonlinear Controls and Robotics research group in 2010 to pursue his doctoral research. Soon after entering graduate school at the University of Florida, he was accepted to an international exchange program (ATLANTIS CRISP) and subsequently received a M.S. in biomedical engineering from Politecnico di Milano in 2012. Upon returning to the United States, he received M.S. degrees in biomedical engineering and mechanical engineering at the University of Florida in 2012 and 2014, respectively. Ryan's research focuses on functional electrical stimulation and Lyapunov-based nonlinear control.